University of Cyprus

DEPARTMENT OF MECHANICAL AND MANUFACTURING ENGINEERING

Ultrasound Enhanced Drug Delivery: Pressure and Temperature activation approaches

DOCTOR OF PHILOSOPHY DISSERTATION

CHRISTOPHOROS MANNARIS

2014

University of Cyprus

DEPARTMENT OF MECHANICAL AND MANUFACTURING ENGINEERING

Ultrasound Enhanced Drug Delivery: Pressure and Temperature activation approaches

CHRISTOPHOROS MANNARIS

A Dissertation Submitted to the University of Cyprus in Partial Fulfillment of the Requirements for the Degree of Doctor of Philosophy

MAY 2014

VALIDATION PAGE

Doctoral Candidate: Christophoros Mannaris

Doctoral Thesis Title: Ultrasound Enhanced Drug Delivery: Pressure and Temperature activation approaches

The present Doctoral Dissertation was submitted in partial fulfillment of the requirements for the Degree of Doctor of Philosophy at the ***Department of Mechanical and Manufacturing Engineering*** *and was approved on the 14th May. 2014 by the members of the* ***Examination Committee.***

Examination Committee:

Research Supervisor:

Michalakis A. Averkiou, Associate Professor,
University of Cyprus, MME Department ----------

Committee Members:

Vassilis Sboros, Associate Professor,
Heriot Watt University, UK ----------

Triantafyllos Stylianopoulos, Lecturer
University of Cyprus, MME Department ----------

Andreas Alexandrou, Professor
University of Cyprus, MME Department ----------

Constantinos Pitris, Associate Professor
University of Cyprus, ECE Department ----------

DECLARATION OF DOCTORAL CANDIDATE

The present doctoral dissertation was submitted in partial fulfillment of the requirements for the degree of Doctor of Philosophy of the University of Cyprus. It is a product of original work of my own, unless otherwise mentioned through references, notes, or any other statements.

Christophoros Mannaris

……

Περίληψη

Η μεταφορά φαρμάκων με υπέρηχους αποσκοπεί στη βελτίωση της θεραπευτικής αποτελεσματικότητας με την αύξηση της ποσότητας χορήγησης και τη μείωση των παρενεργειών. Νέα είδη φαρμάκων έχουν τη δυνατότητα απελευθέρωσης του φαρμάκου με την εφαρμογή ενός εξωτερικού ερεθίσματος. Σκιαγραφικά υπερήχων (μικροφυσαλλίδες) που αρχικά αναπτύχθηκαν για σκοπούς απεικόνισης, μπορούν τώρα να φορτωθούν με φάρμακα είτε στο εσωτερικό τους είτε στο κέλυφος. Οι υπερηχογράφοι μπορούν να παίξουν έναν διπλό ρόλο ως απεικονιστικό και θεραπευτικό εργαλείο. Η απεικόνιση μικροφυσαλλίδων στην κυκλοφορία γίνεται συνήθως με υπερήχους χαμηλής έντασης ενώ με υψηλή ένταση μπορούν να καταστρέψουν τις μικροφυσαλλίδες και να προκαλέσουν την απελευθέρωση φαρμάκων στην περιοχή ενδιαφέροντος. Λιποσώματα ευαίσθητα στη θερμοκρασία έχουν σχεδιάστεί ούτως ώστε να απελευθερώνουν φάρμακα που εσωκλείουν κάτω από ήπια αύξηση θερμοκρασίας (42 °C). Υπέρηχοι ψηλής έντασης μπορούν να προκαλέσουν αύξηση θερμοκρασίας σε έναν όγκο μέσα στο σώμα για στοχευόμενη παροχή φάρμακων από τα λιποσώματα.

Αυτή η διατριβή ερευνά τις ακουστικές αρχές και τη λεπτομερή ταλάντωση των μικροφυσαλλίδων που προκαλείται με υπερηχητικά κύματα για θεραπευτικές εφαρμογές. Κυριος στόχος είναι να γίνει κατανοητή η αλληλεπίδραση των μικροφυσαλλίδων με τους υπερήχους, το φάρμακο και τον ιστό και να παραχθούν έτσι οι παράμετροι για την καλύτερη δυνατή μεταφορά φαρμάκων στη περιοχή ενδιαφέροντος. Αναπτύσσονται νέες μέθοδοι και πειραματικές διατάξεις, όπου με την αποφυγή του κορεσμού των σημάτων κατά τη χρήση μηχανής υπερήχων, γίνεται μια πιο ακριβής διερεύνηση των απεικονιστικών και θεραπευτικών ιδιοτήτων νέων μικροφυσαλλίδων φορτωμένων με φάρμακα. Πειράματα μεταφοράς φαρμάκων σε καρκινικά κύτταρα καταδεικνύουν αυξημένη θεραπευτική αποτελεσματικότητα με την ενεργοποίηση των μικροφυσαλλίδων με υπερήχους.

Παρουσιάζεται επίσης μια νέα πειραματική διάταξη η οποία δίνει για πρώτη φορά τη δυνατότητα διεξαγωγής *in vitro* πειραμάτων για την ενεργοποίηση λιποσωμάτων ευαίσθητων στη θερμοκρασία. Θεωρητικές προβλέψεις αύξησης θερμοκρασίας με υπερήχους επικυρώνονται πειραματικά. Επιτυγχάνεται σημαντική απελευθέρωση μέχρι και 80% της δοξορουβικίνης από τα λιποσώματα.

Διερευνάται επίσης η σημαντηκότητα και οι πιθανές επιρροές του πεδίου έντασης των μετατροπέων στην στοχευόμενη θεραπεία με υπέρηχους τόσο με μηχανικούς όσο και με θερμικούς μηχανισμούς ενεργοποίησης.

Abstract

Image-guided ultrasound-mediated drug delivery shows great promise in improving the therapeutic efficacy of chemotherapeutic agents by increasing the local drug deposition and reducing systemic side effects. Novel drug-loaded agents with the ability to release the encapsulated drug upon the application of an external stimulus are being developed. Microbubble ultrasound contrast agents (UCA), originally intended for imaging purposes, are now used as a drug delivery vehicle with the drugs encapsulated in the lumen or attached on their shell. Ultrasound scanners adopt a double role as both an imaging and a therapy device by tracking the microbubbles in circulation using low-amplitude US while high-amplitude ultrasound is used to destroy the microbubbles and trigger the drug release on site. Temperature sensitive liposomes (TSL) loaded with drugs are designed to release their payload with mild hyperthermia (42 °C). TSLs can be co-administrated with UCA and monitored in circulation using ultrasound. High intensity focused ultrasound can be used to induce hyperthermia in a tumor inside the body thus locally delivering the drug from TSLs.

This thesis investigates the physical acoustics and detailed microbubble response to ultrasound used in therapeutic applications in an attempt to better understand the mechanism of microbubble interaction with ultrasound, the drug and tissue and derive the optimal conditions to use in ultrasound-enhanced drug delivery. *In vitro* experimental setups and methods are developed for limiting signal saturation in order to accurately measure backscattered echoes from UCA and determine their response to a large range of acoustic pressures. The therapeutic efficacy of novel Doxorubicin liposome-loaded microbubbles following ultrasound activation is also evaluated on human glioblastoma cells.

A novel *in vitro* experimental setup for the activation of drug loaded TSLs is presented allowing studies for the controlled release of TSL with ultrasound-induced hyperthermia to be carried out *in vitro* which to the best of our knowledge is the first of its kind. The acoustic conditions for the desired hyperthermia are derived theoretically and validated experimentally. Using our setup, an 80% release of doxorubicin from TSLs is achieved.

The importance of the diffraction pattern produced by the transducer and its effect on both temperature and pressure activation approaches of drug delivery is addressed.

Acknowledgements

I would like to thank Dr. Michalis. A. Averkiou, my supervising professor, for his continuous advice, encouragement and support throughout this work. He was always willing to help out with the experiments and his aspirations on the quality of my work often exceeded my own. Even though we never got to go mountain biking together as he promised, I feel that our relationship developed to more than a typical student-supervisor relationship. Mike, I have learned a great deal from you over these last 7 years. It was both an honor and a privilege working with you.

Marios Lampaskis, my colleague with the ability to offer a vast amount of information on nearly any subject, is greatly appreciated for his help in numerical analysis and development of the complicated MATLAB codes. Above all, he is thanked for the endless discussions over lunch, the beers and Zivania which were sometimes a necessity, and his true friendship.

Christina Keravnou, who I saw developing from a shy undergraduate student to a very capable researcher and co-author, is thanked for all her help with the experiments and analysis of the endless amount of data we collected. Christina, I could always count on your help and know that I have learned a lot from you.

Mr. Kypros Stylianou, our laboratory technician who is so much more than that, is sincerely thanked for all his help in designing and building any experimental setup that came into our minds. Only Kypros could successfully insert a 200μm thread into a 250μm microfil tube with a naked eye. His exceptional skills and willingness to help has helped me more than he can imagine.

I would like to thank my parents, whose love and support over the years has never faded. They have set the standards high and one day I hope to be as good a parent as they have been to me.

Last and most important of all, I want to thank my wife and best friend Vana. She always believed in me, she is my rock that was by my side “through better and through worse”. She always said that behind every great man there is an even greater woman and I want to use this opportunity to tell her that I too believe it is true. The birth of our two wonderful boys, Demetris and Panayiotis was the highlight of this journey and the major incentive for completing this degree. Boys, I love you.

to my wife and kids

Contents

List of Figures

List of Tables

1
Introduction

1.1 Medical diagnostic ultrasound and microbubbles

Ultrasonography is widely used to visualize soft tissues, organs, vessels, muscles, joints, and tendons. It has numerous advantages over other imaging modalities, such as low cost, real-time visualization, portability (it is often referred to as a bedside imaging modality), and safety (it is free of ionizing radiation). Ultrasound has an excellent safety record, making it particularly appealing in prenatal evaluations and continuous patient monitoring. It is routinely used in cardiology with echocardiograms to provide information about the size and shape of the heart, its pumping capacity, and the location and extent of any damage to the myocardium. In oncology, ultrasound imaging is used to locate abnormalities in otherwise healthy tissue, diagnose malignant lesions [1] and differentiate between cystic and solid lesions.

Ultrasound imaging involves the use of high frequency sound waves. It is based on the pulse-echo principle where short pulsed waves typically in the MHz range are transmitted into tissue by an ultrasound probe. Inhomogeneities in the tissue (variations in density and compressibility) partially scatter the incident wave producing echoes that are received by the same transducer. The amplitude of the received echoes determines the grayscale level of the formed image and the time-of-flight is converted into the distance traveled in the tissue i.e. the depth of the scattering surface. The lateral (horizontal) position of the imaged object is determined by the location of the receiving transducer element. Thus a tissue or B-mode (brightness mode) image is formed. Optimized processing algorithms and computing power allow for real-time imaging with typical frame rates in the order of tens of frames per second.

Imaging blood flow is of high diagnostic value. In the heart, blood flow in the coronary arteries and through the valves determines the heart's overall condition. In the carotid arteries blood flow around an atherosclerotic plaque reveals the extent of occlusion, and helps in patient management. Blood clots in leg veins (deep vein thrombosis) are similarly diagnosed while the health of a fetus can be evaluated by blood flow measurements through the umbilical cord.

Doppler ultrasound is used to measure blood flow and relies on the phenomenon of the *apparent* change in the transmitted frequency when a sound emitting source moves relative to the observer (the Doppler Effect). The change in frequency is proportional to the relative velocity as shown in equation 1.1.

where Δf is the frequency change, f_o is the transmitted frequency, v is the relative speed of the source to the observer and c is the speed of the wave in the medium.

In practice, a series of pulses is transmitted and received. Echoes from stationary tissue remain unaltered from pulse to pulse (and cancel out) whereas echoes from moving scatterers (in this case the red blood cells) induce a change in frequency, which can be detected and processed to produce either a color flow display or a Doppler waveform. Examples of Doppler imaging in the diagnosis of carotid artery stenosis are shown in Fig.1-1. Doppler imaging can help visualize the blood flow around the plaque (Fig. 1-1 a-b) and the blood velocity before and after the stenosis can be accurately measured. Measuring peak systolic velocity (PSV) is still considered the most important component of the carotid Doppler examination and is used for grading carotid stenosis [2]. The distinction between occlusion and near occlusion is of extreme importance because patients with near occlusion, indicated by the presence of trickle flow (Fig. 1-1 c-d), may be benefited from surgery, while total occlusion precludes it [3].

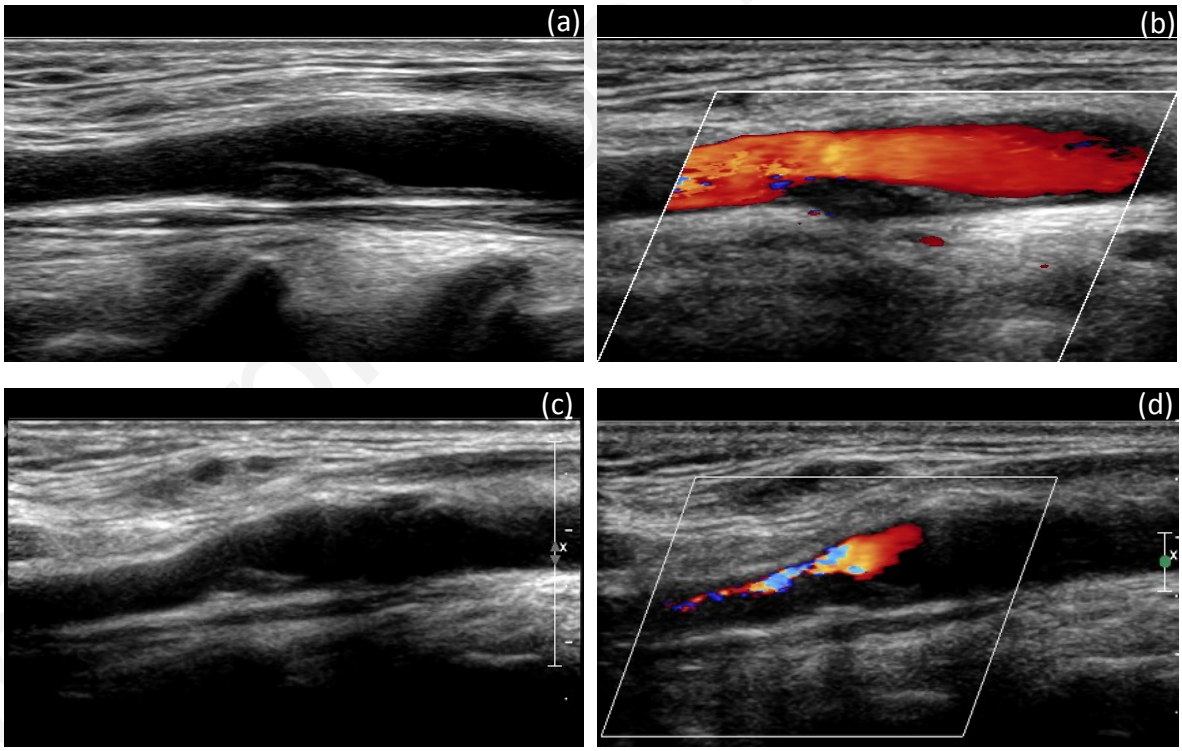

Figure 1-1: Doppler imaging in the diagnosis of carotid artery stenosis. (a),(c) baseline B-Mode images of a left internal carotid artery. The plaques can be observed but the extent of the occlusion cannot be accurately determined. (b) with Doppler imaging the blood flow around the plaque can be easily visualized and the blood velocity before and after the stenosis can be measured. (d) Trickle flow detected with Doppler imaging might change the diagnosis and treatment of a patient.

While Doppler techniques work well in large vessels with high blood velocities they are unable to detect low velocity blood flow in the microcirculation despite continuing advances in the sensitivity of diagnostic ultrasound systems. The main difficulty these techniques share is that the red blood cells are weak reflectors of ultrasound with received amplitudes 40–60 dB smaller than that of tissue and the removal of this tissue signal places a lower limit on the ability to detect low velocity blood flow. Overcoming this limitation is important because perfusion of atherosclerotic plaques is a biomarker of atherosclerotic development [4, 5] while the quantification of the flow profile in the vasa vasorum has been shown to contain valuable information in identifying vulnerable plaques [6]. In oncology, measurements of the blood flow in the tumor microvasculature would be useful in the detection and characterization of the lesion as well as in therapy monitoring [7, 8]. A method to overcome the difficulties in imaging blood flow on a smaller scale is to inject brighter reflectors than red blood cells into the vascular system. Gas-filled microbubbles are one such reflector.

Microbubbles in medical imaging were accidentally introduced by Gramiak and Shah in 1968 [9] when opacification of the right ventricle was observed following an injection of saline into the ascending aorta and cardiac chambers. In the following decades, active research led to the development of several agents; in 1994 Albunex (Molecular Biosystems, San Diego, CA) became the first commercially available contrast agent to be approved for human use in the United States followed shortly by Levovist, (Bayer Schering Pharma AG, Berlin, Germany) [10]. These early agents had a relatively short half-life mainly due to the high solubility of the air core. Replacing the air core with perfluorocarbons improved the stability of ultrasound contrast agents (UCA). Optison (GE Healthcare, Chalfont St Giles, UK), and SonoVue (Bracco, Milan, Italy), were the first examples of such UCA to be approved for clinical use. Table 1-1 summarizes the current clinically approved ultrasound contrast agents. UCA are blood-pool agents as their typical mean diameters of 2-3 μm (Fig. 1-2) are small enough to pass through the alveolar–capillary barrier of the lungs and large enough to stay within the circulation and not leak into the interstitial space.

Table 1-1: Overview of current clinically approved ultrasound contrast agents. Data collected from the International Contrast Ultrasound Society (ICUS) website .

Name	Manufacturer	Gas	Coating	Approved	Year
Optison	GE Healthcare, Princeton, NJ	C_3F_8	human albumin	USA, EU	1997
Definity	Lantheus Medical Imaging, N. Billerica, MA	C_3F_8	phospholipids	USA, Canada, Mexico, Israel, New Zealand, India, Australia, EU, Korea, Singapore, UAE	2001
Imagent	MCOR Pharmaceuticals, Inc. San Diego, CA	C_6F_{14}	phospholipids	USA	2002
SonoVue	Bracco International, Milan, Italy	SF_6	phospholipids	EU, Norway, Switzerland, China, Singapore, Hong Kong, S. Korea, Iceland, India	2001
Sonazoid	Daiichi Pharmaceutical Co., Tokyo, Japan	C_4F_{10}	phospholipids	Japan	2006

UCA exhibit high echogenicity (ability to reflect sound waves) since they are resonant scatterers at diagnostic ultrasound frequencies. When an acoustic wave encounters a gas microbubble, an asymmetric nonlinear oscillation occurs where the gas expands during the negative pressure portion of the wave in a significantly different way to the compression during the positive pressure portion of the wave. This results in an asymmetric-nonlinear bubble oscillation. Instead of producing a sinusoidal echo with a clean frequency spectrum like the transmitted signal in Fig. 1-3(a) it produces an odd looking echo with asymmetric top and bottom as shown in Fig. 1-3(b). This asymmetry produces harmonics which can be utilized to enhance the signals from the bubbles and effectively distinguish them from the surrounding tissue (Fig. 1-3(c)).

Nonlinear microbubble specific detection techniques like pulse inversion [11, 12] and power modulation [13, 14] utilize the nonlinear signature produced by UCA to suppress the linear tissue signal and provide microbubble specific images. These techniques do not rely on the translational movement of the microbubbles, but instead depend only on their radial response. Thus, microbubbles are imaged everywhere in the body and even in the microcirculation where the blood flow velocities are very low [15, 16].

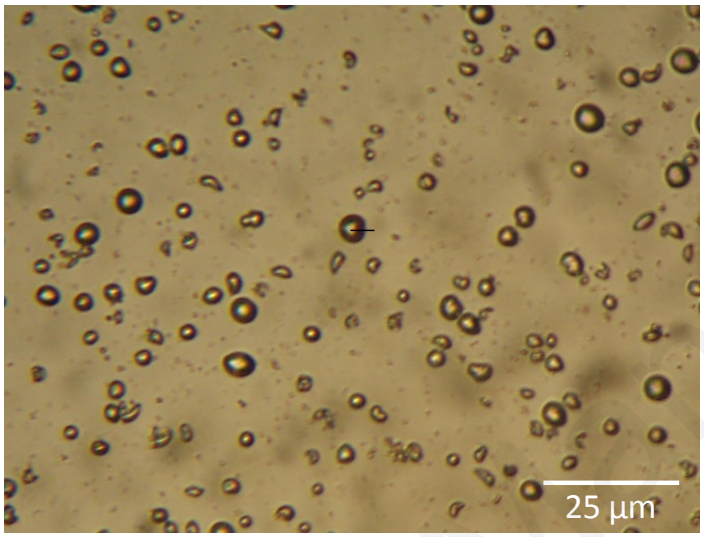

Figure 1-2: Ultrasound contrast microbubbles (SonoVue) viewed under a microscope.

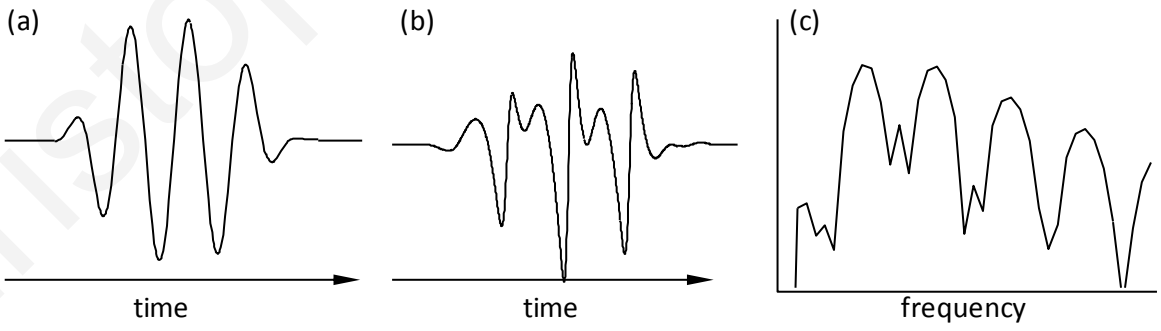

Figure 1-3: (a) Incident ultrasonic wave; (b) nonlinear scattered signal from bubbles; (c) frequency spectrum of bubble echoes seen in (b). The first major hump is the fundamental, and the subsequent ones are the second, third, and fourth harmonics.

UCAs have subsequently been used in various clinical applications including cardiology for myocardial perfusion, oncology for tumor detection and characterization [17] and molecular imaging [18]. CEUS is useful in both detecting lesions (Fig. 1-4) and providing quantitative information about their perfusion enabling accurate identification and characterization of lesions, as well as optimal monitoring of their development and response to therapy [19-21].

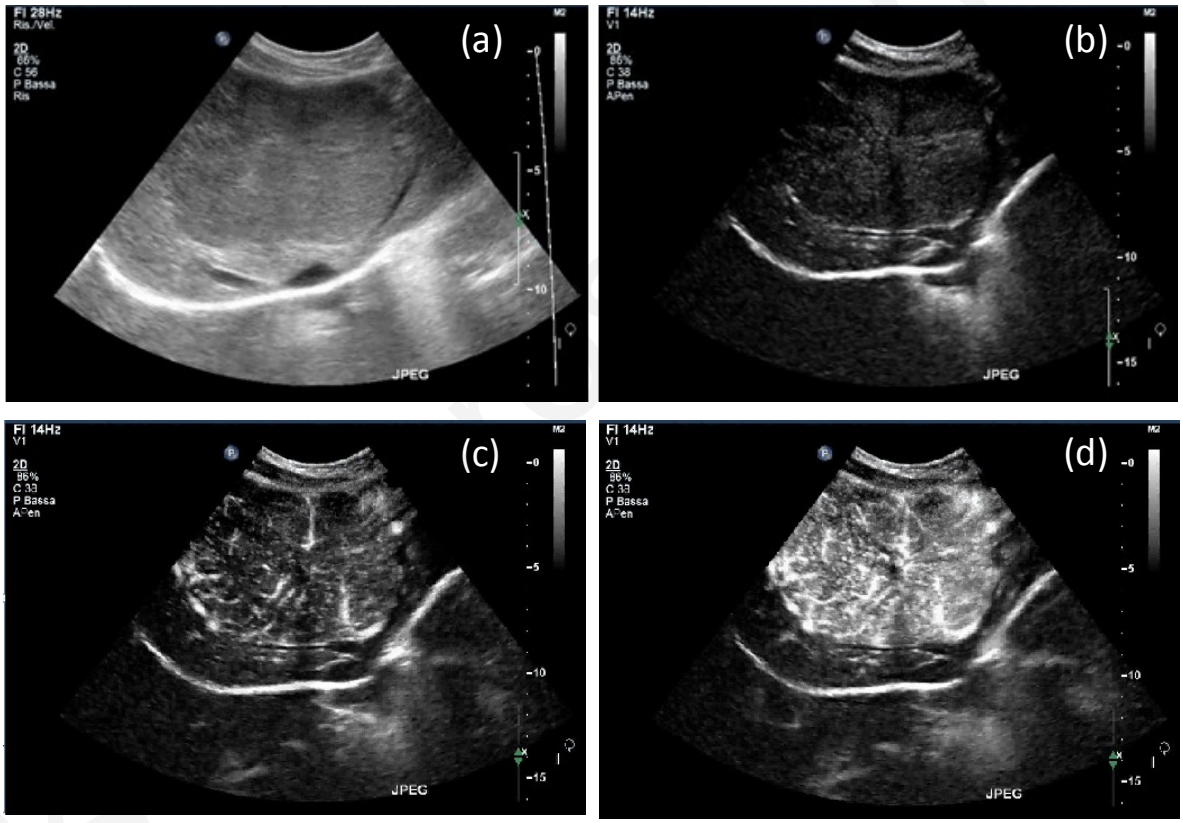

Figure 1-4: (a) B-Mode imaging of a benign FNH lesion. Lesion cannot be easily distinguished due to its similar texture and appearance with normal parenchyma. Smaller lesions would be very difficult to detect. (b) CEUS imaging before UCA arrival. The image is almost black due to the cancellation of the linear tissue echoes. CEUS imaging; immediately after contrast arrival (c) and during peak intensity (d) clearly showing the macrovascular flow patterns of this lesion.

1.2 Therapeutic applications of ultrasound

The use of ultrasound in therapy predates its use as an imaging technique. The ability of ultrasound to interact with tissue and cause biological changes with possible therapeutic effects was recognized as early as 1927 [22]. Today, low intensity ultrasound is used in physiotherapy, fracture repair, sonophoresis (the enhancement of drug penetration through the skin), sonoporation (increasing cell permeability to drugs and other molecules by temporarily modifying the cell membrane structure), and gene therapy where ultrasound facilitates the transfer of genes into diseased tissues and organs [23, 24]. High intensity ultrasound is used in lithotripsy [25], tumor ablation [26], gene and DNA transfection [27], and the facilitation of drug delivery to the brain by opening of the blood brain barrier [28].

The mechanisms of interaction between therapeutic ultrasound and tissue to produce biological effects can be categorized into two main types: thermal and mechanical. Tissue heating is the main aim of many ablative therapeutic applications and probably the best known and understood effect. Heat generation in tissue results from the acoustic absorption of ultrasound energy and is proportional to the intensity and frequency of the sound beam as well as the thermoviscous properties of the medium, such as the absorption coefficient and specific heat capacity.

In low intensity applications, mild hyperthermia on the order of a few degrees above normothermic levels has been shown to increase perfusion in the targeted area and hence increase the delivery of drugs and nutrients as well as the removal of cellular waste. This leads to the relief of inflammation, muscle spasms, and pain, as well as accelerated healing and decreased joint stiffness [29]. Drug delivery with temperature-sensitive drug carriers has also been shown to improve with ultrasound induced mild hyperthermia [30].

At higher intensities, temperatures in excess of 56 °C can be achieved rapidly, leading to protein denaturation and cell death. Spherically curved transducers have the ability to concentrate ultrasound energy at a confined focus inside the body reaching acoustic pressures several-fold the source pressure, hence the name of the therapeutic technique: high intensity focused ultrasound (HIFU). The skin and intermediate structures to the focal point are unaffected because the ultrasound signal passes through them over a wider area and at lower intensities. Approved HIFU applications in the clinic include selective tissue ablation such as solid tumors in the prostate [31] and the treatment of uterine fibroids [32]. Furthermore, several completed and ongoing clinical trials that evaluate HIFU for the treatment of breast, kidney and liver tumors [29, 33], palliative

treatment of bone cancer patients [34] as well as a method of haemostasis [35] confirm the emergence of HIFU as an attractive alternative to traditional surgery.

Acoustic cavitation is the most widely known of the mechanical mechanisms associated with ultrasound and considered by many as the one with the most critical role in ultrasound enhanced drug delivery. Acoustic cavitation can be defined as the growth, oscillation and collapse of air cavities in a fluid medium under the influence of varying pressure field of an acoustic pulse. Non-inertial (or stable) cavitation under low intensity ultrasound involves stable volumetric oscillations of the bubble lasting for several cycles where the bubble radius varies linearly about an equilibrium value. During high intensity ultrasound, inertial (or transient) cavitation occurs where the bubble expands to several times its original size, oscillates nonlinearly for very few cycles and then violently collapses resulting in the possible generation of shockwaves, high velocity micro-jets and extreme localized pressures and temperatures [36, 37]. If inertial cavitation occurs near a rigid boundary e.g. a cell membrane or vessel wall, temporary pores may form. This leads to enhanced extravasation where the drug leaves the circulation to the surrounding interstitium [38]. Pore openings on cell membranes temporarily increase the permeability allowing the delivery of macromolecules into the cytoplasm a process known as sonoporation [39].

Cavitation activity increases with a corresponding increase of cavitation nuclei. One of the major obstacles in the utilization of acoustic cavitation for drug delivery was the limited availability of the latter *in vivo*. This was overcome by the introduction of UCA as cavitation nuclei with several studies reporting enhanced therapeutic effects in their presence while at the same time reducing the required in-situ pressure [40, 41]. Gene and DNA transfection [42], blood brain barrier disruption [43] triggered protein deposition [44], thrombolysis [45], tissue ablation, histotripsy [46] and targeted drug delivery [47] are only a few of the applications where acoustically driven microbubbles are used.

Other non-thermal ultrasound related bio-effects such as acoustic radiation force and acoustic streaming have also been proposed as a mechanism to enhance the delivery of therapeutic substances [48].

1.3 Ultrasound enhanced drug delivery

In 2009, a review on the "Clinical uses of microbubbles in diagnosis and treatment" by Cosgrove and Harvey [49] predicted that the therapeutic applications of microbubbles

and ultrasound will have even more impact on human health than diagnostic applications. Recent literature suggests that HIFU applications are indeed shifting towards enhancing the delivery of drugs and genes and UCA have a key role to play in this process. The development of new drug-loaded agents with the ability to release their payload upon the application of an external stimulus has provided applications like triggered and targeted drug delivery with a whole new dynamic [49]. Drugs encapsulated in the lumen or attached on the shell of microbubbles or liposomes are delivered intravenously and monitored in circulation using medical imaging modalities such as US and/or MRI [47]. Focused ultrasound is the method of choice in research for efficient local deposition of the drug thereby reducing undesired toxicity in the surrounding area. Pressure and temperature activation methods of drug delivery are discussed in the following sections.

1.4 Pressure (mechanical) activation

Pressure activation refers to the use of ultrasound energy as the stimulus for localized drug delivery. A key component of ultrasound-triggered local drug delivery is the ability to image the drug-delivery vehicle in real time. Microbubbles are ideal for this purpose. Targeted drug delivery to specific tissue with microbubbles was proposed as early as 1999 [50] by the incorporation of binding ligands into the shell. These microbubbles would adhere to the targeted tissue and selective bubble destruction with high intensity ultrasound would be used to locally deliver the payload. Over the years, several additional methods of ultrasound-enhanced drug delivery with pressure activation have been proposed. For instance, co-administration of approved drugs with approved contrast microbubbles has been used in sonothrombolysis, where intra-arterial thrombi have been dissolved enabling complete vessel recanalization primarily through cavitation [45, 47]. Microbubble-enhanced extravasation and sonoporation have also improved delivery of drugs, plasmid DNA, and other particles that normally have difficulty escaping from the bloodstream and permeating cell membranes. While co-administration of microbubbles with cytotoxic drugs (either in free or liposomal form) has seen little success mainly due to continued access to untargeted tissues resulting in undesired side effects [51], loading the drug *into* the microbubbles, which are unable to leave the circulation due to their relatively large size, minimizes this issue.

While the literature strongly supports microbubble-enhanced drug delivery, there is a large discrepancy with respect to the optimal ultrasound conditions required, and in

many cases the results are simply a case of trial and error. There are studies where the microbubbles are subjected to ultrasonic pulses ranging from a few cycles [27] up to tens of thousands of cycles [52] or even continuous wave excitations [53]. The pressures used also vary greatly from a few kPa [46] up to several MPa [54]. Often enough, ultrasound induced bio-effects (thermal and mechanical) are seldom taken into consideration. The diffraction pattern (shape of the sound field) produced by the transducer is also erroneously overlooked. Microbubbles at different locations (perhaps even a few mm apart) may respond differently due to the different acoustic pressures and possibly produce different bio-effects. Several questions remain unanswered and the mechanism of microbubble interaction with ultrasound, the drug and the cells is not fully understood.

1.5 Temperature (thermal) activation

Liposomes containing drugs are known to reduce systemic exposure as well as increase the accumulation of drug in tumors [30] mainly due to their small size which allows extravasation. The relatively slow passive release of the drug however has limited the drug effectiveness despite the larger drug concentrations present. Temperature sensitive liposomes (TSL) designed to modify their membrane structure and quickly release their encapsulated drug when heated near their phase transition temperature (T_m) have provided a solution for this obstacle [55]. Low temperature sensitive liposomes (LTSL) with transition temperatures in the non-destructive hyperthermia range (i.e. 39-42°C) are more commonly used.

Several sources of hyperthermia have been considered over the years, including superficial heating with water baths [56], microwave radiation [57], infra-red radiation [58], and heating with invasive catheters [59]. The use of ultrasound as an external energy source to trigger drug release from TSL offers some distinct advantages over the rest of the methods and it is thus becoming increasingly more popular [30, 60]. In addition to the non-invasive nature of ultrasound, the acoustic field produced by a transducer can be accurately modeled. The field varies in amplitude and different areas in the field experience different acoustic pressures. The acoustic pressure is directly proportional to the energy deposition upon the targeted tissue and thus the effective temperature elevation in the region of interest can also be predicted [61]. Recent advances in electronic and mechanical ultrasound beam steering have enabled accurate control over the acoustic field allowing for local hyperthermia to be induced with millimeter accuracy in a selected region of interest

deep inside the body while maintaining physiological temperatures in the surrounding tissue and along the path of ultrasound propagation [62, 63]. Addition of a paramagnetic contrast agent in the TSL allows MRI tracking of the TSL in circulation as well as quantification of the drug release and subsequent uptake by the tumor tissue [64]. The combined benefits of ultrasound, hyperthermia and drug loaded TSL show great potential in increasing the therapeutic index in cancer treatment with several preclinical reports demonstrating improved delivery of various chemotherapeutic agents into tumors of various types while temperature-induced delivery of TSL encapsulated doxorubicin (DOX) has entered phase III of clinical trials [65].

1.6 Image-guided ultrasound-mediated drug delivery

Image-guided ultrasound-mediated drug delivery shows great promise in improving the therapeutic index of a chemotherapeutic agent by increasing the local deposition and reducing the systemic side effects [66]. A key ingredient is the real-time tracking of the drug-delivery vehicle *in vivo* using low mechanical index (MI) imaging. Once at the desired location, high amplitude ultrasound may be used to trigger the drug release on site. Clinically approved microbubbles used for imaging purposes are designed to offer maximum contrast-to-tissue ratio (CTR) under non-destructive pressures. CTR is defined as the ratio of the scattered intensity from the microbubbles to the scattered intensity from tissue and it is an index of the ability to image the contrast agent in the presence of tissue. Novel drug loaded microbubbles intended for therapeutic purposes should take into consideration both the drug loading capacity as well as the imaging properties. Studying the CTR and destruction characteristics of these novel agents is important since it allows the development of the optimal imaging conditions for tracking the microbubbles *in vivo* without causing destruction and premature release of the drug.

Ultrasound scanners can be a valuable tool in drug delivery applications. Diagnostic ultrasound together with UCAs have been used to induce sonoporation [67], gene and drug delivery [68], sonothrombolysis [69], and blood brain barrier opening [70]. A clinical pilot study for the treatment of pancreatic cancer combining a commercial ultrasound scanner with UCAs has also been reported [71]. Ultrasound scanners have also been used in the past as a research tool to investigate bubble dynamics thus adopting a double role as both an imaging and a therapy device. Sboros et al. [72] reported on the backscatter of UCA suspensions as a function of concentration and pressure. A major

problem often encountered however, is signal saturation [73, 74]. The dynamic range of the backscattered signals varies dramatically depending on the bubble concentration and the MI used. Typically, to image the small signals from the microcirculation, high receive gains are used and this results in signal saturation in areas of larger vessels with higher bubble concentrations. If low receive gains are used, then the small signals from the microcirculation are not detected. This problem becomes even worse at higher MIs, typically used for therapeutic applications. More often than not, signal saturation with increasing pressure and bubble concentration results in a dramatic decrease in CTR and is a limiting factor in achieving accurate image guidance during drug delivery approaches. In addition, signal saturation may lead to erroneous results and false conclusions during perfusion quantification with contrast enhanced ultrasound [74, 75].

1.7 Scope of this work

This dissertation explores the physical acoustics and bubble dynamics related with the use of ultrasound in drug delivery approaches. The response of contrast agent microbubbles to a wide range of ultrasound parameters is investigated in great detail and validated with experiments. The optimum parameters for ultrasound enhanced drug delivery with microbubbles are derived. The therapeutic efficacy of novel drug loaded microbubbles following ultrasound activation is evaluated on human glioblastoma cells and new methods for accurate characterization of contrast agents with an ultrasound scanner are developed. Ultrasound induced temperature elevation is investigated experimentally and compared to theoretical predictions based on the Bioheat equation [76]. A novel setup is developed allowing for the first *in vitro* study of localized drug release from thermosensitive liposomes with ultrasound-induced hyperthermia. The importance of the diffraction pattern produced by the transducer and its effect on both thermal and mechanical bioeffects is addressed.

The interaction of ultrasound with UCA and with tissue is key in the two main approaches used in ultrasound enhanced drug delivery, namely pressure and temperature activation. The biggest challenge in cancer therapy is increasing the therapeutic index (the ratio of the average toxic dose to the average therapeutic dose) of anti-cancer pharmaceuticals. To achieve this, a fundamental understanding of the underline mechanisms involved is required.

Chapter 2 focuses on the physical acoustics and detailed microbubble response to ultrasound used in therapeutic applications. Two *in vitro* set-ups were considered: (a) a set-up with the microbubbles suspended in a large enclosure of deionized water; and (b) one with the microbubbles enclosed in a micron-sized cellulose tube which mimics the *in vivo* scenario of microbubbles in a capillary. A wide range of ultrasonic pulse parameters is investigated in our experiments where the peak rarefactional pressure is varied between 0.05 to 1.5 MPa, the pulse duration from 10 to 20000 cycles, and the pulse repetition frequency (PRF) from 50 Hz to 1.0 KHz, in an attempt to better understand the interactions of microbubbles with ultrasound which would be the first step towards finding the optimal conditions for drug delivery. The question whether a microbubble would continue to oscillate for the full duration of a driving pulse (at a destructive pressure) or completely get destroyed before the end of the pulse is addressed. The detailed diffraction pattern of the transducer and its effect on the microbubble response is considered and the effect of microbubble concentration on ultrasound propagation is also addressed.

The knowledge gained in Chapter 2 is applied in Chapter 3 where the therapeutic efficacy of novel Doxorubicin liposome-loaded microbubbles [77] following ultrasound activation is evaluated on human glioblastoma cells. Ultrasound mediated drug delivery on cell suspensions is performed *in vitro* using a 1 MHz single element transducer for a range of pressures (200-600 kPa). Dox release and uptake is quantified using fluoroscopy and flow cytometry respectively while the cell viability is evaluated using an MTT colorimetric assay forty-eight hours after treatment. The imaging characteristics of this hybrid imaging/therapeutic agent [77] are also investigated with a Philips iU-22 (Philips Medical Systems, Bothell, WA, USA) ultrasound scanner and compared to the commercially available contrast agent SonoVue. The CTR and destruction curves under different excitation pressures ($0.05<MI<0.75$) are obtained in a tissue mimicking Cardiac Doppler flow phantom.

The microbubble imaging characterization methods presented in Chapter 3 are further improved and refined in Chapter 4. An important aspect of targeted drug delivery is the ability to image the drug-delivery vehicle *in vivo* either at low non-destructive pressures, to track microbubbles co-administered with a drug, or at high destructive pressures during the activation of drug loaded microbubbles. The problem of signal saturation observed when ultrasound scanners are used for investigating bubble dynamics is addressed and a solution is provided. The question of microbubble response with increasing acoustic amplitude and concentration is investigated. Signal saturation with

increasing pressure and bubble concentration was carefully avoided by continuously adjusting the scanner's 2D analog gain and accounting for it in the quantification software. The pressure was varied from 0.06 MPa up to 2.6 MPa peak negative pressure (above FDA diagnostic limit) while various concentrations, were considered. The intensity-concentration relationship was investigated at both low and high pressures. The CTR as a function of MI, without the effect of signal saturation, was calculated for a range of concentrations.

In Chapter 5 the thermal mechanisms of ultrasound-tissue interaction and in particular ultrasound induced hyperthermia for the activation of thermosensitive liposomes is thoroughly investigated with experiments, and theoretical modeling. Custom made single element transducers are used for all the experiments presented. A detailed characterization of the acoustic field of these transducers is carried out using a calibrated 0.4 mm element membrane hydrophone (Precision Acoustics Ltd, Dorchester, UK) and the results are compared to the theoretical predictions obtained using the Rayleigh integral. A model the Penne's Bioheat equation [76] is used to simulate the resulting temperature elevation in our samples and calculate the acoustic conditions needed for the desired temperature elevation. The theoretical predictions are then validated with measurements of the induced temperature elevation in glycerol.

The work presented in Chapter 5 attempts to fill a notable gap in the literature where a plethora of reports mentioning *in vivo* studies with ultrasound as a source of hyperthermia are published while reports for *in vitro* work are scarce. *In vitro* work is a logical precursor to *in vivo* work since is allows simplifications of the system under study, offers a more predictable and controlled environment and is usually both time and cost efficient. The main obstacle encountered is the lack of an appropriate medium in which the experiments are to be carried out. An ideal medium should be biocompatible, it should not interact with liposomes in any way that may potentially compromise their stability and it should have a high ultrasound thermoviscous absorption coefficient so that it may be heated with ultrasound energy. Finding such a biocompatible, inert and high absorption coefficient medium still eludes researchers to date.

The design of a dual compartment holder overcomes the need for an "ideal" medium and allows studies for the controlled release of thermosensitive liposomes with ultrasound-induced hyperthermia to be carried out *in vitro* which to the best of our knowledge is the first of its kind and may prove to be a valuable tool in developing and testing new temperature sensitive nanomaterials. The proposed method resembles the *in*

vivo scenario where ultrasound induces hyperthermia in the tumor tissue and the TSL (accumulated in the tumor interstitial spaces) are heated by thermal conduction. *In vitro* activation of TSLs and doxorubicin release using the dual compartment setup are also evaluated.

Finally, the overall results from this thesis are further discussed and analyzed in chapter 6 and conclusions are drawn.

References

[1] M. Brannigan, et al., "Blood flow patterns in focal liver lesions at microbubble-enhanced US," Radiographics, vol. 24, pp. 921-35, Jul-Aug 2004.

[2] A. V. Alexandrov, et al., "Correlation of peak systolic velocity and angiographic measurement of carotid stenosis revisited," Stroke, vol. 28, pp. 339-342, 1997.

[3] W. E. H. C. A. Brant, Fundamentals of diagnostic radiology. Philadelphia: Lippincott, Williams & Wilkins, 2006.

[4] S. B. Feinstein, "The powerful microbubble: from bench to bedside, from intravascular indicator to therapeutic delivery system, and beyond," Am J Physiol Heart Circ Physiol, vol. 287, pp. H450-7, Aug 2004.

[5] D. Staub, et al., "Contrast-enhanced ultrasound imaging of the vasa vasorum: from early atherosclerosis to the identification of unstable plaques," JACC Cardiovasc Imaging, vol. 3, pp. 761-71, Jul 2010.

[6] M. Averkiou, et al., "Vascular Ultrasound Imaging with Contrast Agents: Carotid Plaque Neovascularization and the Hyperplastic Vasa Vasorum Network," in Ultrasound and Carotid Bifurcation Atherosclerosis, A. Nicolaides, et al., Eds., ed: Springer London, 2012, pp. 121-136.

[7] E. Leen, et al., "Dynamic contrast enhanced ultrasound assessment of the vascular effects of novel therapeutics in early stage trials," Eur Radiol, vol. 22, pp. 1442-1450, 2012.

[8] K. Wei, et al., "Quantification of myocardial blood flow with ultrasound-induced destruction of microbubbles administered as a constant venous infusion," Circulation, vol. 97, pp. 473-483, 1998/02/10/ 1998.

[9] R. Gramiak and P. M. Shah, "Echocardiography of the aortic root," Invest Radiol, vol. 3, pp. 356-66, Sep-Oct 1968.

[10] T. Faez, et al., "20 years of ultrasound contrast agent modeling," IEEE Transactions on Ultrasonics, Ferroelectrics, and Frequency Control, vol. 60, pp. 7-20, 2013.

[11] M. A. Averkiou, et al., "Pulsing schemes for the detection of nonlinear echoes from contrast microbubbles," 9th European Symposium on Ultrasound Contrast Imaging, Jan 2004 2004.

[12] D. H. Simpson, et al., "Pulse inversion Doppler: a new method for detecting nonlinear echoes from microbubble contrast agents," IEEE Trans Ultrason Ferroelectr Freq Control, vol. 46, pp. 372-82, 1999.

[13] M. Averkiou, et al., "Ultrasound contrast imaging research," Ultrasound Q, vol. 19, pp. 27-37, Mar 2003.

[14] G. Brock-Fisher, et al., "Means for increasing sensitivity in non-linear ultrasound imaging systems," USA Patent 5,577,505, 26 Nov 1996, 1996.

[15] M. Averkiou, et al., "Quantification of Tumor Microvascularity with Respiratory Gated Contrast Enhanced Ultrasound for Monitoring Therapy," Ultrasound in Medicine and Biology, vol. 36, pp. 68-77, 2010.

[16] V. Sboros and M. X. Tang, "The assessment of microvascular flow and tissue perfusion using ultrasound imaging," Proceedings of the Institution of Mechanical Engineers, Part H: Journal of Engineering in Medicine, vol. 224, pp. 273-290, 2010.

[17] S. R. Wilson and P. N. Burns, "Liver mass evaluation with ultrasound: the impact of microbubble contrast agents and pulse inversion imaging," Semin Liver Dis, vol. 21, pp. 147-59, May 2001.

[18] J. R. Lindner, "Microbubbles in medical imaging: current applications and future directions," Nature reviews. Drug discovery, vol. 3, pp. 527-532, 2004/06// 2004.

[19] M. Averkiou, et al., "Ultrasound contrast imaging research," Ultrasound Quarterly, vol. 19, pp. 27-37, 2003.

[20] E. Leen, et al., "Prospective multicenter trial evaluating a novel method of characterizing focal liver lesions using contrast-enhanced sonography," American Journal of Roentgenology, vol. 186, pp. 1551-1559, 2006.

[21] C. Strouthos, et al., "Indicator dilution models for the quantification of microvascular blood flow with bolus administration of ultrasound contrast agents," IEEE Transactions on Ultrasonics, Ferroelectrics, and Frequency Control, vol. 57, pp. 1296-1310, 2010.

[22] G.F.S, "The physical and biological effects of high-frequency sound-waves of great intensity. R. W. Wood and A. L. Loomis. (Phil. Mag., Sept., 1927)," Journal of the Franklin Institute, vol. 205, pp. 151-153, 1928.

[23] S. Mitragotri, "Healing sound: the use of ultrasound in drug delivery and other therapeutic applications," Nat Rev Drug Discov, vol. 4, pp. 255-60, Mar 2005.

[24] G. ter Haar, "Therapeutic applications of ultrasound," Progress in Biophysics and Molecular Biology, vol. 93, pp. 111-129, 2007.

[25] C. C. Church, "A theoretical study of cavitation generated by an extracorporeal shock wave lithotripter," Journal of the Acoustical Society of America, vol. 86, pp. 215-27, Jul 1989.

[26] J. E. Kennedy, et al., "High-intensity focused ultrasound for the treatment of liver tumours," Ultrasonics, vol. 42, pp. 931-5, Apr 2004.

[27] A. A. Rahim, et al., "Spatial and acoustic pressure dependence of microbubble-mediated gene delivery targeted using focused ultrasound," J Gene Med, vol. 8, pp. 1347-57, Nov 2006.

[28] K. Hynynen, "Focused ultrasound for blood-brain disruption and delivery of therapeutic molecules into the brain," Expert Opinion on Drug Delivery, vol. 4, pp. 27-35, 2007.

[29] V. Frenkel, "Ultrasound mediated delivery of drugs and genes to solid tumors," Advanced Drug Delivery Reviews, vol. 60, pp. 1193-1208, 2008.

[30] S. Dromi, et al., "Pulsed-high intensity focused ultrasound and low temperature - Sensitive liposomes for enhanced targeted drug delivery and antitumor effect," Clinical Cancer Research, vol. 13, pp. 2722-2727, 2007.

[31] J. E. Kennedy, "High-intensity focused ultrasound in the treatment of solid tumours," Nature Reviews Cancer, vol. 5, pp. 321-327, 2005.

[32] E. A. Stewart, et al., "Focused ultrasound treatment of uterine fibroid tumors: Safety and feasibility of a noninvasive thermoablative technique," American Journal of Obstetrics and Gynecology, vol. 189, pp. 48-54, 2003.

[33] A. Napoli, et al., "MR-guided high-intensity focused ultrasound: Current status of an emerging technology," CardioVascular and Interventional Radiology, vol. 36, pp. 1190-1203, 2013.

[34] R. Catane, et al., "MR-guided focused ultrasound surgery (MRgFUS) for the palliation of pain in patients with bone metastases - Preliminary clinical experience," Annals of Oncology, vol. 18, pp. 163-167, 2007.

[35] R. J. Siegal, et al., "High intensity focused ultrasound: A method of hemostasis," Echocardiography, vol. 18, pp. 309-315, 2001.

[36] K. Hynynen, "The threshold for thermally significant cavitation in dog's thigh muscle *in vivo*," Ultrasound Med Biol, vol. 17, pp. 157-69, 1991.

[37] P. Marmottant and S. Hilgenfeldt, "Controlled vesicle deformation and lysis by single oscillating bubbles," Nature, vol. 423, pp. 153-6, May 8 2003.

[38] M. R. Bohmer, et al., "Focused ultrasound and microbubbles for enhanced extravasation," Journal of Controlled Release, vol. 148, pp. 18-24, Nov 20 2010.

[39] K. Kooiman, et al., "Increasing the Endothelial Layer Permeability Through Ultrasound-Activated Microbubbles," IEEE Transactions on Biomedical Engineering, vol. 57, pp. 29-32, Jan 2010.

[40] J. M. Escoffre, et al., "Doxorubicin delivery into tumor cells with ultrasound and microbubbles," Molecular Pharmaceutics, vol. 8, pp. 799-806, 2011.

[41] C. D. Arvanitis, et al., "Cavitation-Enhanced Extravasation for Drug Delivery," Ultrasound in Medicine and Biology, vol. 37, pp. 1838-1852, 2011.

[42] R. E. Vandenbroucke, et al., "Ultrasound assisted siRNA delivery using PEG-siPlex loaded microbubbles," Journal of Controlled Release, vol. 126, pp. 265-273, 2008.

[43] M. A. O'Reilly and K. Hynynen, "Ultrasound enhanced drug delivery to the brain and central nervous system," International Journal of Hyperthermia, vol. 28, pp. 386-396, 2012.

[44] R. Bekeredjian, et al., "Augmentation of cardiac protein delivery using ultrasound targeted microbubble destruction," Ultrasound Med Biol, vol. 31, pp. 687-91, May 2005.

[45] C. A. Molina, et al., "Microbubble administration accelerates clot lysis during continuous 2-MHz ultrasound monitoring in stroke patients treated with intravenous tissue plasminogen activator," Stroke, vol. 37, pp. 425-9, Feb 2006.

[46] M. R. Bohmer, et al., "Ultrasound triggered image-guided drug delivery," Eur J Radiol, vol. 70, pp. 242-53, May 2009.

[47] S. Hernot and A. L. Klibanov, "Microbubbles in ultrasound-triggered drug and gene delivery," Adv Drug Deliv Rev, vol. 60, pp. 1153-66, Jun 30 2008.

[48] M. J. Shortencarier, et al., "A method for radiation-force localized drug delivery using gas-filled lipospheres," Ieee Transactions on Ultrasonics Ferroelectrics and Frequency Control, vol. 51, pp. 822-831, Jul 2004.

[49] D. Cosgrove and C. Harvey, "Clinical uses of microbubbles in diagnosis and treatment," Medical and Biological Engineering and Computing, vol. 47, pp. 813-826, 2009.

[50] A. L. Klibanov, "Targeted delivery of gas-filled microspheres, contrast agents for ultrasound imaging," Advanced Drug Delivery Reviews, vol. 37, pp. 139-157, 1999.

[51] R. R. Patil, et al., "Engineered nanocarriers of doxorubicin: A current update," Critical Reviews in Therapeutic Drug Carrier Systems, vol. 25, pp. 1-61, 2008.

[52] A. Ghanem, et al., "Focused ultrasound-induced stimulation of microbubbles augments site-targeted engraftment of mesenchymal stem cells after acute myocardial infarction," J Mol Cell Cardiol, vol. 47, pp. 411-8, Sep 2009.

[53] T. Zenitani, et al., "Accelerating effects of ultrasonic thrombolysis with bubble liposomes," Journal of Medical Ultrasonics, vol. 35, pp. 5-10, 2008.

[54] J. H. Hwang, et al., "Vascular effects induced by combined 1-MHz ultrasound and microbubble contrast agent treatments *in vivo*," Ultrasound Med Biol, vol. 31, pp. 553-64, Apr 2005.

[55] D. Needham and M. W. Dewhirst, "The development and testing of a new temperature-sensitive drug delivery system for the treatment of solid tumors," Advanced Drug Delivery Reviews, vol. 53, pp. 285-305, 2001.

[56] D. Needham and M. W. Dewhirst, "The development and testing of a new temperature-sensitive drug delivery system for the treatment of solid tumors," Adv Drug Deliv Rev., vol. 53, pp. 285-305, 2001.

[57] M. L. Hauck, et al., "Phase I trial of doxorubicin-containing low temperature sensitive liposomes in spontaneous canine tumors," Clinical Cancer Research, vol. 12, pp. 4004-4010, 2006.

[58] R. Salomir, et al., "Local delivery of magnetic resonance (MR) contrast agent in kidney using thermosensitive liposomes and MR imaging-guided local hyperthermia: A feasibility study *in vivo*," J Magn Reson Imaging, vol. 22, pp. 534-540, 2005.

[59] M. Ahmed and S. N. Goldberg, "Combination radiofrequency thermal ablation and adjuvant IV liposomal doxorubicin increases tissue coagulation and intratumoural drug accumulation," Int J Hyperthermia, vol. 20, pp. 781-802, 2004.

[60] P. R. Patel, et al., "*In vitro* and *in vivo* evaluations of increased effective beam width for heat deposition using a split focus high intensity ultrasound (HIFU) transducer," Int J Hyperthermia, vol. 24, pp. 537-549, 2008.

[61] C. Mannaris, et al., "*In vitro* localized release of thermosensitive liposomes with ultrasound-induced hyperthermia," Ultrasound Med Biol, vol. 39, pp. 2011-20, Nov 2013.

[62] C. J. Diederich and K. Hynynen, "Ultrasound technology for hyperthermia," Ultrasound Med Biol, vol. 25, pp. 871-887, 1999.

[63] C. Mougenot, et al., "Quantification of near-field heating during volumetric MR-HIFU ablation," Medical Physics, vol. 38, pp. 272-282, 2011.

[64] M. de Smet, et al., "Temperature-sensitive liposomes for doxorubicin delivery under MRI guidance," J Control Release, vol. 143, pp. 120-7, Apr 2 2010.

[65] C. D. Landon, et al., "Nanoscale drug delivery and hyperthermia: The materials design and preclinical and clinical testing of low temperature-sensitive liposomes used in combination with mild hyperthermia in the treatment of local cancer," Open Nanomedicine Journal, vol. 3, pp. 38-64, 2011.

[66] R. Deckers and C. T. Moonen, "Ultrasound triggered, image guided, local drug delivery," J Control Release, vol. 148, pp. 25-33, Nov 20 2010.

[67] D. L. Miller and J. Quddus, "Sonoporation of monolayer cells by diagnostic ultrasound activation of contrast-agent gas bodies," Ultrasound in Medicine and Biology, vol. 26, pp. 661-667, 2000.

[68] S. Mehier-Humbert, et al., "Ultrasound-mediated gene delivery: influence of contrast agent on transfection," Bioconjug Chem, vol. 18, pp. 652-62, May-Jun 2007.

[69] F. Xie, et al., "Diagnostic ultrasound combined with glycoprotein IIb/IIIa-targeted microbubbles improves microvascular recovery after acute coronary thrombotic occlusions," Circulation, vol. 119, pp. 1378-1385, 2009.

[70] K. F. Bing, et al., "Blood-Brain Barrier (BBB) Disruption Using a Diagnostic Ultrasound Scanner and Definity® in Mice," Ultrasound in Medicine and Biology, vol. 35, pp. 1298-1308, 2009.

[71] S. Kotopoulis, et al., "Treatment of human pancreatic cancer using combined ultrasound, microbubbles, and gemcitabine: A clinical case study," Med Phys, vol. 40, p. 072902, Jul 2013.

[72] V. Sboros, et al., "Understanding the limitations of ultrasonic backscatter measurements from microbubble populations," Phys Med Biol, vol. 47, pp. 4287-99, Dec 7 2002.

[73] M. Lampaskis and M. Averkiou, "Investigation of the relationship of nonlinear backscattered ultrasound intensity with microbubble concentration at low MI," Ultrasound Med Biol, vol. 36, pp. 306-12, Feb 2010.

[74] T. P. Gauthier, et al., "Perfusion quantification using dynamic contrast-enhanced ultrasound: the impact of dynamic range and gain on time-intensity curves," Ultrasonics, vol. 51, pp. 102-6, Jan 2011.

[75] N. de Jong, "Mechanical index," Eur J Echocardiogr, vol. 3, pp. 73-4, Mar 2002.

[76] H. H. Pennes, "Analysis of tissue and arterial blood temperatures in the resting human forearm," J Appl Physiol, vol. 1, pp. 93-122, Aug 1948.

[77] B. Geers, et al., "Self-assembled liposome-loaded microbubbles: The missing link for safe and efficient ultrasound triggered drug-delivery," J Control Release, vol. 152, pp. 249-56, Jun 10 2011.

2

Investigation of microbubble response to long pulses used in ultrasound-enhanced drug delivery

In current drug delivery approaches microbubbles and drugs can be co-administered while high intensity ultrasound is applied. The mechanism of microbubble interaction with ultrasound, the drug and the cells is not fully understood. The aim of this study was to investigate microbubble response to long ultrasonic pulses used in drug delivery approaches. Two different *in vitro* setups were considered: with the microbubbles suspended in an enclosure; and with the microbubbles flowing in a capillary tube. Acoustic streaming, which influences the observed bubble response, was observed in "typical" drug delivery conditions in the first setup. With the capillary setup streaming was eliminated and accurate bubble responses were recorded. At low nondestructive pressures microbubbles can oscillate for thousands of cycles repeatedly. At high pressures all bubble activity disappeared within about 100 μs despite the length of the pulse, mainly due to violent bubble destruction and subsequent accelerated diffusion. The diffraction pattern of the source greatly influences the bubble response and in different locations of the field different bubble responses are observed.

Published as: C. Mannaris and M. A. Averkiou, "Investigation of microbubble response to long pulses used in ultrasound-enhanced drug delivery," *Ultrasound in Medicine & Biology,* vol. 38, pp. 681-691, 2012/04/2012

2.1 Introduction

The use of ultrasound energy as a therapeutic tool has long been used in physiotherapy [1] and lithotripsy [2] and more recently in tumor ablation [3, 4]. Microbubbles as ultrasound contrast agents were first introduced in echocardiography when Gramiah and Shah [5] used agitated saline to improve aortic delineation. Today, contrast agents are widely used in ultrasound imaging especially in cardiology for the assessment of myocardial perfusion, in oncology for the detection and characterization of tumors [6-9], as well as in molecular imaging [10] where molecular events *in vivo* can now be imaged non-invasively with targeted microbubbles.

In the last few years, there has been an increased interest in the research community in the use of microbubbles as cavitation nuclei and/or drug carriers in order to enhance therapeutic effects. Gene and DNA transfection [11-14], triggered protein deposition [15], thrombolysis [16], tissue ablation, histotripsy [17] and targeted drug delivery [18-22], are only a few of the applications where acoustically driven microbubbles are used. A common goal in all therapeutic applications is to improve the efficacy of the drug delivery in the region of interest while at the same time reducing undesired side effects such as toxicity in the surrounding tissue. Current drug delivery techniques at the pre-clinical stage suffer from low effectiveness and are limited by side effects mainly due to the inefficiency of the drug to pass the barriers of blood vessels (extravasation) and cell membranes (drug uptake).

When microbubbles are exposed to an ultrasound field, the amplitude of the applied ultrasound affects the behavior of the microbubbles. At a very low Mechanical Index, MI < 0.05, the microbubbles undergo almost symmetric oscillations in a linear manner with the driving acoustic pressure and scatter ultrasound at the same frequency as the transmitted frequency. As the pressure increases (0.05 > MI > 0.1), the expansion of the microbubbles during the rarefaction part of the cycle becomes larger than the corresponding compression during positive pressure thus leading to non-linear oscillations and the onset of non-linear scattering. The backscattered ultrasound contains harmonics, sub-harmonics and ultraharmonics which are being utilized in harmonic imaging methods like pulse inversion [23, 24] and power modulation [25, 26]. At even higher acoustic pressures (MI > 0.5), the microbubbles undergo forced compression and expansion which lead to violent destruction of the microbubbles and inertial cavitation [27-29]. During inertial cavitation, large localized increases in stress are observed as well as high velocity jets often termed as micro-streaming [30, 31]. It has been shown, both *in vitro* and *in vivo*, that ultrasound in

the presence of microbubbles can lead to enhanced extravasation as well as increased drug uptake by cells, a process known as sonoporation [32-40]. It is suggested that acoustic cavitation plays a major role in both extravasation and sonoporation. Other ultrasound related bio-effects such acoustic radiation force and acoustic streaming have also been proposed as a mechanism to enhance the delivery of therapeutic substances [41, 42].

When an ultrasonic wave is incident on a contrast agent microbubble, nonlinear oscillation of the microbubble occurs as well as a net pressure gradient across its diameter. This pressure gradient and nonlinear oscillation interaction gives rise to primary acoustic radiation force causing the microbubble to move in the direction of the wave propagation [42, 43]. Acoustic streaming has been studied by many researchers [44-47] and it refers to the transfer of momentum from the acoustic wave to the propagating medium due to attenuation [48, 49]. As a result, there's movement of fluid in the direction of propagation of the ultrasound. Acoustic streaming has been considered as an adjunct diagnostic tool [50, 51] but as we will see in this work it may also present a hindering factor during experiments of interrogating microbubble contrast agents and trying to understand their response to ultrasound.

Ultrasound can be focused to regions inside the body and it thus becomes a noninvasive therapy tool. This together with the enhanced extravasation and cell uptake observed with cavitating microbubbles offers great potential in improving the efficacy of current drug delivery applications whilst reducing undesired side effects. In current drug delivery approaches microbubbles and drugs can be co-administered intravenously while high intensity ultrasound is applied [19]. Novel agents are also being developed where drugs are loaded either on the shell or encapsulated within the lumen of the microbubbles [19]. Diagnostic ultrasound may be used to track drug-loaded bubbles during circulation and once at the desired location, high intensity ultrasound may be used to destroy the microbubbles and deliver the drug load on a specific site.

Despite the vast amount of research however, the exact mechanism of microbubble interaction with ultrasound the drug and the cells is not clearly understood and in a lot of cases, the optimal ultrasound conditions referenced are simply a case of trial and error. There are reports where the microbubbles are subjected to ultrasonic pulses ranging from a few cycles [13, 52] up to tens of thousands of cycles [53] or even continuous wave excitations [54]. The pressures used also vary greatly from a few kilopascals up to 9 MPa [17, 55]. Furthermore, ultrasound induced bio-effects such as localized heating, acoustic radiation force and acoustic streaming are seldom taken into consideration many times resulting in erroneous results.

A better understanding of microbubble response to long ultrasonic pulses used in therapeutic applications is important for the realization of these promising drug delivery and therapeutic applications. In this work, we present an *in vitro* experimental method developed to examine the response of microbubbles using two *in vitro* setups: (a) with the microbubbles suspended in a large enclosure of deionized water; and (b) with the microbubbles enclosed in a capillary. A wide range of ultrasonic pulse settings was considered in our experiments where the amplitude was varied between MIs of 0.05 to 1.5, the pulse duration from 10 to 20000 cycles and the pulse repetition frequency (PRF) from 50 Hz to 1.0 KHz in an attempt to better understand the interactions of microbubbles with ultrasound which would be the first step towards finding the optimal conditions for drug delivery. The question whether a microbubble would continue to oscillate for the full duration of a driving pulse (at a destructive MI) or completely get destroyed before the end of the pulse is addressed.

2.2 Materials and methods

2.2.1 Ultrasonic enclosure

An ultrasonic enclosure was designed to accommodate a transmitter-receiver system consisting of two circular single element transducers (Panametrics-NDT, Waltham, Massachusetts, USA) placed confocally with respect to each other. A schematic of the enclosure is shown in Figure 2-1. Care was taken during the design of the enclosure for the foci of the transducers to be accurately placed at the same spot.

The accuracy of the design was verified using a 0.5 mm needle hydrophone by Precision Acoustics (Dorchester, UK) that was placed at the intersecting foci of the transducers. Any misalignment discrepancies were less than 10% in terms of the maximum pressure amplitude at the confocal region. The transmitter was a 1.0 MHz focused single element transducer (Panametrics V392) with a diameter of 38.1 mm and focal length of 76.2 mm (focusing gain = 10.07). A 2.25 MHz focused transducer (Panametrics C304) of 25.4 mm diameter and 50.8 mm focal length (focusing gain = 15.10) was used as a receiver. The center frequency of the receiving transducer was chosen to be at 2.25 MHz in order to accommodate the 2^{nd} harmonic response (2.0 MHz) from the interrogated microbubbles. The walls of the enclosure were lined with a 10 mm acoustic absorbing material (Aptflex F28, Precision Acoustics, Dorchester, UK), to minimize reflections and contamination of the scattered signal from microbubbles.

The microbubbles were interrogated in the enclosure in two different ways. In the first set-up the microbubbles were freely suspended, i.e., the enclosure was filled with a low concentration of microbubbles diluted in deionized water. In the second set-up, a 200 μm acoustically transparent cellulose capillary taken from a dialysis cartridge (Gambro, Cambridgeshire, UK) was carefully placed at the overlapping foci of the two transducers. The capillary was attached on a 28G Microfil syringe needle (World Precision Instruments, Sarasota, Florida, USA) which was then connected to a gravity feed reservoir via luer lock. The microbubbles were injected into the reservoir and were allowed to flow through the capillary into the detection area. Before each ultrasound exposure, the flow was stopped for the bubbles to remain still inside the capillary. A 3-axis micro-positioning system (Newport, Irvine, California) was used to align the capillary with the two confocal transducers. This capillary setup was designed to better imitate *in vivo* conditions of microbubbles flowing in the microcirculation. The effective "detection area" of this setup, the area from which a response from a microbubble can be detected, is assumed to be the region where the beam widths (defined by the -6 dB points) of the transmitter and receiver (4 and 2 mm respectively) overlap.

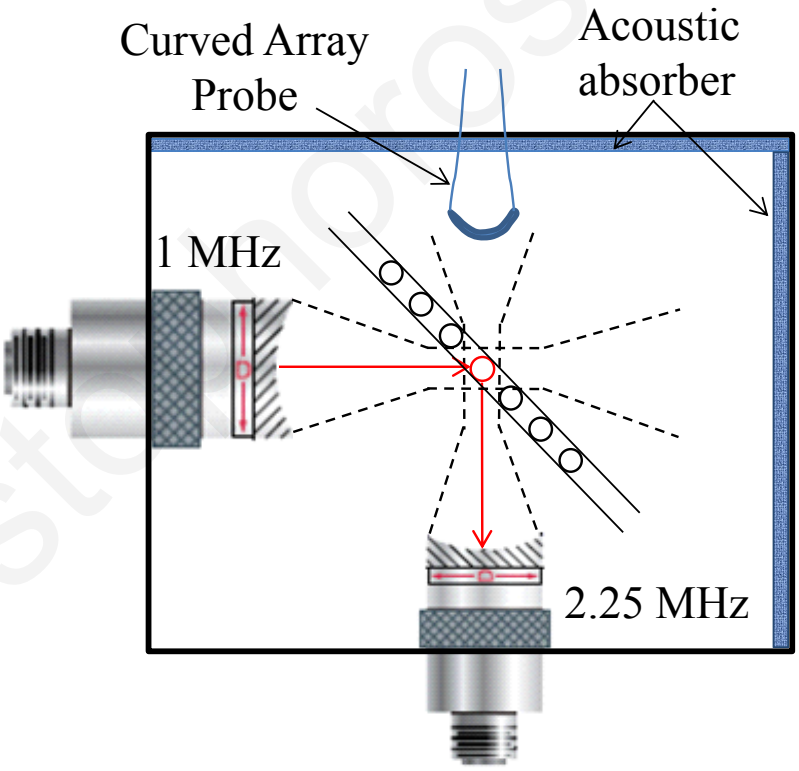

Figure 2-1: Schematic of ultrasonic enclosure accommodating the transmitting and receiving single element transducers and a 200 μm cellulose capillary. Diagnostic ultrasound is used for imaging of the bubble flow.

2.2.2 Instrumentation

Figure 2-2 shows a block diagram of the experimental set-up. A 2-channel, 1 mHz-100 MHz, 14-bit resolution and 1 GS/s sampling rate arbitrary function generator model AFG 3102 (Tektronix, Beaverton, Oregon, USA) was used to generate the signal which was amplified by a radio-frequency power amplifier model AR150A100B (Amplifier Research, Pennsylvania, USA). The self-contained, broadband (150 Watt CW, 0.01-100 MHz) amplifier provided a minimum gain of 52 dB. The pressure amplitude of the transmitted pulses was previously measured with a 0.4 mm element membrane hydrophone (Precision Acoustics Ltd, Dorchester, UK) that offers a flat (±2 dB) frequency response over the range 1-30MHz. The microbubble response was passively captured with the receiver (C304) and digitized by a 500 MHz bandwidth, 20 GS/s sampling rate, digital oscilloscope, DPO 7054 (Tektronix, Beaverton, Oregon, USA). A minimum sampling frequency of 50 MHz was used for digital to analog conversion throughout this work. Finally, the acquired data was transferred to a PC for analysis via a GPIB-USB-HS interface (National Instruments, Austin, Texas, USA).

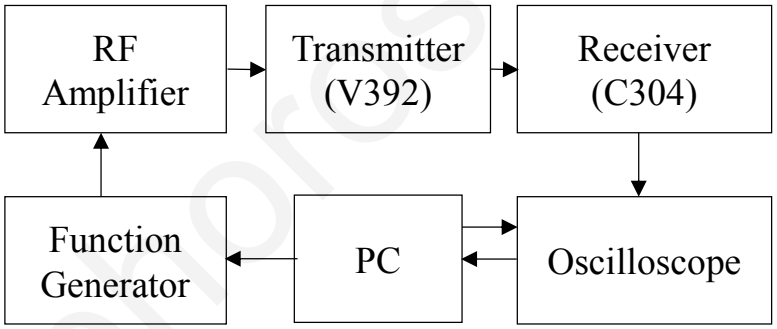

Figure 2-2: Block diagram of the experimental setup

2.2.3 Contrast Agent

SonoVue and BR14 microbubble contrast agents (Bracco, Geneva, Switzerland) were used throughout this work. The agent solutions in our experiments were prepared according to the manufacturer's recommendations. In the suspended microbubbles setup a dilute concentrations (0.005‰ – 0.04‰, which correspond to roughly 1-8 bubbles/μL, and the interrogation volume is 16 μL) were used. These concentrations lie in the low end of the linear range of the relation of intensity versus concentration [56], and are expected to be similar with what is found in the microcirculation of typical *in vivo* scenarios. Before each ultrasound firing, the solution was "softly" stirred and allowed to settle, enough for

the bubbles to stop moving but not float. Slightly higher concentrations were also used in the capillary setup (0.005‰ – 0.2‰). The microbubble solution was placed in a gravity fed reservoir. As mentioned earlier, before ultrasound exposure, the flow was stopped. Both set-ups described above were also observed with diagnostic ultrasound imaging.

2.2.4 Imaging

In all the experiments, a Philips iU22 Ultrasound Scanner (Phillips Ultrasound, Bothell, WA, USA) was used for the imaging of the microbubbles. The ultrasound probe used for imaging was a C8-4v broadband curved array transducer, normally used in obstetrics for intracavity clinical exams. Its thin long shape and wide field of view was convenient for placement inside the ultrasonic enclosure and enabled accurate depiction of the area interrogated by ultrasound (the therapy pulses) in both the open enclosure and the capillary set-up. The imaging frequency was 4-8 MHz and the MI was set to 0.03 to ensure no bubble destruction. Imaging was used to verify both the presence and concentration of the microbubbles and avoid errors such as large air bubbles passing through and clogging of the microtube. During the application of the therapeutic ultrasound the diagnostic ultrasound system was placed in "freeze" (not scanning) to avoid any interference of the imaging pulse with the experiments. Figure 2-3(a) shows a contrast image of the suspended microbubbles in the enclosure before an ultrasound firing. The corresponding image shortly after the therapy pulse was fired (10 cycles, MI 0.9) is shown in Figure 2-3(b). Figures 2-3(c) and (d) show the microbubble-filled capillary before and after an ultrasound firing respectively. The area where the bubbles are destroyed can be clearly seen in both setups [Figs. 2-3(b) and (d)]. When the bubble concentration dropped, it was easily observed from the image and a new solution was prepared. It is noted that a higher concentration of microbubbles was used in these images for demonstration purposes.

2.2.5 Ultrasound exposure conditions

A typical ultrasound firing consisted of a series of tone bursts (pulses). The number of cycles used was varied from 10 to 20000. The amplitude of the pulses spanned a range of MI of 0.05 to 1.5. The pulse repetition frequency (PRF) was varied between 50 to 1000 Hz. The pulses were fired repeatedly in order to study the bubble destruction over time. For all experiments, the center frequency of the pulses used was 1.0 MHz since this is the frequency that is used in many published drug delivery publications.

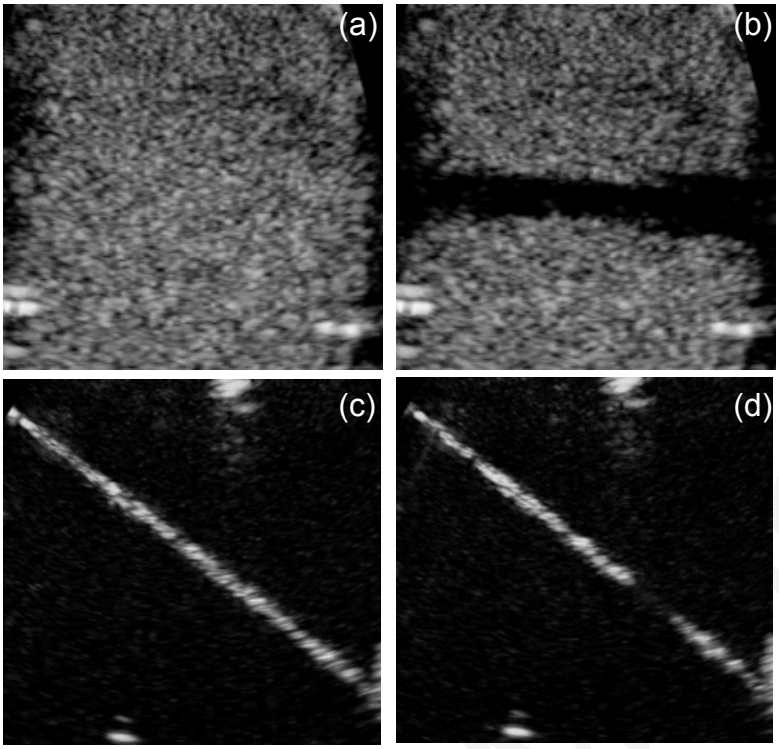

Figure 2-3: Ultrasound images showing microbubbles; (a) in suspension before excitation, (b) in suspension after excitation, (c) in the capillary before excitation, (d) in the capillary after excitation. Power modulation nonlinear imaging is used. Destruction area (due to the therapy pulses) is clearly seen

2.3 Results

2.3.1 Microbubbles suspended in open enclosure

The response of the microbubbles (a solution with concentration 0.005‰) to a series of 1 MHz, 10-cycle tone bursts spaced 20 ms apart (PRF = 100 Hz) is shown in Figure 2-4. Scattered pulses from microbubbles at MIs 0.1, 0.2 and 0.4 are shown in Figure 2-4(a)-(c), respectively. The horizontal axis is time in milliseconds and the vertical axis is the scattered pressure in kPa. It is noted that every condition was repeated 50 times and the experiment was done for concentrations 0.005, 0.02, and 0.04 ‰. Table 2-1 shows the mean and standard deviation of the RMS value of the scattered pressure. The waveforms shown in Fig. 2-4 (a)-(c) are chosen to have amplitude close to the mean value. The spectra of the waveforms are shown in Fig. 2-4 (d)-(f). In Fig. 2-4 (g)-(i) the reduction in normalized amplitude (with respect to the maximum value) as a function of time (after repeated sonifications with 100 Hz PRF) is shown. At MI 0.1, the normalized amplitude of the scattered pressure stays close to 1 suggesting that the microbubbles remained intact after all ultrasound firings. At MI 0.2, there's a gradual decrease in amplitude of the response, suggesting disruption of the microbubbles and slow diffusion of the gas. Finally

at MI 0.4, there is even faster decay of the amplitude suggesting that the microbubbles are destroyed after only a few firings. It is also noted that the spectra of MI=0.2 and MI=0.4 [Fig. 2-4 (e) – (d)] show a broadening associated with bubble destruction and as expected this broadening is highest at the highest MI.

Table 2-1: Mean and standard deviation of the RMS amplitude of the scattered pressure from microbubbles suspended in the open enclosure (Statistics out of 50 samples). C= 0.005‰

MI	RMS scattered pressure (kPa)	σ (kPa)
0.1	0.22	0.07
0.2	0.43	0.15
0.4	1.17	0.36

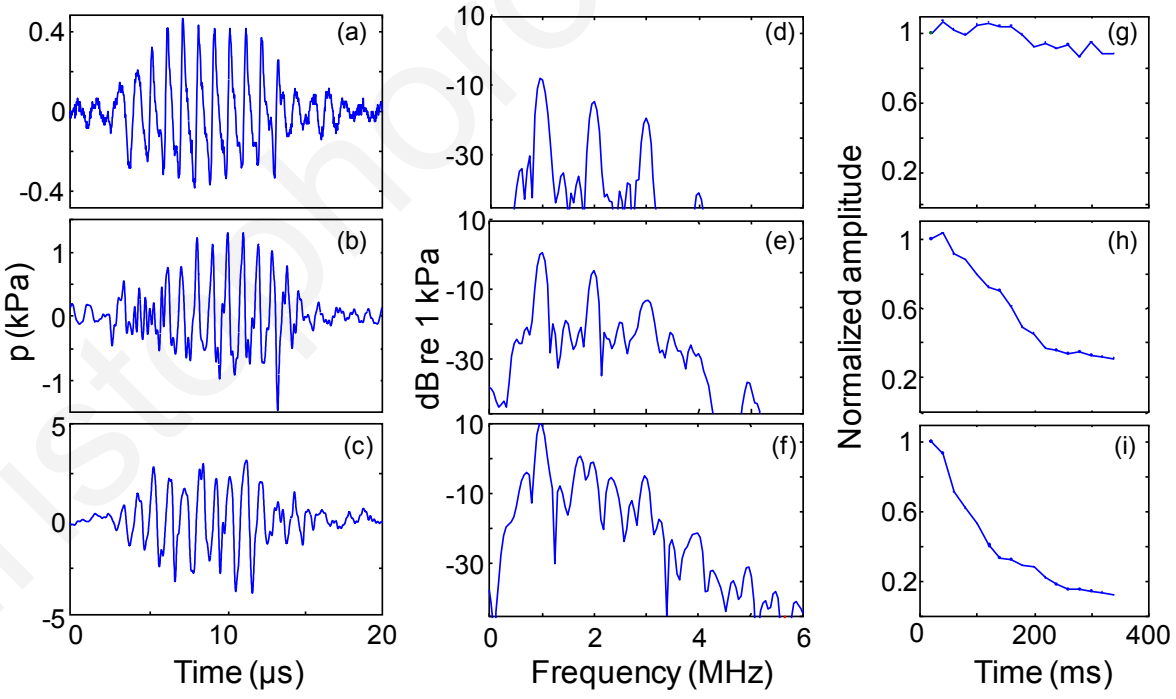

Figure 2-4: Scattered ultrasound pulses (1 MHz, 10 cycles) from microbubbles diluted in the open enclosure at, MI=0.1 (a), MI=0.2 (b), and MI=0.4(c) and their corresponding spectra (d)-(e). Normalized amplitude as a function of time (after repeated sonifications with 100 Hz PRF) for MI = 0.1(g), 0.2(h) and 0.4(i).

Longer pulses (100-20000) over a range of acoustic amplitudes were also considered. However, with very long pulses it was not possible to study the response of microbubbles with our set-up as they moved away from the interrogation region (confocal area) due to acoustic streaming [Tjotta [57]; Starrit et al. [58]]. The presence of acoustic streaming in the microbubble solution was confirmed with ultrasound imaging where video loops of moving microbubbles during the excitations have been recorded. Table 2-2 summarizes the pressures at which streaming was first observed for 10, 80, 500 and 2000 cycles. As expected, the observed onset of streaming as a function of input pressure is inversely proportional to the pulse duration (number of cycles) and ultimately duty cycle. Calculation of the spatial average intensity and predicted velocities according to the work of Tjotta [57] for the given parameters are also shown in Table 2-2. We observe that for 80, 500 and 2000 cycles, the calculated intensities and velocities where streaming was first detected are very similar. For 10 cycles however we observe that the resulting intensity and expected velocity is higher but nevertheless streaming is not detected. One explanation is that at such high MI any microbubbles that lie in the acoustic field are destroyed and we are unable to visualize them.

Table 2-2: Onset of observed acoustic streaming and its dependence on MI and the number of cycles at PRF = 50 Hz. Calculated spatial average intensities and predicted velocities are also shown.

# of cycles	Streaming Threshold	Spatial Average intensity (mW/cm^2)	Calculated Streaming velocity ($mm\ s^{-1}$)
10	Not detected (up to MI 1.1)	20.21	0.114
80	0.2	5.34	0.030
500	0.1	8.35	0.047
2000	< 0.05	8.35	0.047

2.3.2 Microbubbles in capillary

The second setup used in this work was designed to better mimic *in vivo* conditions and specifically flow in a capillary vessel. The microbubbles were allowed to flow through a 200 μm diameter capillary tube rather than being freely suspended in water. As confirmed with our results and ultrasound imaging, streaming was completely eliminated.

Figure 2-5 shows scattered pulses (200-cycle tone bursts spaced 10 ms apart) from microbubbles, at a concentration of 0.2‰. Scale breaks in the x-axis are used for better visualization of the individual pulses. MIs of 0.1, 0.2 and 0.4 are shown in Figure 2-5(a)-(c) respectively. In a similar fashion to the freely suspended bubbles, we observe that MI 0.1 is non-destructive (intensity remains constant with time), MI 0.2 is destructive (intensity gradually decreases), and MI 0.4 and above is highly destructive (bubble disappears before the end of the 1st pulse). Further increase in pressure does not produce any difference in the destruction pattern other than the expected increase in the amplitude of the scattered echo. Two segments of the 1st pulse are selected [dotted rectangles in Fig. 2-5(c)] for further analysis. A Blackman-Harris window is applied to the selected segments in order to limit leakage in the frequency spectra. The time waveform and frequency spectrum of the first segment are shown in Figures 2-6(a) and (b), respectively whereas the time domain and spectrum of the 2nd segment are shown in Figure 2-6(c) and (d). The dramatic reduction of higher harmonics in Figure 2-6(d) indicates that the microbubbles have been destroyed (the remaining signal is the linear scattering from the capillary itself). Results for longer tone bursts follow similar trends where at MIs > 0.4 all bubble activity disappears within about 100 cycles or 100 μs.

Figure 2-7(a)-(c) shows scattered pulses from microbubbles using 200, 1000 and 2000-cycle pulses at an MI of 0.4. At this MI the microbubbles are destroyed by the first pulse and the gas diffuses in the liquid before the second pulse arrives. As a matter of fact, for excitations greater than 100 cycles the microbubbles are always destroyed and diffused with the first pulse, independent of the pulse length.

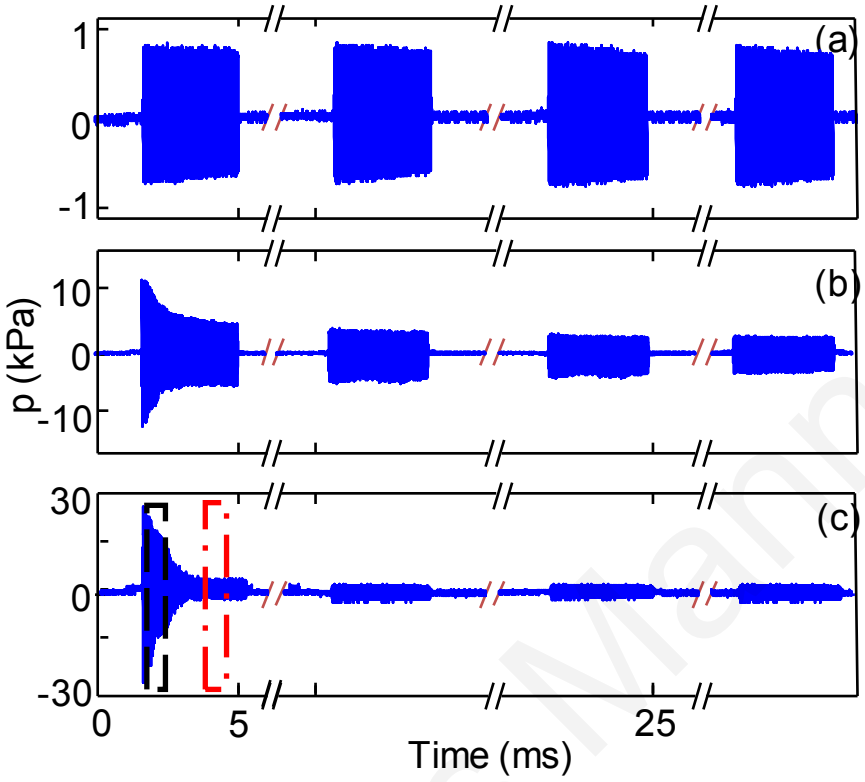

Figure 2-5: Scattered ultrasound pulses (200 cycles, PRF=100 Hz) from microbubbles in a capillary, for MI = 0.1(a), 0.2(b), and 0.4(c).

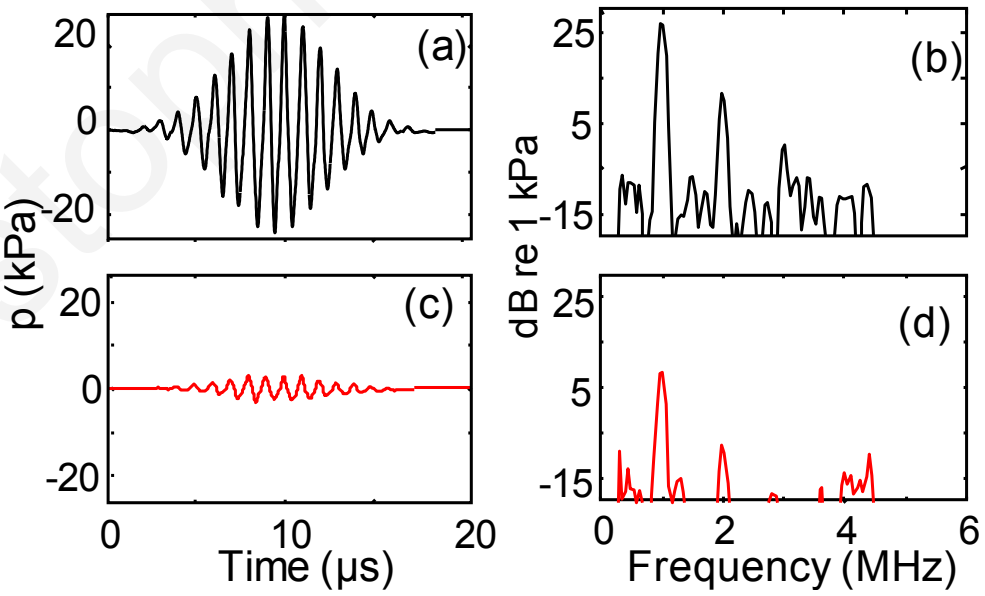

Figure 2-6: (a) time waveform and (b) spectrum of 1st selected region of pulse at MI 0.4 [shown in fig 2-5(c)]. (c) time waveform and (d) spectrum of 2nd selected region.

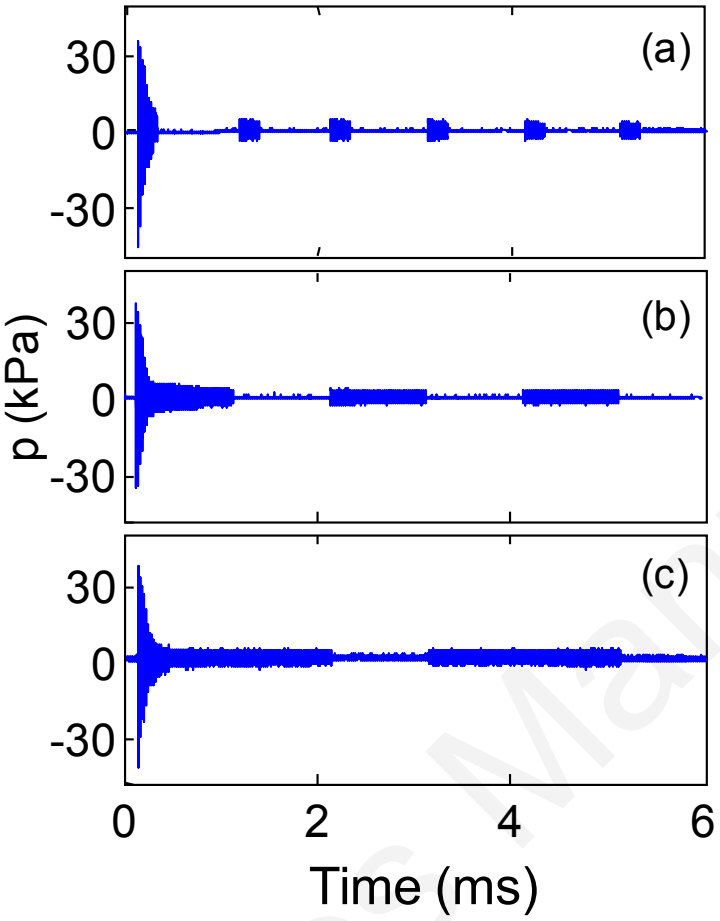

Figure 2-7: Pulses scattered from microbubbles in the capillary set-up. (a) 200 cycles, MI 0.4; (b) 1000 cycles, MI 0.4; and (c) 2000 cycles, MI 0.4.

2.4 Discussion

The response of contrast agent microbubbles to long of ultrasonic pulses similar to the ones used in therapeutic applications has been studied in two different experimental setups: (a) with the microbubbles suspended in a large enclosure of deionized water and (b) with the microbubbles enclosed in a capillary. It has been shown that acoustic streaming generated by the ultrasound in microbubble suspensions induces bubble movement and does not allow for the study of bubble response to long pulses. Experimental setups similar to the one described here where the microbubbles are freely suspended in a medium (even in the case where microbubbles are placed in OptiCell™-like enclosures) probably experience acoustic streaming with the consequences described above.

While acoustic radiation force may be present in capillaries and the microcirculation, [42, 43] it is generally accepted that acoustic streaming is not a factor in small vessels. Enclosing the microbubbles in a cellulose capillary tube eliminates acoustic

streaming and allows a more accurate observation and measurement of the bubble response, while at the same time closely resembles the *in vivo* scenario of microbubbles in the microcirculation. At MIs greater than 0.4, the microbubbles were destroyed and no response was detected after about 100 cycles or 100 μs (at 1 MHz) irrespective of the pulse length. Figure 2-8(a) shows the response to a 200 cycle burst at MI 0.4 and Figure 2-8(c) shows the response to a 1000 cycle burst at the same MI. The first 100 μs of each response are isolated and shown in Figures 2-8(b) and (d), respectively. The destruction pattern followed is nearly identical in both cases. Published reports of drug delivery suggest that pulses with thousands of cycles are more effective in delivering the drugs [53]. A question is being raised whether the enhanced drug delivery seen with longer ultrasound pulses at such high pressures is related to the microbubble response or whether other biological factors play an important role.

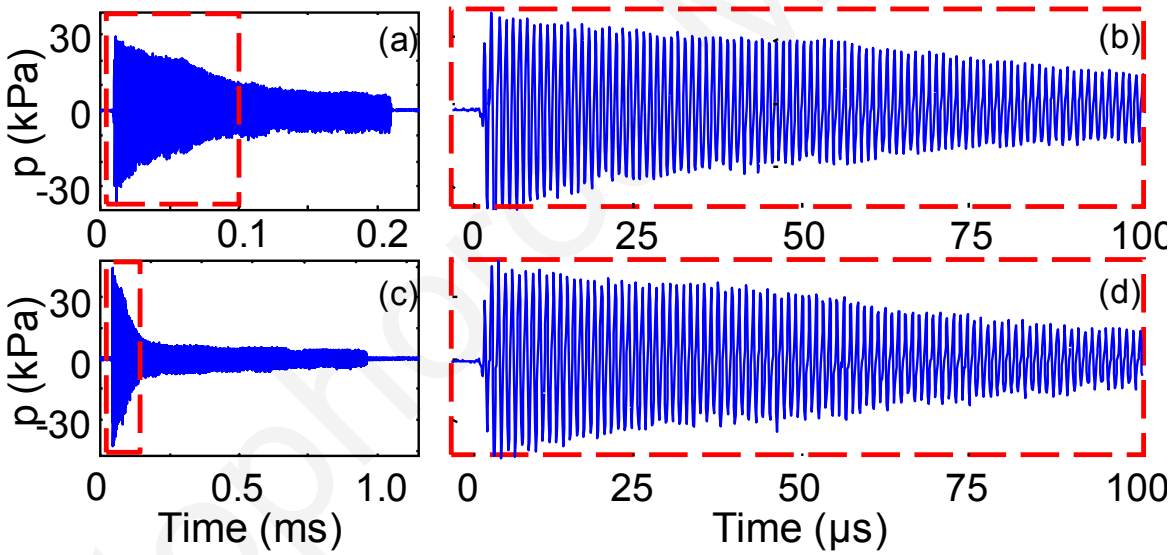

Figure 2-8: Pulses scattered from microbubbles in the capillary set-up. (a) 200 cycle pulse at MI 0.4; (c) 1000 cycle pulse at MI 0.4. (b), (d) Isolation of the first 100 μs of the 30 pulses shown in (a) and (c), respectively. The destruction pattern followed is nearly identical in (b) and (d)

The bubble concentration in the experiments was very carefully controlled and concentrations that are expected to be found *in vivo* in the capillary bed were used. The concentrations were 0.005<C<0.2‰ and they were all in the linear range of intensity versus concentration curve [56] to ensure that acoustic shadowing was not present. Despite the fact that we have not used a mechanical filter to select a certain bubble population (e.g. less than 3 microns) it is assumed that the bubbles that responded to the ultrasound pulses were in the range 1-10 microns as any smaller or larger bubbles would be far away from resonance at the driving frequency.

An important factor often overlooked in drug delivery applications is the detailed shape (diffraction pattern) of the focused sound field. The field varies in amplitude and different bubbles in the field experience a different acoustic pressure. In Figure 2-9 we show the calculated field of the focused source used in our experiments. In Figure 2-9(a) the central axial plane is shown and in (b) the focal plane. The contours were drawn so that the following four MI ranges were shown: 0-0.05, 0.05-0.1, 0.1-0.2, 0.2-0.5, and 0.5-1.0. Thus, some bubbles undergo stable (non-destructive) oscillation and some are violently destroyed. For example the bubbles in the red area of the contour plot are eliminated in 75-100 cycles (as discussed above) whereas the bubbles in the grey area are undergoing stable oscillations, and the ones in the white areas are possibly not excited at all.

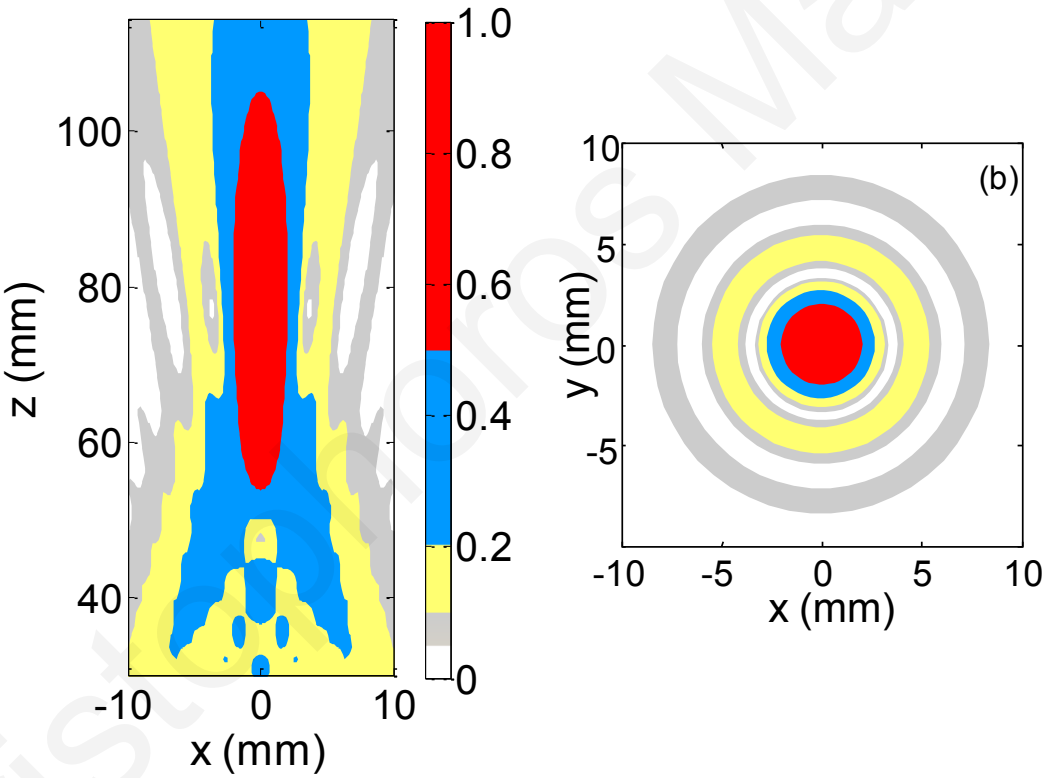

Figure 2-9: Contour plots of the MI of (a) the axial plane and (b) focal plane of the transmitter. The red area is 0.5<MI<1, the blue area is 0.2<MI<0.5, the yellow area is 0.1<MI<0.2, the gray area is 0.05<MI<0.1 and white denotes MI's less than 0.05.

Another consideration for very long pulses intended for drug delivery applications is the possibility for ultrasound induced heating. For example, when 1 MHz continuous wave ultrasound with 0.5 MPa amplitude is used a temperature rise of 2 degrees Celsius would be expected in tissue within 3 seconds. In the case of pulsed excitation, when a single 20,000-cycle pulse of 2 MPa is used a temperature rise of 0.2 degrees would result in tissue. Repeated sonications would result in further temperature rise. The center

frequency of the pulses investigated in this work was kept constant at 1.0 MHz. In the future we are planning to investigate the effect of frequency when long ultrasonic pulses such as the ones used in therapeutic applications are used.

Based on the observed bubble behavior two options for drug delivery are suggested that must be confirmed with *in vivo* experiments: (a) a long pulse (100-1000 cycles) at low amplitude, MI<0.1 for a prolonged stable nonlinear oscillation; and (b) a 100 cycle pulse at high amplitude, MI>0.4, for a destructive highly nonlinear oscillation. Longer than 100 cycles pulses at high amplitude do not produce any added benefit in terms of the bubble oscillation. However, it is possible that the longer high amplitude ultrasound pulses have an effect on the cell membrane permeability and it must be further investigated.

2.5 Conclusion

Acoustic streaming influences experimental setups where microbubbles are freely suspended and allowed to move around. Enclosing the microbubbles in a capillary eliminated streaming and accurate results of bubble oscillations to very long ultrasound pulses were obtained. The diffraction pattern of a focused source can greatly influence bubble oscillations and must be considered when designing acoustic conditions for ultrasound-enhanced drug delivery. It is possible to repeatedly oscillate a microbubble for 1000's of cycles at MI<0.1. At higher pressures (MI > 0.4) all bubble activity disappears within about100 cycles despite the length of the excitation pulse, mainly due to gas diffusion.

Acknowledgements

This project was funded by the EU Project SONODRUGS (NMP4-LA-2008-213706).
The authors would like to thank Prof. Nico de Jong and Dr. Marcel Bohmer for valuable technical discussions and Bracco Siusse SA for supplying SonoVue and BR14.

References

[1] R. W. Wood and A. L. Loomis, "The physical and biological effects of high frequency sound waves of great intensity," Philosophical Magazine, vol. 4, pp. 417–436, 1927.

[2] C. C. Church, "A theoretical study of cavitation generated by an extracorporeal shock wave lithotripter," Journal of the Acoustical Society of America, vol. 86, pp. 215-27, Jul 1989.

[3] T. Yu, et al., "A review of research into the uses of low level ultrasound in cancer therapy," Ultrason Sonochem, vol. 11, pp. 95-103, Apr 2004.

[4] J. E. Kennedy, et al., "High-intensity focused ultrasound for the treatment of liver tumours," Ultrasonics, vol. 42, pp. 931-5, Apr 2004.

[5] R. Gramiak and P. M. Shah, "Echocardiography of the aortic root," Invest Radiol, vol. 3, pp. 356-66, Sep-Oct 1968.

[6] M. Bruce, et al., "Vascular flow and perfusion imaging with ultrasound contrast agents," Ultrasound Med Biol, vol. 30, pp. 735-43, Jun 2004.

[7] S. R. Wilson and P. N. Burns, "Liver mass evaluation with ultrasound: the impact of microbubble contrast agents and pulse inversion imaging," Semin Liver Dis, vol. 21, pp. 147-59, May 2001.

[8] E. Leen, et al., "Potential role of doppler perfusion index in selection of patients with colorectal cancer for adjuvant chemotherapy," Lancet, vol. 355, pp. 34-37, 2000/01/01/ 2000.

[9] E. Quaia, et al., "Comparison of visual and quantitative analysis for characterization of insonated liver tumors after microbubble contrast injection," AJR Am J Roentgenol, vol. 186, pp. 1560-70, Jun 2006.

[10] J. R. Lindner, "Microbubbles in medical imaging: current applications and future directions," Nat Rev Drug Discov, vol. 3, pp. 527-32, Jun 2004.

[11] P. A. Dijkmans, et al., "Microbubbles and ultrasound: from diagnosis to therapy," Eur J Echocardiogr, vol. 5, pp. 245-56, Aug 2004.

[12] S. Mehier-Humbert, et al., "Ultrasound-mediated gene delivery: influence of contrast agent on transfection," Bioconjug Chem, vol. 18, pp. 652-62, May-Jun 2007.

[13] A. A. Rahim, et al., "Spatial and acoustic pressure dependence of microbubble-mediated gene delivery targeted using focused ultrasound," J Gene Med, vol. 8, pp. 1347-57, Nov 2006.

[14] R. E. Vandenbroucke, et al., "Ultrasound assisted siRNA delivery using PEG-siPlex loaded microbubbles," Journal of Controlled Release, vol. 126, pp. 265-73, Mar 20 2008.

[15] R. Bekeredjian, et al., "Augmentation of cardiac protein delivery using ultrasound targeted microbubble destruction," Ultrasound Med Biol, vol. 31, pp. 687-91, May 2005.

[16] C. A. Molina, et al., "Microbubble administration accelerates clot lysis during continuous 2-MHz ultrasound monitoring in stroke patients treated with intravenous tissue plasminogen activator," Stroke; a Journal of Cerebral Circulation, vol. 37, pp. 425-429, 2006/02// 2006.

[17] M. R. Bohmer, et al., "Ultrasound triggered image-guided drug delivery," Eur J Radiol, vol. 70, pp. 242-53, May 2009.

[18] D. B. Ellegala, et al., "Imaging tumor angiogenesis with contrast ultrasound and microbubbles targeted to alpha(v)beta3," Circulation, vol. 108, pp. 336-41, Jul 22 2003.

[19] S. Hernot and A. L. Klibanov, "Microbubbles in ultrasound-triggered drug and gene delivery," Adv Drug Deliv Rev, vol. 60, pp. 1153-66, Jun 30 2008.

[20] A. L. Klibanov, "Microbubble contrast agents: targeted ultrasound imaging and ultrasound-assisted drug-delivery applications," Invest Radiol, vol. 41, pp. 354-62, Mar 2006.

[21] G. E. Weller, et al., "Ultrasound imaging of acute cardiac transplant rejection with microbubbles targeted to intercellular adhesion molecule-1," Circulation, vol. 108, pp. 218-24, Jul 15 2003.

[22] G. E. R. Weller, et al., "Ultrasonic imaging of tumor angiogenesis using contrast microbubbles targeted via the tumor-binding peptide arginine-arginine-leucine," Cancer Research, vol. 65, pp. 533-539, Jan 15 2005.

[23] M. A. Averkiou, et al., "Pulsing schemes for the detection of nonlinear echoes from contrast microbubbles," 9th European Symposium on Ultrasound Contrast Imaging, Jan 2004 2004.

[24] D. H. Simpson, et al., "Pulse inversion Doppler: a new method for detecting nonlinear echoes from microbubble contrast agents," IEEE Trans Ultrason Ferroelectr Freq Control, vol. 46, pp. 372-82, 1999.

[25] M. Averkiou, et al., "Ultrasound contrast imaging research," Ultrasound Q, vol. 19, pp. 27-37, Mar 2003.

[26] G. Brock-Fisher, et al., "Means for increasing sensitivity in non-linear ultrasound imaging systems," USA Patent 5,577,505, 26 Nov 1996, 1996.

[27] R. E. Appel, "Possibility of microcavitation from diagnostic ultrasound," IEEE Trans Ultrason Ferroelectr Freq Control, vol. 33, pp. 139-42, 1986.

[28] C. K. Holland and R. E. Apfel, "Thresholds for transient cavitation produced by pulsed ultrasound in a controlled nuclei environment," Journal of the Acoustical Society of America, vol. 88, pp. 2059-69, Nov 1990.

[29] W. T. Shi, et al., "Destruction of contrast microbubbles and the association with inertial cavitation," Ultrasound Med Biol, vol. 26, pp. 1009-19, Jul 2000.

[30] P. Marmottant and S. Hilgenfeldt, "Controlled vesicle deformation and lysis by single oscillating bubbles," Nature, vol. 423, pp. 153-6, May 8 2003.

[31] A. A. Doinikov and A. Bouakaz, "Acoustic microstreaming around a gas bubble," Journal of the Acoustical Society of America, vol. 127, pp. 703-9, Feb 2010.

[32] M. R. Bohmer, et al., "Focused ultrasound and microbubbles for enhanced extravasation," J Control Release, vol. 148, pp. 18-24, Nov 20 2010.

[33] K. Iwanaga, et al., "Local delivery system of cytotoxic agents to tumors by focused sonoporation," Cancer Gene Therapy, vol. 14, pp. 354-363, Apr 2007.

[34] M. Kinoshita and K. Hynynen, "Intracellular delivery of Bak BH3 peptide by microbubble-enhanced ultrasound," Pharmaceutical Research, vol. 22, pp. 716-720, May 2005.

[35] K. Kooiman, et al., "Increasing the Endothelial Layer Permeability Through Ultrasound-Activated Microbubbles," Ieee Transactions on Biomedical Engineering, vol. 57, pp. 29-32, Jan 2010.

[36] P. Li, et al., "Impact of myocardial contrast echocardiography on vascular permeability: comparison of three different contrast agents," Ultrasound Med Biol, vol. 30, pp. 83-91, Jan 2004.

[37] P. Li, et al., "Impact of myocardial contrast echocardiography on vascular permeability: an *in vivo* dose response study of delivery mode, pressure amplitude and contrast dose," Ultrasound Med Biol, vol. 29, pp. 1341-9, Sep 2003.

[38] D. M. Skyba, et al., "Direct *in vivo* visualization of intravascular destruction of microbubbles by ultrasound and its local effects on tissue," Circulation, vol. 98, pp. 290-3, Jul 28 1998.

[39] J. H. Wible, et al., "Microbubbles induce renal hemorrhage when exposed to diagnostic ultrasound in anesthetized rats," Ultrasound in Medicine and Biology, vol. 28, pp. 1535-1546, Nov-Dec 2002.

[40] A. Yudina, et al., "Evaluation of the Temporal Window for Drug Delivery Following Ultrasound-Mediated Membrane Permeability Enhancement," Mol Imaging Biol, Jun 3 2010.

[41] A. F. H. Lum, et al., "Ultrasound radiation force enables targeted deposition of model drug carriers loaded on microbubbles," Journal of Controlled Release, vol. 111, pp. 128-134, Mar 10 2006.

[42] M. J. Shortencarier, et al., "A method for radiation-force localized drug delivery using gas-filled lipospheres," Ieee Transactions on Ultrasonics Ferroelectrics and Frequency Control, vol. 51, pp. 822-831, Jul 2004.

[43] P. Dayton, et al., "Acoustic radiation force *in vivo*: A mechanism to assist targeting of microbubbles," Ultrasound in Medicine and Biology, vol. 25, pp. 1195-1201, Oct 1999.

[44] C. E. Bradley, "Acoustic streaming field structure: The influence of the radiator," Journal of the Acoustical Society of America, vol. 100, pp. 1399-1408, Sep 1996.

[45] X. G. Shi, et al., "Quantitative investigation of acoustic streaming in blood," Journal of the Acoustical Society of America, vol. 111, pp. 1110-1121, Feb 2002.

[46] G. Zauhar, et al., "Studies of acoustic streaming in biological fluids with an ultrasound Doppler technique," British Journal of Radiology, vol. 71, pp. 297-302, Mar 1998.

[47] W. Nyborg, "Acoustic streaming," in Physical acoustics. vol. 2B, W. Mason, Ed., ed New York: Academic Press, 1965, pp. 265-331.

[48] F. A. Duck, "Radiation stress and its bio-effects. European Committee for Medical Ultrasound Safety (ECMUS)," Eur J Ultrasound, vol. 11, pp. 61-4, Mar 2000.

[49] K. G. Baker, et al., "A review of therapeutic ultrasound: Biophysical effects," Physical Therapy, vol. 81, pp. 1351-1358, Jul 2001.

[50] K. R. Nightingale, et al., "A Novel Ultrasonic Technique for Differentiating Cysts from Solid Lesions - Preliminary-Results in the Breast," Ultrasound in Medicine and Biology, vol. 21, pp. 745-751, 1995.

[51] F. Duck, "Acoustic streaming and radiation pressure in diagnostic applications," in Safety of Diagnostic Ultrasound Barnett S and K. G, Eds., ed Carnforth, UK: Parthenon, 1998, pp. 87–98.

[52] A. van Wamel, et al., "Vibrating microbubbles poking individual cells: drug transfer into cells via sonoporation," Journal of Controlled Release, vol. 112, pp. 149-55, May 15 2006.

[53] A. Ghanem, et al., "Focused ultrasound-induced stimulation of microbubbles augments site-targeted engraftment of mesenchymal stem cells after acute myocardial infarction," J Mol Cell Cardiol, vol. 47, pp. 411-8, Sep 2009.

[54] T. Zenitani, et al., "Accelerating effects of ultrasonic thrombolysis with bubble liposomes," Journal of Medical Ultrasonics, vol. 35, pp. 5-10, 2008.

[55] J. H. Hwang, et al., "Vascular effects induced by combined 1-MHz ultrasound and microbubble contrast agent treatments *in vivo*," Ultrasound Med Biol, vol. 31, pp. 553-64, Apr 2005.

[56] M. Lampaskis and M. Averkiou, "Investigation of the relationship of nonlinear backscattered ultrasound intensity with microbubble concentration at low MI," Ultrasound Med Biol, vol. 36, pp. 306-12, Feb 2010.

[57] S. Tjotta, "Some non-linear effects in sound fields☆," Journal of Sound and Vibration, vol. 6, pp. 255-267, 1967.

[58] H. C. Starritt, et al., "An experimental investigation of streaming in pulsed diagnostic ultrasound beams," Ultrasound Med Biol, vol. 15, pp. 363-73, 1989.

2.6 Appendix A – Transducer Frequency Response Calibration

Single element transducers are often used as receivers due to the high sensitivity they exhibit compared to needle and membrane hydrophones. This allows detection of small signals like acoustic responses from microbubbles that may have amplitudes as low as a few Pascal. However, single element transducers also have a finite frequency response (compared to the flat frequency response of needle and membrane hydrophones) that causes underestimation of signals containing frequencies that lie away from the transducer's center frequency (e.g. 1 and 3 MHz signals are underestimated when received by a 2 MHz transducer). For accurate measurement of the scattered acoustic pressure from microbubbles, the received signals must be corrected for the transducer's frequency response.

While the manufacturer provides a frequency response curve for each transducer, this curve is obtained by a standard pulse/echo test where tone bursts are reflected off a silica target and received by the same transducer. This represents an integration of transmit and receive effects. The receive transfer function alone which is important when transducers are used as receivers is needed. In this appendix, we describe the procedure to calculate the receive transfer function of the transducer in order to correct the received echoes from microbubbles and obtain more accurate results.

The transfer function, *H(f),* of a linear time-invariant system (a transducer in our case) is defined as the relation between the input and output. As a first step, a chirp containing the frequencies 0.1-6 MHz was designed in Matlab using the following equation:

$$y = \exp[-(\frac{\omega t}{N_{cyc}\pi})^{2m}] * \sin[\omega t + \frac{(\omega t)^2}{2.8\pi N_{cyc}}] \quad \text{(A.1)}$$

where m is the envelope, N_{cyc} is the number of cycles, $\omega=2\pi f$, and f is the center frequency.

For the above chirp, m=2, N_{cyc} = 20 and f = 2 were used. A waveform according to (A.1) was transferred to the arbitrary function generator and the open circuit voltage *A(z=0,t)* or *A(t)* was measured with the oscilloscope [Figure A-1(a)]. The Fourier transform of *A(t)* was calculated to give us *A(f)* shown in Figure A-1(b). In effect *A(t)* represents the input signal that reaches the transducer from the function generator. The same chirp signal was then transmitted in water with the C304 transducer and was captured by the membrane hydrophone at the focus [*p(z=d,t)*] or *B(t)*. Figure A-1(c) and (d) show

B(t) and its Fourier transform *B(f)* respectively. To calculate *H(f)* however, the output at the face of the transducer, *C(f, z=0)* is required where,

$$C(f) = \frac{B(f)}{G(f)} \tag{A.2}$$

The focusing gain, *G(f)* is calculated using,

$$G = \frac{\pi f a^2}{cd} \tag{A.3}$$

where *d* is the focal length and *a* is the radius of the source.

The transducer transfer function is given by,

$$H(f) = \frac{C(f)}{A(f)} \tag{A.4}$$

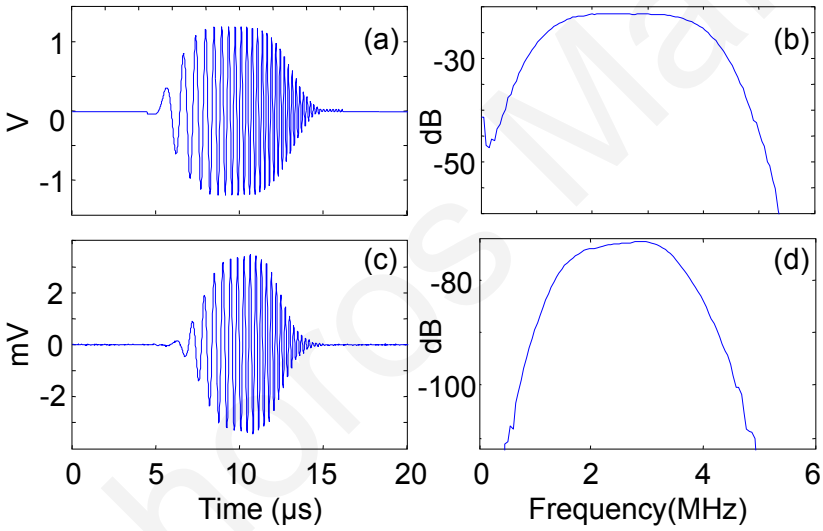

Figure A-1: (a)-(b) Open circuit chirp input, A(t), and its Fourier transform, A(f); (c)-(d) Output, B(t), at the focus (z=d) received by membrane hydrophone and its Fourier transform, B(f).

Figure A-2 depicts the calculated normalized transfer function, $H(f)_n$, which shows the center frequency at 1.9 MHz and the -6 dB down points are at 1.0 and 3.5 MHz.

Once the transducer transfer function is calculated then any measured scattered waveform $p_s(t)$ can be corrected using the following equation:

$$p_{sc}(f) = \frac{p_s(f)}{H(f)_n} \tag{A.5}$$

where $p_s(f)$ is the Fourier transform of a time waveform $p_s(t)$. Finally the inverse Fourier transform is used to get $p_{sc}(t)$ which is the corrected time waveform.

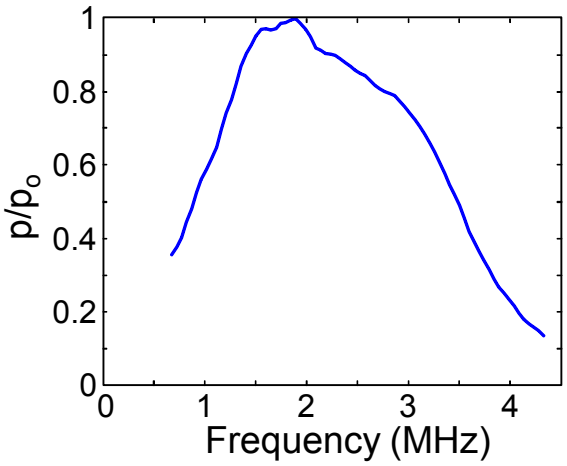

Figure A-2: Frequency response curve of C304 transducer obtained experimentally.

Figure A-3(a) shows the bubble response, $p_s(t)$,to a 1 MHz, 10 cycle burst at MI 0.4. Its Fourier transform, $p_s(f)$ is shown in Fig. A-3(b). In Fig. A-3(c) equation A.5 is used to calculate the corrected spectrum, $p_{sc}(f)$, and finally Fig. A-3(d) shows the corrected waveform, $p_{sc}(t)$.We observe that the 1st harmonic level has increased by 5 dB and the 3rd harmonic by 3 dB, whereas the 2nd harmonic remained the same. We also observe that the amplitude of the corrected waveform has increased by a factor of 2.

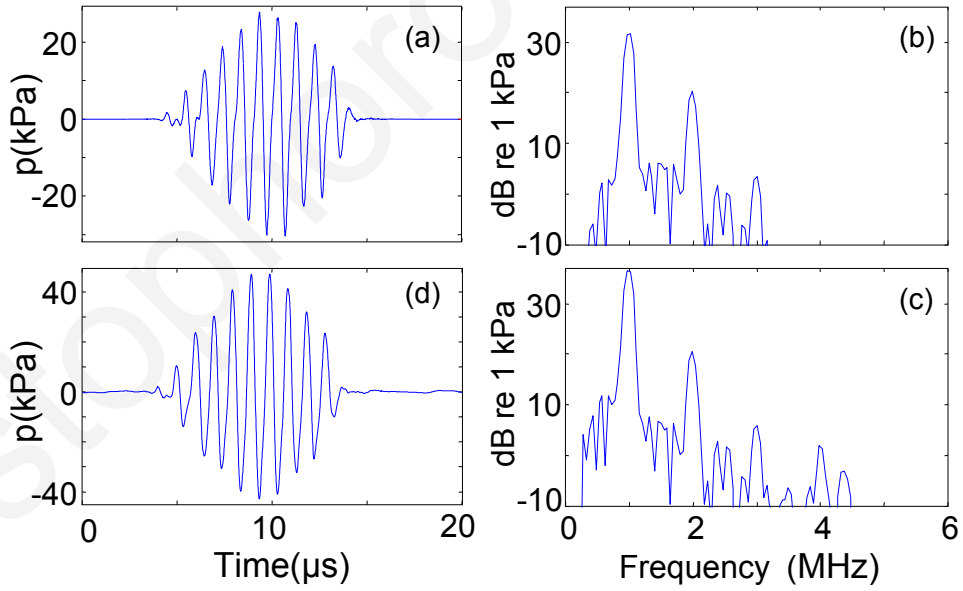

Figure A-3: Bubble response to 1 MHz, 10-cycle burst at MI 0.4. (a) time waveform, $p_s(t)$, (b) Fourier transform of (a), $p_s(f)$, (c) corrected spectra $p_{sc}(f)$ and (d) inverse Fourier transform of (c) to give corrected time waveform, $p_{sc}(t)$.

To complete the calibration of the single element transducer, we also need to calculate the receive sensitivity, i.e. what is the produced electrical signal for a given pressure. To do this, a 6 cycle, 2.25 MHz pulse was received at the focus with both the membrane hydrophone and the single element transducer. Care was taken for the

amplitude of the transmitted pulse to be low in order to avoid nonlinear propagation and the production of harmonics. Since the sensitivity of the calibrated membrane hydrophone is known, the sensitivity of the transducer can be easily calculated. The sensitivity of the C304 transducer was found to be 4725 mV/MPa at 2.25 MHz (compared to 63 mV/MPa of the membrane hydrophone).

3

Doxorubicin Liposome-Loaded Microbubbles for Contrast Imaging and Ultrasound-Triggered Drug Delivery

.Targeted drug delivery under image guidance is gaining more interest in the drug delivery field. The use of microbubbles as contrast agents in diagnostic ultrasound provides new opportunities in noninvasive image guided drug delivery. In the present study, the imaging and therapeutic properties of novel doxorubicin liposome-loaded microbubbles are evaluated. The results showed that at scanning settings (1.7 MHz and mechanical index 0.2), these microbubbles scatter sufficient signal for nonlinear ultrasound imaging and can thus be imaged in real time and be tracked *in vivo*. *In vitro* therapeutic evaluation showed that ultrasound at 1 MHz and pressures up to 600 kPa in combination with the doxorubicin liposome-loaded microbubbles induced 4-fold decrease of cell viability compared to treatment with free doxorubicin or doxorubicin liposome-loaded microbubbles alone. The therapeutic effectiveness is correlated to an ultrasound-triggered release of doxorubicin from the liposomes and an enhanced uptake of the free doxorubicin by glioblastoma cells. The results obtained demonstrate that the combination of ultrasound and the doxorubicin liposome-loaded microbubbles can provide a new technology of noninvasive image guided-drug delivery.

Published as: Escoffre, J.-M *., C. Mannaris, et al *. (2013). "Doxorubicin liposome-loaded microbubbles for contrast imaging and ultrasound-triggered drug delivery." IEEE Transactions on Ultrasonics, Ferroelectrics, and Frequency Control **60**(1): 78-87.

*Escoffre, J.-M and C. Mannaris contributed equally to this work

3.1 Introduction

Doxorubicin (DOX) is one of the most powerful anticancer drugs prescribed on its own or in combination with other agents. Due to its broad spectrum of activity, it is widely used for the treatment of solid tumors and hematological malignancies [1]. However, the use of free DOX in clinical application is still rather limited because of the severe systemic side effects associated with its use. To overcome these major problems, the DOX has been encapsulated inside PEGylated liposomes preventing their recognition by the reticuloendothelial system [2]. This formulation results in the passive accumulation of liposomes in the leaky tumor vasculature due to the enhanced permeability and retention effect [3]. Doxil®, a clinical approved liposomal DOX formulation, is nowadays indicated for the treatment of cancer such as Kaposi's sarcoma and ovarian cancer [2, 4]. Although, Doxil® strongly reduced the cardiotoxicity of DOX in clinical trials [5], other adverse effects have been reported such as patients suffering from mucositis and the hand and foot syndrome due to the localization of liposomes in skin capillaries [6]. Both the pharmacological actions of DOX as well as its toxicological effects are related to tissue concentration of DOX [1]. For that reason, the development of a more efficient and targeted delivery method is required to increase the local concentration of DOX at the desired site while minimizing side effects to healthy tissues.

Image guided ultrasound mediated drug delivery shows great promise in improving the therapeutic ratio of a chemotherapeutic agent by increasing the local deposition and reducing the systemic side effects [7-9]. The combination of ultrasound waves and ultrasound contrast agents (microbubbles) is known to enhance the vascular extravasation and the intracellular delivery of drugs [10-14]. The exposure of microbubbles to ultrasound causes the expansion and the compression of microbubbles during the respective rarefaction and compression phases of the ultrasound wave. These oscillations may cause liquid flow around the microbubbles, known as microstreaming [15, 16]. At even higher acoustic pressures, the microbubbles undergo large oscillations, which lead to violent collapse and destruction of the microbubbles and in some cases inertial cavitation where the microbubble disruption might be accompanied by the generation of shock waves in the medium close to the microbubbles [17]. In the case of an asymmetrical collapse, jet formation may also occur when a collapsing microbubble is located near the cell membrane [18]. These different physical phenomena can transiently enhance the permeability of tumor vasculature and cells and therefore, the extravasation and the intracellular uptake of the drugs [19, 20].

A key ingredient in ultrasound-triggered local drug delivery is the ability to image the drug delivery vehicle in real time. Ideally, the drug carrier should be able to be tracked *in vivo* using low mechanical index (MI) imaging and once at the desired location, high MI ultrasound may be used to trigger the drug release on site. Another approach is to image the microbubble destruction process with Doppler-based methods [21].

Several studies reported on the synergistic effect of DOX and ultrasound. These studies focused mainly on the intracellular delivery of free or encapsulated DOX by ultrasound alone [22-25] or co-injected with contrast agent [26-29]. However, a major limitation of the co-administration approach is that liposomes can still extravasate and accumulate in untargeted tissues such as the skin capillaries resulting in undesired side effects [6]. To minimize this side effect, one of strategies is to develop a drug-loaded microbubbles [28, 30, 31]. Geers *et al.,* designed doxorubicin liposomes-loaded microbubbles. Hence the DOX is encapsulated in liposome particles that bind to the lipid shell of the microbubbles through a covalent link [28]. The clinical potential of the DOX liposome-loaded microbubbles rests on the ultrasound-triggered DOX delivery monitored by ultrasound contrast imaging.

The aim of this study is first to investigate the imaging characteristics of the liposome-loaded microbubbles and to compare their performances to those of a commercially available contrast agent (SonoVue®, Bracco Research, Geneva, Switzerland). Then, the therapeutic effectiveness of the DOX liposome-loaded microbubbles in human glioblastoma cells was evaluated and the mechanism of DOX delivery was investigated.

3.2 Material and Methods

3.2.1 Preparation of microbubbles

3.2.1.1 Unloaded microbubbles

Unloaded microbubbles were prepared via the method described by Geers *et al.* [26]. Briefly, microbubbles were prepared from a lipid solution of 1,2-dipalmitoyl-sn-glycero-3-phosphocholine (DPPC) and 1,2-distearoyl-sn-glycero-3-phosphoethanolamine-N-[PDP(polyethylene glycol)-2000] (DSPE-PEG-PDP) (Avanti polar lipids, Albaster, AL) in a 1:2:7 glycerine-propyleneglycol-H_2O solvent (Sigma-Aldrich, Bornem, Belgium). The molar ratio of the lipids in the lipid solutions was respectively 65:35. This lipid solution was prepared as follows: the different lipids dissolved in $CHCl_3$ were mixed and the

solvent was evaporated. Afterwards, the remaining lipid-film was dissolved in glycerine-propyleneglycol-H_2O. One milliliter of the mixture was transferred to a glass vial and its headspace was filled with C_4F_{10} gas (F2 chemicals, Preston, UK) before mechanical agitation. Finally, unloaded microbubbles were obtained by high speed shaking of the lipid solution in a Capmix™ device (3M-ESPE, Diegem, Belgium) during 15s. The size and the concentration of the microbubbles in the dispersion (i.e. number of microbubbles/mL) were determined with a Beckman-Coulter Multisizer 4 (Beckman-Coulter, Brea, CA). The unloaded microbubbles showed an average volume diameter of 3.6 µm. The microbubble dispersions contained respectively 1.23×10^9 microbubbles/mL.

3.2.1.2 Dox liposome-loaded microbubbles

DOX liposome-loaded microbubbles were prepared by adding adequate amounts of DOX liposomes functionalized with DSPE-PEG-MALEIMIDE (Avanti Polar Lipids, Albaster, AL) to the lipid-solution before mechanical activation (Figure 3-1). The DOX-liposomes were prepared via the method described by Lentacker *et al.,* [32]. Briefly, adequate amounts of DPPC, DSPE-PEG-MALEIMIDE and cholesterol (dissolved in $CHCl_3$) were transferred to a round-bottom flask and the solvent was evaporated using a Rotavap. The remaining lipid-film was then hydrated with ammonium sulfate buffer (250 mM) and the liposomal-solution was extruded through a 200 nm filter. To remove the excess of ammonium sulfate the liposome dispersion was peletized in a Beckman L8-M ultracentrifuge at 10,000 g. Finally, DOX liposomes were obtained by incubating the obtained liposomal dispersion with a sufficient amount of DOX in HCl (10 mg/mL in H_2O) at 50°C for 2 hours. Afterwards the nonencapsulated DOX was removed by ultracentrifugation at 10,000 g (Beckman L8-M ultracentrifuge). Finally adequate amounts of DOX-liposomes were mixed with the (DPCC, DSPE-PEG-SPDP) lipid solution as described in the previous section and were transferred into glass vials and its headspace was filled with C_4F_{10}. After 15 sec of mechanical agitation, the loaded microbubbles showed an average volume diameter of 4 µm. The microbubble dispersions contained approximately 1.04×10^9 microbubbles/mL.

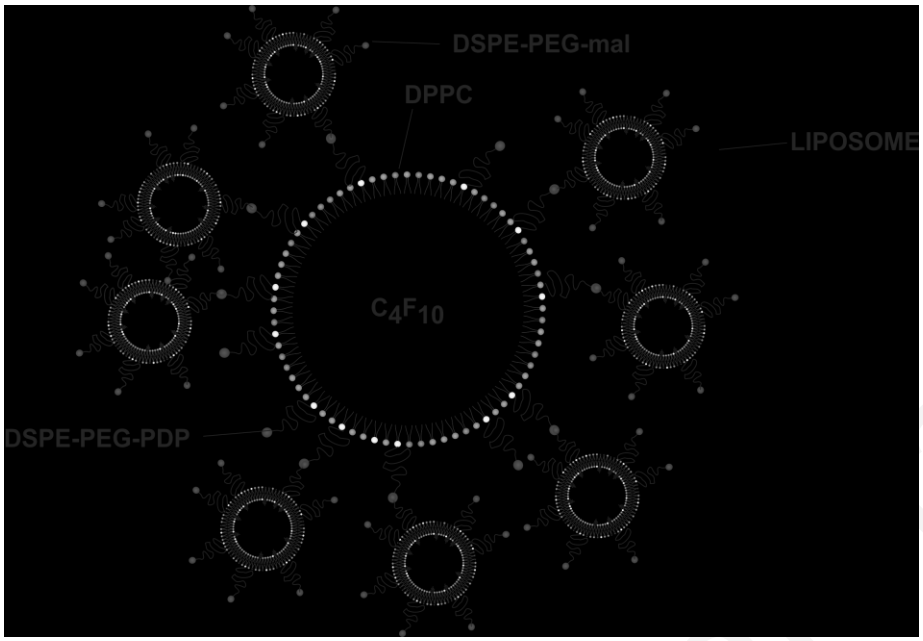

Figure 3-1: Schematic presentation of DOX liposome-loaded microbubbles. The microbubbles are filled with the hydrophobic C4F10 gas. DOX-containing liposomes are coupled to the microbubble's surface through covalent thiol-maleimide linkages. The DOX liposome-loaded microbubbles showed an average volume diameter of 4 μm while the DOX-loading liposomes are 200 nm in diameter.

3.2.2 Acoustic characterization

3.2.2.1 Microbubble imaging

In this section, the imaging characteristics of the unloaded microbubbles and DOX liposome-loaded microbubbles were investigated and compared to SonoVue® using the setup shown in Figure 3-2. The microbubbles were diluted to a concentration of 0.2 $^{o}/_{oo}$ (0.2 mL of contrast agent in 1 L of de-ionized water), which lies in the low end of the linear range of the relation of intensity versus concentration [33], and this is similar to what is usually used clinically (normally 2.4 mL injected in 5 L of blood) [21]. The original concentration of all three types of microbubbles used in this study is 10^8 microbubbles/mL thus consistency was maintained. The solution was continuously mixed by a magnetic stirrer to avoid flotation and to ensure uniform distribution of the microbubbles while a peristaltic pump (Masterflex; Cole-Palmer, Vernon Hills, IL, USA) was used to draw the solution into a rubber based tissue mimicking Cardiac Doppler flow phantom (Model 523A; ATS Laboratories Inc., Bridgeport, CT, USA). Contrast enhanced ultrasound imaging of the microbubbles was performed with the C5-1 curvilinear transducer of a Philips iU-22 (Philips Medical Systems, Bothell, WA, USA) ultrasound scanner. The

transducer was placed so as to image the 8 mm diameter flow channel of the phantom at a depth of 12 cm. Power modulation nonlinear pulsing scheme [34, 35] was used at a transmit center frequency of 1.7 MHz.

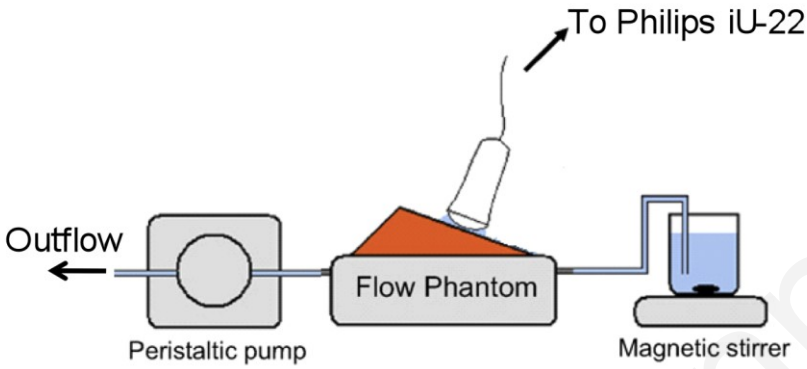

Figure 3-2: Flow phantom setup. A peristaltic pump draws the samples into a tissue mimicking flow phantom (attenuation coefficient 0.5 dB/cm/MHz). Imaging done by a C5-1 curvilinear transducer and a Philips iU-22 ultrasound scanner.

The Contrast-to-Tissue ratio (CTR) under different excitation pressures was measured using the setup described above. CTR is defined as the ratio of the scattered intensity from the microbubbles to the scattered intensity from tissue and it is an index of the ability to image contrast agent in the presence of tissue. Acoustic pressures ranging from 0.06 to 0.98 MPa corresponding to mechanical indices (MI) of 0.05 to 0.75 were used. A continuous infusion of the microbubble solution was passed through the phantom and 5 frames per MI were acquired at a frame rate of 0.5 Hz. The total volume in the field of view was about 5 mL (radius = 4 mm, length = 10 cm), so a flow rate of 200 mL/min (6.7 mL in 2 sec) was used to make sure the region of interest (ROI) was refreshed with new microbubbles for each frame so that microbubble destruction would not be an issue. QLAB software (Philips Healthcare, Andover, MA, USA) was used in the analysis of the data. QLAB allows for selection of one or more ROIs and produces time-intensity curves from the image loops. The intensity is obtained from uncompressed envelope detected data squared and then averaged from all pixel values in the ROI. Two regions of interest were selected, one inside the tube lumen and one outside the tube. CTR as a function of MI was obtained by dividing the backscattered intensity from the microbubbles by the backscattered intensity from tissue (in absolute scale units). In Figure 3-3, examples of the ROI selection during a CTR experiment are shown for low, medium and high MI.

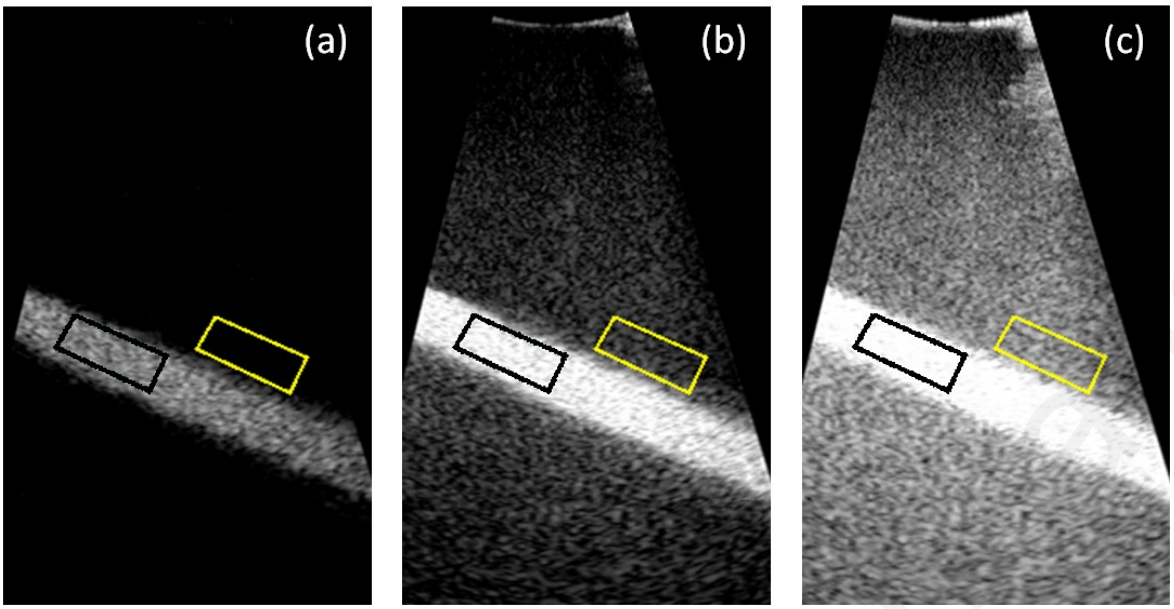

Figure 3-3: Selection of regions of interest in QLAB for CTR calculation at (a) MI 0.05, (b) MI 0.3, (c) MI 0.7. Two identical regions were selected at the same depth, one inside the tube lumen (contrast) and one outside the tube (tissue).

3.2.2.2 Microbubble destruction

The setup shown in Fig. 3-2 was also used to investigate the destruction of the unloaded and DOX liposome-loaded microbubbles when exposed to ultrasound at MIs 0.05 to 0.75. The destruction threshold of the microbubbles would allow us to determine the optimal MI to image and track the microbubbles *in vivo* without causing destruction and premature release of the drug as well as to optimize the imaging of the microbubble destruction process with a Doppler-based method. Similar to the CTR experiments, the results were compared to SonoVue®.

A freshly made solution of microbubbles (C = 0.2 $^{o}/_{oo}$) was pumped into the flow phantom and the flow was stopped. The microbubbles were then insonified for 10 seconds at a frame rate of 10 Hz (100 ms interval). The 10 sec imaging duration was selected so that it would be long enough to determine the ultrasound effect on the microbubbles (rate of destruction) while at the same time short enough to avoid any microbubble flotation. QLAB was used to select a single ROI in the middle of the tube and the decrease in intensity as a function of time was measured.

3.2.3 DOX delivery by microbubble-assisted ultrasound

3.2.3.1 Cell culture

Human glioblastoma cells (U-87 MG) were derived from a malignant glioma (ECACC European Collection of Cell Cultures, Salisbury, U.K.). Cells were grown as a monolayer in Dulbecco's Modified Eagle Medium (DMEM) (Gibco-Invitrogen, Carlsbad, CA) supplemented with 10% heat-inactivated fetal calf serum (FCS) (Gibco-Invitrogen, Carlsbad, CA). The cells were routinely sub-cultured every 4 days and incubated at 37°C in humidified atmosphere with a 5% CO_2 incubator.

3.2.3.2 Ultrasound set-up

Ultrasound waves were generated from a single element transducer with a center frequency of 1 MHz. The 13 mm diameter transducer was focused at 30 mm with a wide focal spot (i.e. beamwidth at -6dB = 5 mm). The transducer was driven with an electrical signal generated by an arbitrary waveform generator (Agilent, Santa Clara, CA) and amplified with a power amplifier (ADECE, Artannes sur Indre, France). The peak negative pressure of the acoustic wave was measured in a separate set-up using a calibrated PVDF needle hydrophone (0.2 mm diameter, Precision Acoustics, Dorchester, U.K.) at the natural focal distance of the transducer.

3.2.3.3 DOX delivery

U-87 MG cells were trypsinized, washed once and resuspended in OptiMEM (Gibco-Invitrogen, Carlsbad, CA) supplemented with 1% FCS. During the procedure, the cell suspension was maintained in a water bath at 37°C (Grant Instruments Ltd., Cambridge, U.K.). The cell suspension (3×10^5 cells in 1.5 mL) was then placed in a polystyrene cuvette (Fisher Scientific SAS, Illkirch, France) (45 mm height, 10 mm internal width and 12 mm external width) and 15 µL of unloaded microbubbles alone or DOX liposome-loaded microbubbles were added just before ultrasound application. Thus, a microbubble-cell ratio of 5 was achieved and the final concentration of DOX was of 3 µg/mL. The center of the plastic cuvette was positioned at the focal distance of the transducer in a deionized water tank at 37°C. The cell suspension was kept uniform through a gentle magnetic stirring during ultrasound application. Subsequently, the cell suspension was exposed to 1 MHz sinusoidal ultrasound waves with a pulse repetition period of 100 µs, 40 cycles per pulse and for 30 s (i.e. optimal acoustic parameters for gene and drug delivery, as determined by Escoffre et al., [27]). The applied acoustic pressures were 200 to 600 kPa.

After ultrasound application, 500 µL of cells were cultured in a 24-wells cell culture plates (Corning Life Science B.V., Amsterdam, The Netherlands) and incubated at 37°C in a humidified atmosphere with a 5% CO_2 incubator. Four hours later, 1 mL of OptiMEM-10% FCS was added to each well and incubated at 37°C in humidified atmosphere with a 5% CO_2 incubator for 48 h.

3.2.3.4 Dox uptake

Forty-eight hours after ultrasound triggered DOX delivery, the cell medium was removed and the cells were washed with PBS and collected through centrifugation (i.e., 3 min, 800 g). The cells were resuspended in 500 µL of PBS. Fluorescence histograms were recorded with a flow cytometer (Beckman-Coulter, Fullerton, CA) and analyzed using the Kaluza software supplied by the manufacturer. A minimum of 10,000 events was analyzed to generate each histogram. The gate was arbitrary set for the detection of red fluorescence [27].

3.2.3.5 Dox release

The experimental procedure was adapted from De Smet *et al.,* 2010 [36] and performed at 37°C. The DOX release from DOX liposomes or DOX liposome-loaded microbubbles was determined by measuring the intensity of fluorescence (λ_{ex} = 485 nm and λ_{em} = 590 nm) at 37°C and 10 min after treatment. A volume of 15 µL of unloaded microbubbles alone or DOX liposome-loaded microbubbles was added to the plastic cuvette containing 1.5 mL of OptiMEM-1% FCS just before ultrasound application. Subsequently, the solution was exposed to ultrasound. Three experimental groups were selected: (1) DOX liposomes or DOX liposome-loaded microbubbles after Triton X-100 at 10% v/v, which induces DOX release by dissolving the liposomes (Positive control), (2) DOX liposomes or DOX liposome-loaded microbubbles alone (Negative control), (3) Combination of DOX liposomes or DOX liposome-loaded microbubbles with ultrasound. After ultrasound application, 150 µL of the solution were introduced in 96-wells plate (Corning Life Science B.V., Amsterdam, The Netherlands). The percentage of DOX release was calculated according to:

—— (3.1)

in which I_{100} and I_{exp} are respectively the fluorescence intensity of positive control and the negative control or the combination of DOX liposome-loaded microbubbles with ultrasound.

3.2.3.6 Cell viability

The cell viability was evaluated using an MTT assay. Forty-eight hours after treatment, the cell medium was replaced with 0.5 mg/mL MTT solution (Molecular Probes-Invitrogen, Carlsbad, CA) and the cells were incubated at 37°C in humidified atmosphere with a 5% CO_2 incubator for 1.5 hours. Afterwards, the MTT solution was substituted by the DMSO solution (Sigma-Aldrich, St. Louis, MO) and the cells were incubated for 10 min under gentle agitation at room temperature. The absorbance was then measured at 570 nm (OD_{570}) to determine the amount of formed formazan and at 690 nm (OD_{690}) as a reference. The cell viability was calculated as follows [32]:

(3.2)

3.2.3.7 Statistical analysis

Data are presented as mean ± standard error of the mean (SEM) of five independent experiments. Statistical analysis was performed using the nonparametric Mann-Whitney test. Significance was defined as $p < 0.05$ (NS, non-significance; *$p < 0.05$; **$p < 0.01$; ***$p < 0.001$).

3.3 Results

3.3.1 Ultrasonic characterization

In this section the experimental measurements of CTR and destruction properties of the microbubbles are presented.

3.3.1.1 Contrast-to-tissue ratio

The contrast-to-tissue ratio for SonoVue® as a function of the mechanical index as well as the scattered intensity is shown in Fig. 3-4A (uncompressed data shown in decibels (dB)). The backscattered intensity from microbubbles (ROI inside the tube) is shown in black (line with solid dots) and for tissue (ROI outside the tube) in blue (line with 'x'). The calculated CTR is shown in red (line with '□'). SonoVue® microbubbles exhibit a higher CTR at low, non-destructive MIs as shown in our results. At MIs of 0.05 and 0.1 the CTR reaches 22 and 27 dB respectively. The best CTR for this setting of the ultrasound scanner is found at MI = 0.2 (29 dB). At this setting however, the pressure is high enough to destroy the microbubbles and real-time imaging is not possible [(real time contrast imaging

with Sonovue is carried out at non-destructive pressures (MI < 0.1)]. At higher MIs, incomplete tissue cancellation due to nonlinear propagation of ultrasound causes the tissue signal to increase considerably while the corresponding increase in the microbubble signal is less. As a result, the overall CTR decreases. The white area indicates the non-destructive MIs, and the grey area the destructive MIs.

The CTR for unloaded microbubbles is shown in Fig. 3-4B. A CTR of 13 and 18 dB is measured for non-destructive MIs of 0.05 and 0.1 respectively. Even though these are 9 dB less than SonoVue®, there is still enough microbubble signal for imaging. The best CTR for these scanning settings is 25 dB and is reached at MI = 0.26. Similar to SonoVue®, the CTR drops at higher MIs. Bubble size, concentration, gas content, frequency, shell elasticity and thickness are among the various parameters influencing the microbubble response (and consequently the CTR).

Loading of the microbubbles with the DOX-liposomes had an insignificant impact on the imaging properties of the microbubble as the results for DOX liposome-loaded microbubbles (shown in Fig. 3-4C) are nearly identical to the results of the unloaded microbubbles shown in Fig. 3-4B. One small difference is that loading of the microbubbles with DOX-liposomes seems to make them a slightly "tougher" and the destruction threshold (as described in the next section) increases. Real-time non-destructive imaging at this optimal setting (CTR = 25 dB) may be possible with the drug-loaded microbubbles.

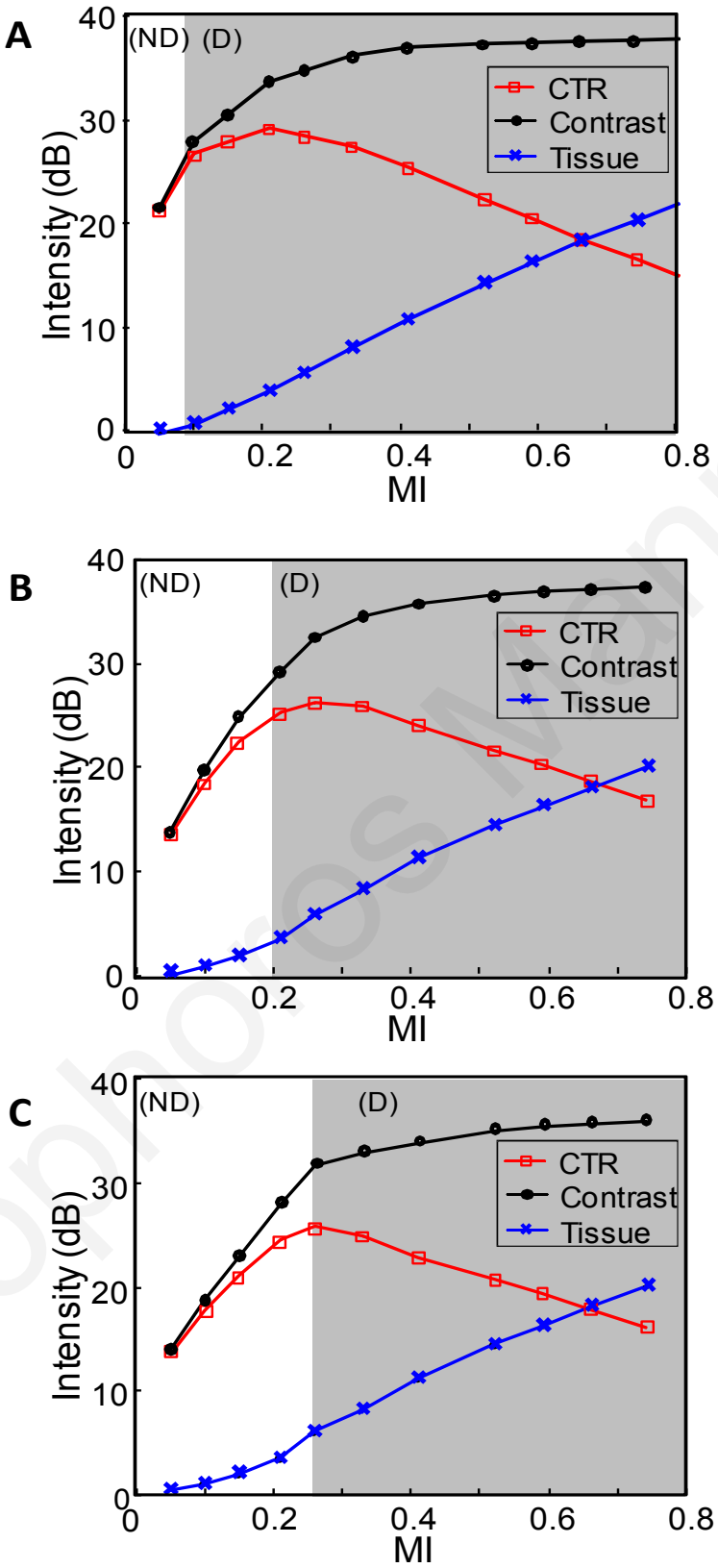

Figure 3-4: Contrast to tissue ratio for (A) SonoVue® microbubbles, (B) unloaded microbubbles and (C) DOX liposome-loaded microbubbles. The backscattered intensity from microbubbles (ROI inside the tube) is shown in black (line with solid dots) and for tissue (ROI outside the tube) in blue (line with 'x'). The calculated CTR is shown in red (line with '□'). The white area indicates the non-destructive MIs, and the grey area the destructive MIs.

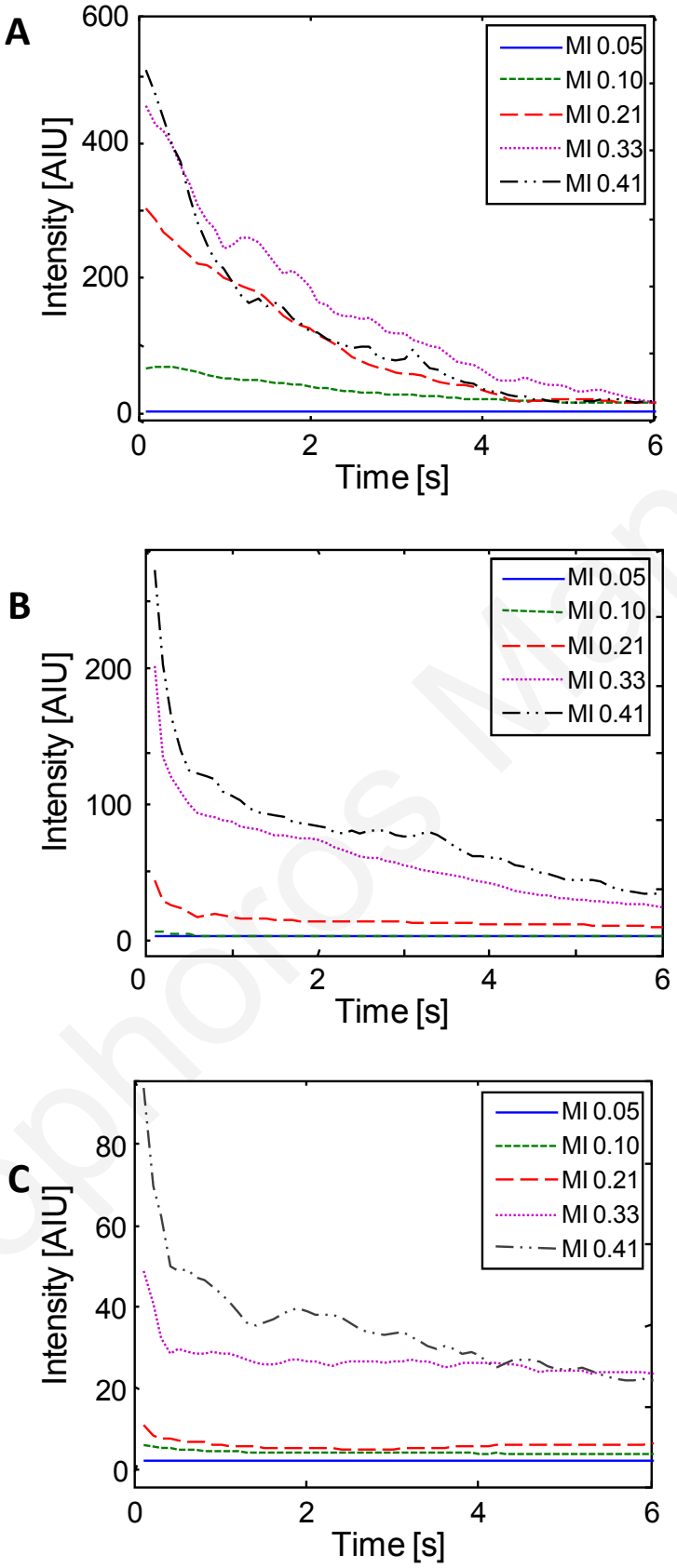

Figure 3-5: Kinetics of destruction of (A) SonoVue® microbubbles, (B) unloaded microbubbles and (C) DOX liposome-loaded microbubbles. MIs of 0.05, 0.1, 0.21, 0.33 and 0.41 are applied for 6 seconds (60 frames).

3.3.1.2 Microbubble destruction

The microbubble destruction patterns for various MIs are shown in Fig. 3-5. The time axis is given in seconds and the signal intensity in arbitrary intensity units (AIU). MIs of 0.05, 0.1, 0.21, 0.33 and 0.41 were used and ultrasound was applied for 6 seconds (60 frames). Higher pressures and longer exposure times followed the same trends (data not shown). The destruction of SonoVue® microbubbles is shown in Fig. 3-5A. At MI 0.05 the intensity remains constant throughout the insonation period indicating that there is no destruction whereas at MI 0.1, the intensity gradually decreases, indicating that destruction is taking place. Over 6 seconds (60 frames) are required for the overall intensity to drop to half its initial value. Higher pressures steadily become more destructive as expected and at MI 0.4 the majority of the bubbles are destroyed within 2-3 seconds.

Figure 3-5B demonstrates the destruction patterns of unloaded microbubbles. Unlike SonoVue®, the scattered intensity at MI of 0.1 remains constant throughout the insonation period indicating that there is no destruction. Destruction is first observed at MI 0.21 where in the first second, the intensity drops by a factor of 2 before reaching steady state. At higher MIs, a sudden drop in the scattered intensity within the first 5-6 frames followed by a constant decay throughout the insonation period is observed.

The corresponding results for DOX liposome-loaded microbubbles are shown in Fig. 3-5C. Similar to the unloaded microbubbles, MIs of 0.05 and 0.10 are non destructive since the intensity remains constant throughout the insonation time. MI 0.21 is a little destructive as a slight decrease in intensity is observed in the first 4-5 frames. Clear destruction can be seen at MI 0.33 where the intensity drops to 50% of its initial value within 4-6 frames before reaching a plateau. Similar trends were observed at higher MIs.

3.3.2 Evaluation of therapeutic efficiency and mechanism of drug delivery

3.3.2.1 Enhancement of Dox-induced glioblastoma cell death by Dox liposome-loaded microbubbles and ultrasound

Cell viability was assessed by the MTT assay 48h after treatment with DOX liposome-loaded microbubbles and ultrasound and the results are shown in Fig. 3-6. When the U-87 MG cells were insonated at 600 kPa (MI=0.6) with only the presence of unloaded microbubbles, the cell viability was 87 ± 2% (Fig. 3-6). Similar cell viability was obtained at 200 and 400 kPa with the unloaded microbubbles. As shown in Fig. 3-6, the cell viability after treatments with free DOX and DOX liposomes-loaded microbubbles alone were 67 ± 1% and 71 ± 1%, respectively. The cytotoxicity induced by the treatment with DOX liposome-loaded microbubbles alone can be ascribed to the presence free DOX-

liposomes in the vial after mechanical activation, which can be endocytosed by the cells causing thus cytotoxicity. The combination of DOX liposome-loaded microbubbles and ultrasound at 200 kPa induced a 2-fold decrease of cell viability compared to free DOX or DOX liposome-loaded microbubbles alone (***$p < 0.001$).

Increasing the acoustic pressure to 400 and 600 kPa caused a 3- and 4-fold decrease of cell viability respectively when compared to free DOX or DOX liposome-loaded microbubbles alone (***$p < 0.001$). These results clearly showed that the combination of DOX liposome-loaded microbubbles with ultrasound induced a synergistic effect on the U-87 MG cell death.

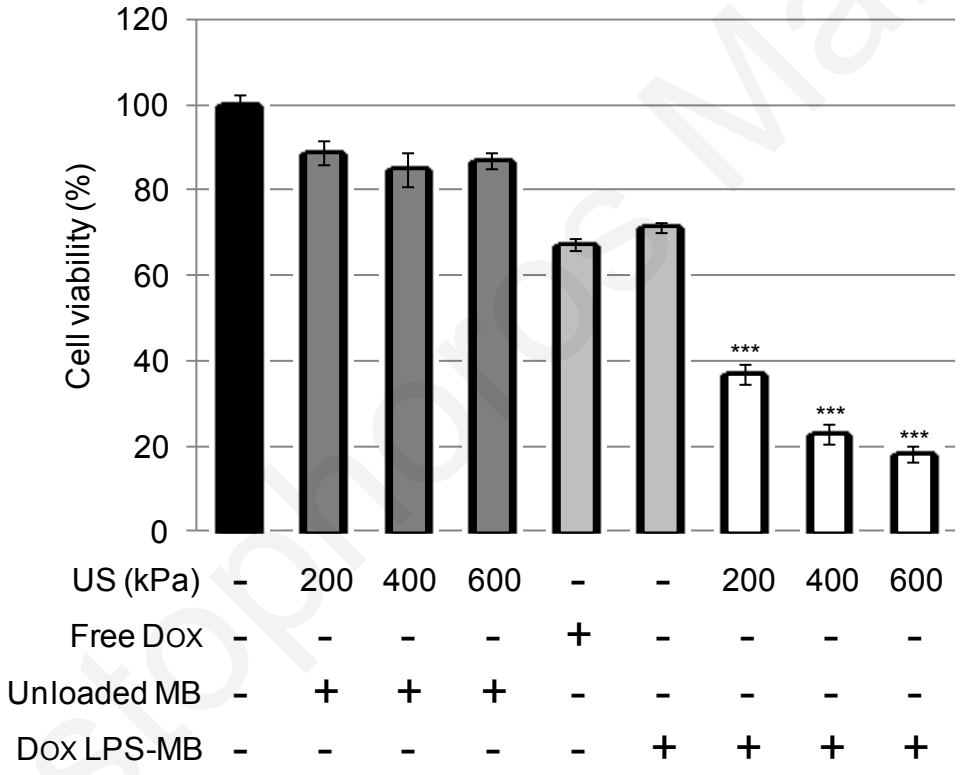

Figure 3-6: Enhancement of doxorubicin-induced cell death by ultrasound combined with DOX liposome-loaded microbubbles. U-87 MG cells were incubated with 3 µg/mL doxorubicin alone (Free DOX), or with DOX liposome-loaded microbubbles alone (DOX LPS-MB) or combined with ultrasound at 200 kPa, 400 kPa and 600 kPa for 30s. Forty-eight hours after the treatment, cell viability was measured by a MTT assay. Data expressed as mean ± SEM was calculated from five independent experiments. Statistical analysis was performed using the nonparametric Mann-Whitney test. Significance was defined as $p < 0.05$ (*$p < 0.05$, **$p < 0.01$ and ***$p < 0.001$).

3.3.2.2 Enhancement of Dox release from Dox liposome-loaded microbubbles after insonation.

Due to the high intra-liposomal DOX amount, the native DOX fluorescence is quenched. Release of DOX from the aqueous intra-liposomal medium will result in the dilution of the free DOX in the extra-liposomal medium leading to an increment of fluorescence intensity. The latter is proportional to the amount of DOX in the medium. The DOX release was assessed by spectrofluorometry after insonation of DOX liposome-loaded microbubbles. The insonation at 600 kPa of DOX liposome-loaded microbubbles induced a significant increase of DOX release from the liposomes loaded on the microbubbles (***$p < 0.001$ compared to the incubation of DOX-loaded microbubbles in the medium of cell culture) (Figure 3-7). These results reveal that the combination of DOX liposome-loaded microbubbles with ultrasound induced an active release of doxorubicin from liposomes.

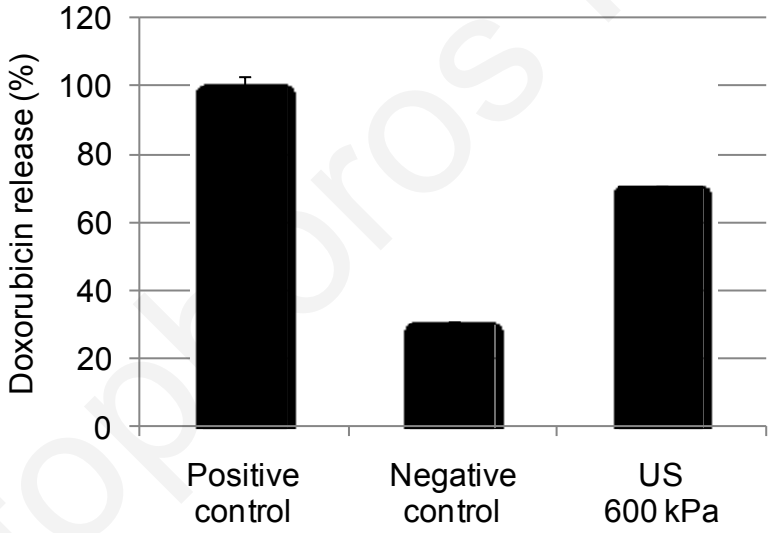

Figure 3-7: Enhancement of DOX release from DOX liposome-loaded microbubbles after insonation. DOX liposome-loaded microbubbles were incubated with (Positive control) or without (Negative control) Triton X-100 at 10% v/v in OptiMEM-1% FCS. In addition, these same microbubbles were insonated at the optimal acoustic pressure of 600 kPa. Data expressed as mean ± SEM was calculated from five independent experiments. Statistical analysis was performed using the nonparametric Mann-Whitney test. Significance was defined as $p < 0.05$ (*$p < 0.05$, **$p < 0.01$ and ***$p < 0.001$).

3.3.2.3 Enhancement of Dox uptake by Dox liposome-loaded microbubbles and ultrasound

Flow cytometry was used for quantitative determination of DOX uptake in the U-87 MG glioblastoma cells. The native fluorescence of the DOX was used to directly measure cellular uptake, fluorescence intensity being directly proportional to the internalized amount of DOX. The insonation of U-87 MG glioblastoma cells at 600 kPa (i.e. optimal acoustic pressure for cell viability) with the unloaded microbubbles did not show an increase in the fluorescence intensity (solid line) as shown in Fig. 3-8. The result is similar to that obtained with untreated cells (data not shown). The treatment of U-87 MG cells with the DOX liposome-loaded microbubbles alone induced a shift of the histogram to the right (dashed line). This result can be explained by the intracellular DOX leakage from DOX-liposomes incorporated by U-87 MG cells. The combination of ultrasound with DOX liposome-loaded microbubbles induced an additional shift of the histogram to the right (short-dash red histogram). This result shows that the cellular uptake of DOX by U-87 MG was significantly ($*p<0.05$) higher in the cells treated with ultrasound and DOX liposome-loaded microbubbles than in the cells treated with DOX liposome-loaded microbubbles alone. These results confirm that the combination of DOX liposome-loaded microbubbles with ultrasound induced an enhancement of free DOX uptake by U-87 MG cells.

3.4 Discussion

The present study examined the imaging and therapeutic properties of DOX liposome-loaded microbubbles for ultrasound induced delivery of DOX under diagnostic ultrasound guidance. We have shown that when interrogated with low non-destructive MI, these microbubbles scatter sufficient signal for nonlinear ultrasound imaging and can therefore be imaged in real time and tracked *in vivo* (Fig. 3-4). Loading of the microbubbles with DOX liposomes has no apparent effect on the acoustic properties of the microbubbles other than slightly increasing the destruction threshold (Fig. 3-5). The therapeutic evaluation of these microbubbles showed that ultrasound insonation of the DOX liposome-loaded microbubbles induced a much higher glioblastoma cell death than treatment with free DOX or DOX liposome-loaded microbubbles alone (Fig. 3-6). We have demonstrated that the enhanced therapeutic efficiency is associated with (i) an ultrasound-triggered release of DOX from the DOX liposome-loaded microbubbles (Fig. 3-7) and (ii) an enhanced uptake of free DOX by the cells (Fig. 3-8). In agreement with our previous

data, these results support the hypothesis that sonoporation improves the cellular uptake of free DOX [27, 28, 32]. Indeed, we demonstrated that microbubbles and ultrasound enhanced significantly the cellular uptake of free DOX and the DOX-associated cytotoxicity compared to the treatment with free DOX alone.

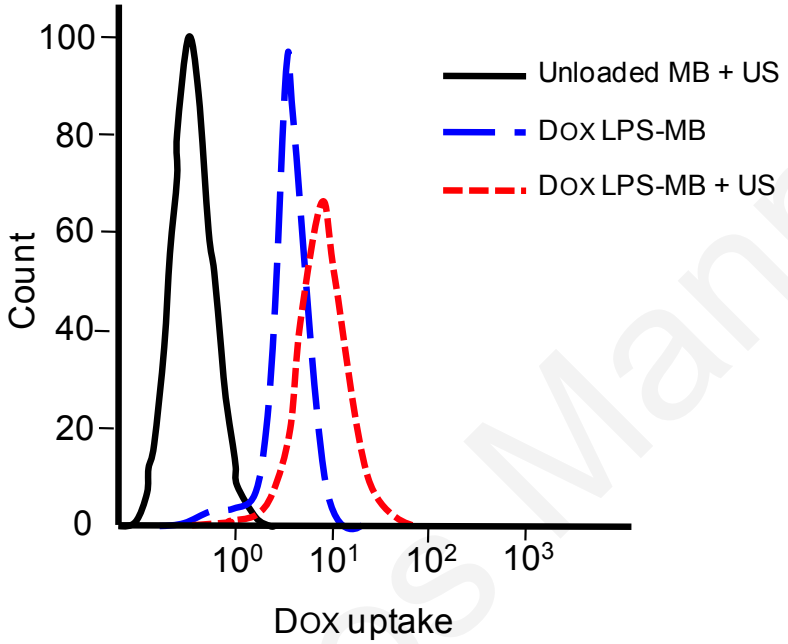

Figure 3-8: Enhancement of doxorubicin uptake into U-87 MG cells with DOX liposome-loaded microbubbles and ultrasound. U-87 MG cells were incubated with unloaded microbubbles (Unloaded MB + US) or DOX liposome-loaded microbubbles (DOX LPS-MB + US) at the final doxorubicin concentration of 3 µg/mL with ultrasound at 600 kPa. In addition, cells were treated with DOX liposome-loaded microbubbles alone (DOX LPS-MB). Forty-eight hours after the treatment, doxorubicin uptake was measured by flow cytometry. Data expressed as mean ± SEM was calculated from five independent experiments.

Based on the results obtained in the present study, we hypothesized that DOX-liposome loaded microbubbles in combination with ultrasound may improve significantly the *in vivo* effectiveness of targeted DOX delivery under ultrasound imaging guidance. Our data support the idea that the design of a hybrid imaging/therapeutic probe is required to reach this double objective. Following intravenous injection, these smart microbubbles may be tracked *in vivo* using conventional ultrasound contrast imaging modes. Once the tumor microvasculature network is filled with the DOX liposome-loaded microbubbles, a high intensity therapeutic ultrasound exposure may induce the destruction of microbubbles, promoting (i) the permeation of tumor endothelium, (ii) the ultrasound-triggered release and (iii) the extravasation of the free DOX into the endothelial and tumor cells [37-39]. The enhanced uptake of DOX in endothelial cells may potentiate the destruction of tumor

microvasculature and breakdown the nutrient supply (i.e., oxygen, nutrients, *etc.*) of the tumor [40]. As free DOX is more cytotoxic than liposomal DOX [41], the local ultrasound-triggered delivery of free DOX in the tumor may enhance the tumor cell death and tumor eradication. We believe that the use of optimal formulation of DOX liposome-microbubbles (i.e. without free Dox liposomes) might exhibit less side effects than free DOX. Thus, in the tissues unexposed to ultrasound, these micro-sized microbubbles would remain intact and there would be no release and extravasation of DOX in these health tissues. This assumption remains to be demonstrated in future *in vivo* studies.

In conventional chemotherapy with Doxil®, a single therapeutic dose corresponds to 40 mg of DOX for an 80 kg adult patient [41]. The concentration of loaded DOX attached to a single microbubble was estimated to be 5×10^{-9} µg [28]. Based on these figures, a total number of 8×10^{12} DOX liposome-loaded microbubbles have to be intravenously injected to reach a similar therapeutic dose. However, the recommended diagnostic doses of current contrast agents (e.g. SonoVue® and Definity®) are respectively 10^9 and 10^{10} microbubbles for an 80 kg adult (i.e. about 1,000 and 100 times lower than that of DOX liposome-loaded microbubbles required to reach a single therapeutic dose of Doxil®). Nevertheless, recent studies have reported a good tolerance with 100- and 1,000-fold higher doses of SonoVue® and Definity® microbubbles in non-human primates and patients [42-46]. Consequently, the injection of a high dose of DOX liposome-loaded microbubbles could be considered for clinical DOX delivery for therapeutic purposes. However, further preclinical studies might be necessary to identify putative toxicity of high lipid concentrations. In addition, the localized delivery character of this approach would likely require a smaller therapeutic dose than the one used in current chemotherapy protocols. Thus, therapeutic effects can be expected in human at recommended diagnostic microbubble doses.

The enhancement of DOX loading efficiency on the microbubbles and the application of consecutive treatments constitute two other alternative approaches to reach the therapeutic dose of Doxil®. The small size of the microbubbles limits the space for DOX loading. Geers *et al.,* reported that the binding of DOX-liposomes on the surface of the microbubbles could increase the amount of loaded doxorubicin [28]. Though they showed that 600 to 1300 DOX-liposomes nanoparticles are bound per single microbubble. And hence the DOX concentration remains rather limited. Nevertheless, the loading efficiency can be further improved by applying multiple layers of DOX-liposomes around the microbubble shell. Finally, Zhao et al., reported that the repeated treatments of epirubicin and microbubble-assisted ultrasound induced an efficient inhibition of marrow leukemic

tumor growth followed by tumor eradication [47]. No side effect associated with this protocol has been reported.

3.5 Conclusion

Our results demonstrated that DOX liposome-loaded microbubbles have good imaging properties and a high therapeutic potential. Thus, the combination of these smart microbubbles and ultrasound presents a new potential strategy for the ultrasound-triggered DOX delivery under diagnostic ultrasound guidance.

References

[1] C. Carvalho, et al., "Doxorubicin: the good, the bad and the ugly effect," Curr Med Chem, vol. 16, pp. 3267-85, 2009.

[2] A. A. Gabizon, "Pegylated liposomal doxorubicin: metamorphosis of an old drug into a new form of chemotherapy," Cancer Invest, vol. 19, pp. 424-36, 2001.

[3] Y. Barenholz, "Doxil(R)--the first FDA-approved nano-drug: lessons learned," J Control Release, vol. 160, pp. 117-34, Jun 10 2012.

[4] C. L. Bennett and E. A. Calhoun, "Pharmacoeconomics of liposomal anthracycline therapy," Semin Oncol, vol. 31, pp. 191-5, Dec 2004.

[5] M. E. O'Brien, et al., "Reduced cardiotoxicity and comparable efficacy in a phase III trial of pegylated liposomal doxorubicin HCl (CAELYX/Doxil) versus conventional doxorubicin for first-line treatment of metastatic breast cancer," Ann Oncol, vol. 15, pp. 440-9, Mar 2004.

[6] R. R. Patil, et al., "Engineered nanocarriers of doxorubicin: a current update," Crit Rev Ther Drug Carrier Syst, vol. 25, pp. 1-61, 2008.

[7] R. Deckers and C. T. Moonen, "Ultrasound triggered, image guided, local drug delivery," J Control Release, vol. 148, pp. 25-33, Nov 20 2010.

[8] A. Fernandez-Fernandez, et al., "Theranostic applications of nanomaterials in cancer: drug delivery, image-guided therapy, and multifunctional platforms," Appl Biochem Biotechnol, vol. 165, pp. 1628-51, Dec 2011.

[9] A. V. Patil, et al., "Real-time technique for improving molecular imaging and guiding drug delivery in large blood vessels: *in vitro* and *ex vivo* results," Mol Imaging, vol. 10, pp. 238-47, Aug 2011.

[10] J. M. Escoffre, et al., "*In vitro* gene transfer by electrosonoporation," Ultrasound Med Biol, vol. 36, pp. 1746-55, Oct 2010.

[11] V. Frenkel, "Ultrasound mediated delivery of drugs and genes to solid tumors," Adv Drug Deliv Rev, vol. 60, pp. 1193-208, Jun 30 2008.

[12] K. Iwanaga, et al., "Local delivery system of cytotoxic agents to tumors by focused sonoporation," Cancer Gene Ther, vol. 14, pp. 354-63, Apr 2007.

[13] I. Lentacker, et al., "Ultrasound exposure of lipoplex loaded microbubbles facilitates direct cytoplasmic entry of the lipoplexes," Mol Pharm, vol. 6, pp. 457-67, Mar-Apr 2009.

[14] Y. Ueno, et al., "Combination of ultrasound and bubble liposome enhance the effect of doxorubicin and inhibit murine osteosarcoma growth," Cancer Biol Ther, vol. 12, pp. 270-7, Aug 15 2011.

[15] A. A. Doinikov and A. Bouakaz, "Acoustic microstreaming around an encapsulated particle," J Acoust Soc Am, vol. 127, pp. 1218-27, Mar 2010.

[16] J. Wu, "Theoretical study on shear stress generated by microstreaming surrounding contrast agents attached to living cells," Ultrasound Med Biol, vol. 28, pp. 125-9, Jan 2002.

[17] C. D. Ohl and B. Wolfrum, "Detachment and sonoporation of adherent HeLa-cells by shock wave-induced cavitation," Biochim Biophys Acta, vol. 1624, pp. 131-8, Dec 5 2003.

[18] C.-D. Ohl, et al., "Sonoporation from Jetting Cavitation Bubbles," Biophysical Journal, vol. 91, pp. 4285-4295, 2006.

[19] A. A. Doinikov and A. Bouakaz, "Theoretical investigation of shear stress generated by a contrast microbubble on the cell membrane as a mechanism for sonoporation," J Acoust Soc Am, vol. 128, pp. 11-9, Jul 2010.

[20] B. D. Meijering, et al., "Ultrasound and microbubble-targeted delivery of macromolecules is regulated by induction of endocytosis and pore formation," Circ Res, vol. 104, pp. 679-87, Mar 13 2009.

[21] C. Greis, "Technology overview: SonoVue (Bracco, Milan)," Eur Radiol, vol. 14 Suppl 8, pp. P11-5, Oct 2004.

[22] V. Frenkel, et al., "Delivery of liposomal doxorubicin (Doxil) in a breast cancer tumor model: investigation of potential enhancement by pulsed-high intensity focused ultrasound exposure," Acad Radiol, vol. 13, pp. 469-79, Apr 2006.

[23] E. Hagtvet, et al., "Ultrasound enhanced antitumor activity of liposomal doxorubicin in mice," J Drug Target, vol. 19, pp. 701-8, Sep 2011.

[24] P. Mohan and N. Rapoport, "Doxorubicin as a molecular nanotheranostic agent: effect of doxorubicin encapsulation in micelles or nanoemulsions on the ultrasound-mediated intracellular delivery and nuclear trafficking," Mol Pharm, vol. 7, pp. 1959-73, Dec 6 2010.

[25] T. Yoshida, et al., "Combination of doxorubicin and low-intensity ultrasound causes a synergistic enhancement in cell killing and an additive enhancement in apoptosis induction in human lymphoma U937 cells," Cancer Chemother Pharmacol, vol. 61, pp. 559-67, Apr 2008.

[26] M. C. Cochran, et al., "Disposition of ultrasound sensitive polymeric drug carrier in a rat hepatocellular carcinoma model," Acad Radiol, vol. 18, pp. 1341-8, Nov 2011.

[27] J. M. Escoffre, et al., "Doxorubicin delivery into tumor cells with ultrasound and microbubbles," Mol Pharm, vol. 8, pp. 799-806, Jun 6 2011.

[28] B. Geers, et al., "Self-assembled liposome-loaded microbubbles: The missing link for safe and efficient ultrasound triggered drug-delivery," J Control Release, vol. 152, pp. 249-56, Jun 10 2011.

[29] C. Y. Lin, et al., "Enhancement of focused ultrasound with microbubbles on the treatments of anticancer nanodrug in mouse tumors," Nanomedicine, vol. 8, pp. 900-7, Aug 2012.

[30] A. F. Lum, et al., "Ultrasound radiation force enables targeted deposition of model drug carriers loaded on microbubbles," J Control Release, vol. 111, pp. 128-34, Mar 10 2006.

[31] F. Yan, et al., "Pharmacokinetics and biodistribution of paclitaxel-loaded microspheres," Arzneimittelforschung, vol. 62, pp. 176-80, Apr 2012.

[32] I. Lentacker, et al., "Design and evaluation of doxorubicin-containing microbubbles for ultrasound-triggered doxorubicin delivery: cytotoxicity and mechanisms involved," Mol Ther, vol. 18, pp. 101-8, Jan 2010.

[33] M. Lampaskis and M. Averkiou, "Investigation of the relationship of nonlinear backscattered ultrasound intensity with microbubble concentration at low MI," Ultrasound Med Biol, vol. 36, pp. 306-12, Feb 2010.

[34] M. Averkiou, et al., "Ultrasound contrast imaging research," Ultrasound Q, vol. 19, pp. 27-37, Mar 2003.

[35] G. A. Brock-Fischer, et al., "Means for increasing sensitivity in non-linear ultrasound imaging systems," 1996.

[36] M. de Smet, et al., "Temperature-sensitive liposomes for doxorubicin delivery under MRI guidance," J Control Release, vol. 143, pp. 120-7, Apr 2 2010.

[37] R. Bekeredjian, et al., "Ultrasound targeted microbubble destruction increases capillary permeability in hepatomas," Ultrasound Med Biol, vol. 33, pp. 1592-8, Oct 2007.

[38] M. R. Bohmer, et al., "Focused ultrasound and microbubbles for enhanced extravasation," J Control Release, vol. 148, pp. 18-24, Nov 20 2010.

[39] S. M. Stieger, et al., "Enhancement of vascular permeability with low-frequency contrast-enhanced ultrasound in the chorioallantoic membrane model," Radiology, vol. 243, pp. 112-21, Apr 2007.

[40] M. S. Gordon, et al., "Tumor angiogenesis and novel antiangiogenic strategies," Int J Cancer, vol. 126, pp. 1777-87, Apr 15 2010.

[41] S. T. Duggan and G. M. Keating, "Pegylated liposomal doxorubicin: a review of its use in metastatic breast cancer, ovarian cancer, multiple myeloma and AIDS-related Kaposi's sarcoma," Drugs, vol. 71, pp. 2531-58, Dec 24 2011.

[42] D. Bokor, "Diagnostic efficacy of SonoVue," Am J Cardiol, vol. 86, pp. 19G-24G, Aug 17 2000.

[43] D. Bokor, et al., "Clinical safety of SonoVue, a new contrast agent for ultrasound imaging, in healthy volunteers and in patients with chronic obstructive pulmonary disease," Invest Radiol, vol. 36, pp. 104-9, Feb 2001.

[44] T. Fritz, et al., "Preclinical studies of MRX-115: safety evaluations of a myocardial perfusion agent," Acad Radiol, vol. 3 Suppl 2, pp. S185-7, Aug 1996.

[45] S. E. Grauer, et al., "MRX 115, an echocardiographic contrast agent, produces myocardial opacification after intravenous injection in primates: studies before and

after occlusion of left anterior descending coronary artery," Acad Radiol, vol. 3 Suppl 2, pp. S405-6, Aug 1996.

[46] E. C. Unger, et al., "Therapeutic applications of lipid-coated microbubbles," Adv Drug Deliv Rev, vol. 56, pp. 1291-314, May 7 2004.

[47] Y. Z. Zhao, et al., "Enhancing chemotherapeutic drug inhibition on tumor growth by ultrasound: an *in vivo* experiment," J Drug Target, vol. 19, pp. 154-60, Feb 2011.

4

Accurate measurement of microbubble response to ultrasound with a diagnostic ultrasound scanner

Ultrasound and microbubbles are often used to enhance drug delivery and the suggested mechanisms are extravasation and sonoporation. Drug delivery schemes with ultrasound and microbubbles at both low and high acoustic amplitudes have been suggested. A diagnostic ultrasound scanner may play a double role as both an imaging and a therapy device. It was not possible to accurately measure microbubble response with an ultrasound scanner for a large range of acoustic pressures and microbubble concentrations up to now, mainly due to signal saturation issues. A method for continuously adjusting the receive gain of a scanner and limiting signal saturation was developed in order to accurately measure backscattered echoes from microbubbles for Mechanical Index (MI) up to 2.1. The backscattered echoes from microbubbles increased quadratically with MI without reaching any limit. The signal intensity from microbubbles was found to be linear with concentration at both low and high MIs. However, at very high concentrations acoustic shadowing occurs which limits the delivered acoustic pressure in deeper areas. The contrast to tissue ratio was also measured and found to also increase with MI. These results can be used to better guide drug delivery approaches and to also develop imaging techniques for therapy procedures.

Submitted for review; by Christina P. Keravnou*, Christophoros Mannaris* and Michalakis A. Averkiou in IEEE Transactions in Ultrasonics and Ferroelectric Frequency Control.

* C. P. Keravnou and C. Mannaris contributed equally to this work

4.1 Introduction

Ultrasound contrast agents (UCAs) are micron-sized gas filled bubbles stabilized with a lipid or polymeric shell. Delivered intravenously, UCAs are considered a true blood-pool agent as they are small enough to pass through the alveolar–capillary barrier of the lungs and large enough to stay within the circulation. The high echogenicity of microbubbles compared to that of red blood cells is used to enhance image contrast in diagnostic ultrasound. Today, dynamic contrast enhanced ultrasound (DCEUS) is used in the clinic to image and quantify the perfusion of organs by depicting the macro- and microcirculation [1-4]. UCAs have been used in various clinical applications including cardiology [5], oncology [6, 7], and molecular imaging [8]. Recently interest has shifted towards the use of UCAs in therapeutic applications such as gene and DNA transfection [9, 10], thrombolysis [11], tissue ablation [12] and targeted drug delivery [13-16].

A key characteristic of microbubble behavior is that when interrogated with ultrasound pulses they undergo nonlinear oscillations and produce nonlinear scattering. The backscattered ultrasound contains harmonics, sub-harmonics and ultra-harmonics which are being utilized in nonlinear imaging methods like pulse inversion [17, 18] and power modulation [19, 20] which detect signals from harmonic frequencies and cancel out the linear tissue response. As a result, contrast-specific images are formed where only areas perfused with UCAs appear bright whereas everything else appears black. Since the image intensity of a given region is proportional to the amount of UCAs present [21], quantification of the perfusion is possible.

At high acoustic pressures [Mechanical Index (MI) > 0.5], violent destruction of the microbubbles occurs with even the possibility of inertial cavitation [22-24] and the formation of high velocity micro-jets [25]. These physical phenomena have been linked to an increased therapeutic effect due to enhanced extravasation and alteration of the cell membrane permeability, a process referred to as sonoporation [26-29].

Diagnostic ultrasound together with UCAs may be used to induce sonoporation. Several preclinical reports on gene and drug delivery [30-32], sonothrombolysis [33], and blood brain barrier opening [34] with the use of diagnostic ultrasound and microbubbles have been published. A clinical pilot study for the treatment of pancreatic cancer combining a commercial ultrasound scanner with UCAs has also been reported [35]. Ultrasound scanners have been used in the past as a research tool to investigate bubble

dynamics. Sboros et al. [36] reported on the backscatter of UCA suspensions as a function of concentration and pressure.

A major problem often encountered when microbubble properties are investigated using a diagnostic ultrasound scanner is signal saturation [21, 37-39]. The dynamic range of the backscattered signals varies dramatically depending on the bubble concentration and the MI used. Typically, to image the small signals from the microcirculation, high receive gains are used and this results in signal saturation in areas of larger vessels with higher bubble concentrations. If low receive gains are used, then the small signals from the microcirculation are not detected. This problem becomes even worse at higher MI's which are typically used for therapeutic applications. If not taken into consideration, signal saturation may affect CTR calculations as well as the quantification of perfusion and thus lead to false conclusions [37, 40].

In this work, a diagnostic ultrasound scanner was used to study the backscatter echoes of BR14 microbubbles (Bracco S.P.A., Milan, Italy) [41] as a function of pressure and concentration in a tissue flow phantom. The question of microbubble response with increasing acoustic amplitude is addressed. Signal saturation with increasing pressure and bubble concentration, often encountered with commercial scanners, was carefully avoided by continuously adjusting the scanner's 2D analog gain. The pressure was varied from 0.06 MPa up to 2.6 MPa peak negative pressure (above FDA diagnostic limit) while various concentrations, were considered. The intensity-concentration relationship was investigated at both low and high pressures. The contrast to tissue ratio (CTR) as a function of MI and now without the effect of signal saturation was calculated for a range of concentrations. Knowledge of accurate bubble response to ultrasound is key in therapeutic applications such as sonoporation.

4.2 Materials and methods

4.2.1 Experimental setup

Imaging of the microbubbles and measurements of their response to ultrasound were carried out using the flow phantom setup shown in Fig. 4-1. A freshly prepared microbubble solution was placed in a glass beaker and was continuously mixed with a magnetic stirrer. A peristaltic pump (Masterflex; Cole-Palmer, Vernon Hills, IL, USA) was used to draw the solution into an 8-mm wall-less tube of a tissue mimicking flow phantom (Model 523A; ATS Laboratories Inc., Bridgeport, CT, USA) with a flow rate of 200

ml/min. An iU-22 diagnostic ultrasound scanner (Philips Medical Systems, Bothell, WA) was used to interrogate and image the microbubbles.

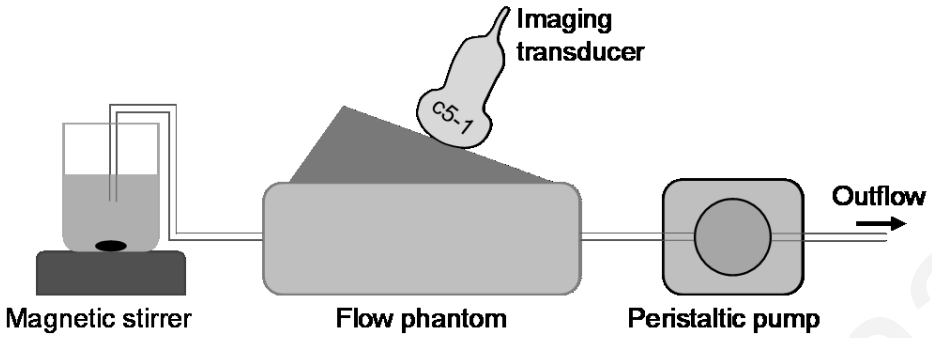

Figure 4-1: Schematic representation of the flow phantom setup.

4.2.2 Microbubbles

BR14 microbubbles were used throughout this work. The microbubbles were prepared according to the manufacturer's specifications. A total of 4 microbubble solutions were prepared with concentrations 0.01‰, 0.05‰, 0.1‰, 0.3‰. The concentrations are given in milliliters of contrast agent per liter of deionized water (e.g. 0.01‰ = 0.01 ml UCA / liter of DI water) and they cover a very wide range of concentrations often used in clinical cases. It is possible though with these microbubble concentrations to encounter the nonlinear propagation artifact [42, 43], and acoustic shadowing [44].

The total experiment time was held below one hour following vial reconstitution in order to limit microbubble deterioration to an absolute minimum. Vial-to-vial reproducibility was addressed by repeating the experiments 3 times using different vials and the results are presented as mean ± standard error of the mean.

4.2.3 Ultrasound scanner settings and imaging

Microbubble interrogation and imaging was performed with a C5-1 probe (curve-linear array) of the Phillips iU-22 diagnostic ultrasound scanner. The penetration setting in harmonic mode (HPEN) was used where a 3.5 cycle hamming windowed pulse with center frequency of 1.5 MHz was transmitted (largest duration at lowest frequency available on B-mode on the C5-1 probe). A single pulse scheme (we avoided pulse inversion) was chosen to eliminate any effects due to motion or destruction of the microbubbles between multiple pulses. The receive center frequency was 3 MHz. The MI was varied from 0.05 to

2.1 (see Table 4-1) which corresponds to peak negative pressures of 0.06 MPa to 2.6 MPa. Research software on the iU22 allowed us to increase the MI beyond the maximum FDA limit of 1.9. The frame rate was set at 1.0 Hz, to ensure that the tube in the image plane was refreshed with new bubbles in every frame.

4.2.4 Image quantification and gain adjustment procedure

Video loops of 8 images (taken over 8 s) were captured for each MI. The quantification software QLAB (Philips Medical Systems, Bothell, WA) was used to measure backscattered signal intensity by placing a region of interest (ROI) in the middle of the phantom tube and calculating the average backscatter intensity from that region. In order to check for the possibility of acoustic shadowing, two smaller ROIs one at the top and one at the bottom of the phantom tube were also placed and the analysis was repeated.

To avoid signal saturation, the compression (dynamic range) was set to the maximum value and a specific 2D gain setting for each MI was carefully selected making sure that the image of the microbubbles was not very close to the maximum value of the color map. A list of the 2D gain settings chosen for each MI is shown in Table 4-1.

Table 4-1: Optimal 2D Gain per MI to avoid signal saturation for concentrations C≤0.1‰ and for C>0.1‰.

MI	Gain (C≤0. 1‰)	Gain (C>0. 1‰)
<0.05	80	77
0.1	70	67
0.3	54	51
0.5	48	45
0.6	44	41
0.8	41	38
1.0	38	35
1.3	34	31
1.6	33	30
2.1	31	28

During the analysis of the data an inverse adjustment to a chosen reference 2D gain value was made so that the results from different gains could be plotted together. If for example, at MI=0.1 the 2D gain was adjusted from a reference 80 dB to 70 dB to avoid signal saturation, then during the analysis of the results, the measured intensity data was increased by 10 dB in order to match the reference value of 80 dB. Similarly, MI=0.3 was increased by 16 dB, MI 0.5 by 32dB and so on (see Table 4-1).

The gain adjustment method is further explained and demonstrated in Figs. 4-2 and 4-3. In Fig. 4-2(a-c) images of the flow phantom in the absence of microbubbles at MIs 0.6, 1.0 and 2.1 with a fixed 2D gain of 44 dB are shown. Images at MIs 0.8, 1.3, and 1.6 also captured but not shown here. A region of interest is chosen in the tissue and its average intensity is measured as a function of MI as shown by the solid line with cross-hair markers in Fig. 4-3. The same procedure is followed at a higher 2D gain (56 dB) and the images acquired are shown in Fig. 4-2(d-e). The corresponding measured intensity-MI relation is shown in Fig. 4-3 (solid line with square markers). When each intensity point on the 44 dB curve is given an additional 12 dB, the line labeled as "Gain 56 corrected" (dashed line with circle markers) in Fig. 4-3 is obtained. Good agreement between the measured and corrected 56 dB 2D gain values is obtained. The measured intensities can be adjusted to any reference value as long as there is no signal saturation. For the work presented here, the maximum 2D gain (80 dB) was chosen as the reference point.

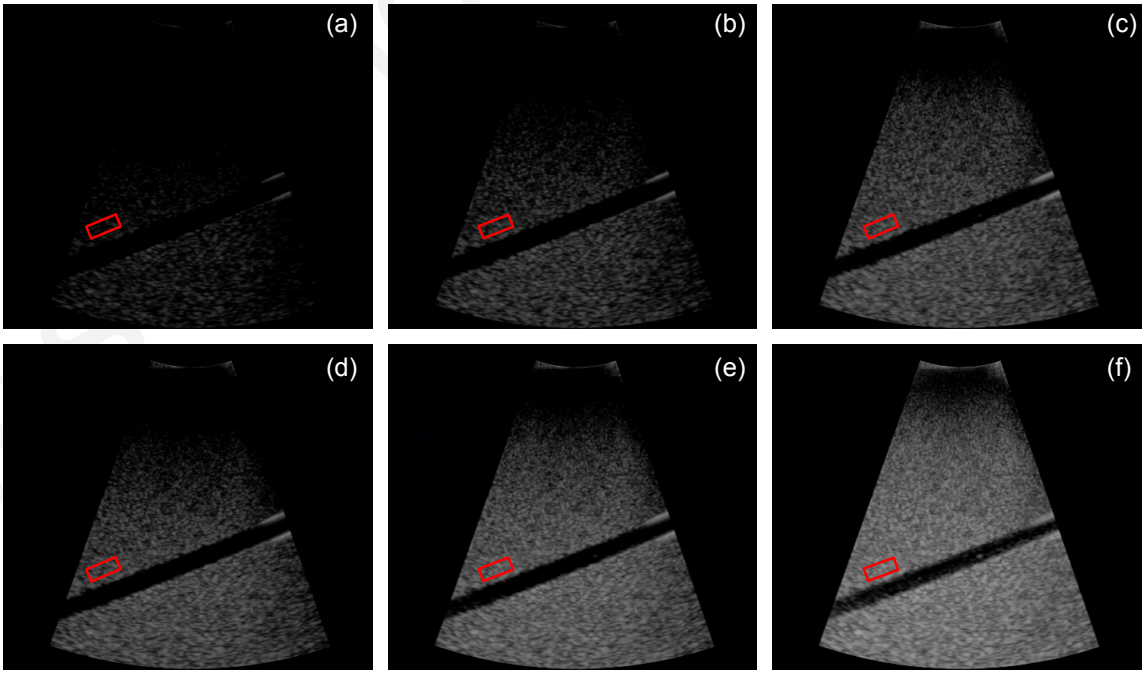

Figure 4-2: Flow phantom images without UCAs. (a-c) 2D Gain set at 44 dB for MI=0.6, 1.0 and 2.1 respectively. (d-f) 2D Gain set at 56 dB for MI=0.6, 1.0 and 2.1 respectively.

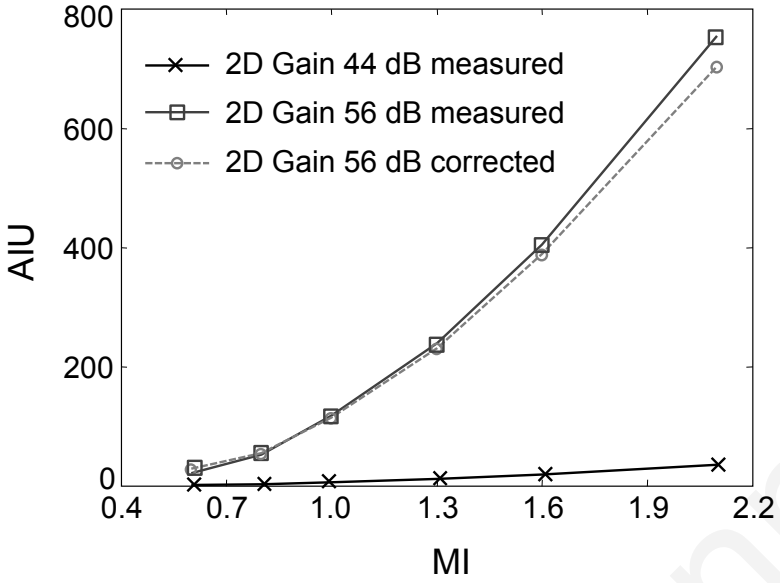

Figure 4-3: Backscatter tissue signal intensity as a function of MI measured at two different 2D Gains (56 and 44 dB) and intensity collected at 44 dB and adjusted to 56 dB.

4.3 Results

In Figure 4-4 images of the phantom vessel filled with microbubbles are shown for two different gain settings. In Fig. 4-4(a-c) images of microbubbles acquired with MIs 0.1, 1.0 and 2.1 respectively are shown. The concentration was 0.1‰ and the 2D gain was held fixed at the default value of 70 dB. While the image in Fig. 4-4(a) offers a clean signal with a high CTR, the bubble backscatter signal in (b) and (c) is saturated (very close to being all white) and the CTR is significantly reduced (the vessel is not easily separated from the tissue). Images of the same microbubble solution under the same pressures are shown in Fig. 4-4 (d-f) with the 2D gain adjusted accordingly. For MI 0.1 the gain was kept at 70 dB, but was reduced to 38 dB for MI 1.0 and 31 dB for MI 2.1 thus limiting saturation and increasing the CTR.

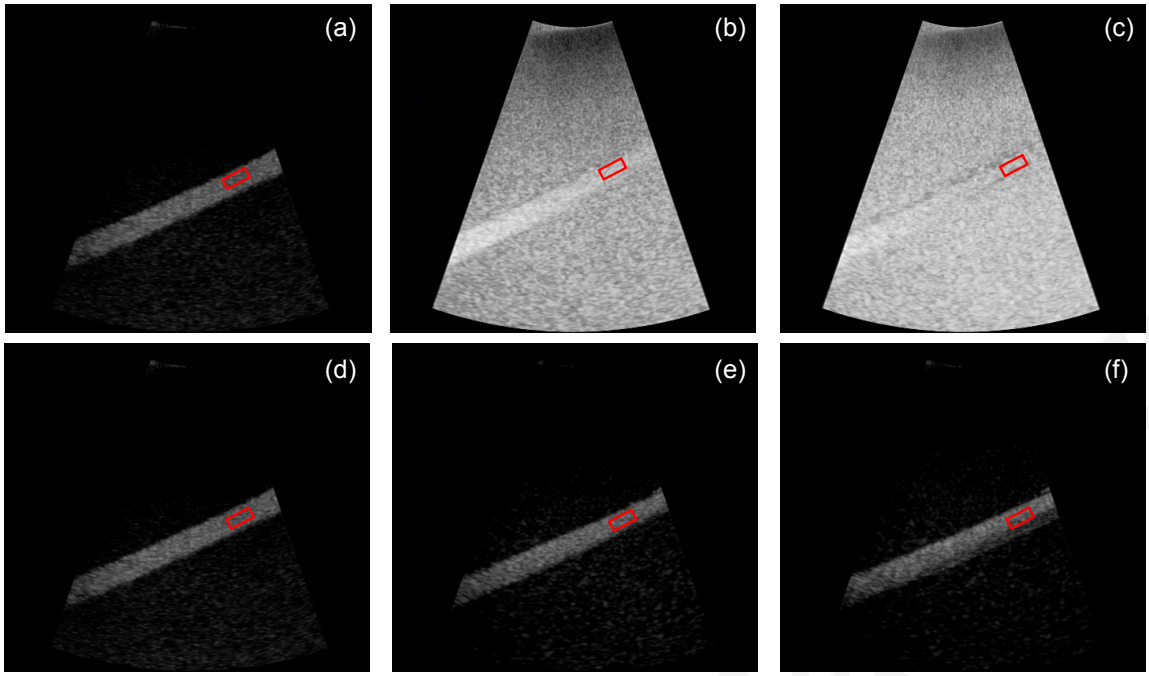

Figure 4-4: Flow phantom images at MI (a) 0.1, (b) 1.0, and (c) 2.1 at constant 2D Gain (70 dB). The images in (d), (e), and (f) are taken at their optimal gain (70, 38, and 31 dB respectively) to avoid saturation. The microbubble concentration is 0.1‰.

A comparison of the microbubble backscatter intensity as a function of MI with and without the gain adjustment method is made in Fig. 4-5. The measured intensity with the 2D gain fixed at 80 dB is shown with the solid line, while the dashed line presents the results after the gain adjustment method was applied. A logarithmic scale was used in this plot in order to better accommodate the large dynamic range of the intensities obtained. With a fixed 2D gain of 80 dB, signal saturation begins as early as MI 0.3 and the signal becomes completely saturated at MI>0.5 where further increase in pressure does not result in any increase in backscatter intensity. When the proposed 2D gain adjustment method is applied however, saturation is eliminated and the true microbubble response to increasing amplitude can be obtained.

Figure 4-6 shows the backscattered intensity as a function of MI for microbubble concentrations 0.1‰, 0.05‰, and 0.01‰. The 2D gain adjustment method used with reference to 80 dB. Figure 4-6(a) displays the entire MI range ($0.05 \leq MI \leq 2.1$), while Figs. 4-6(b, c) zoom into $0 < MI \leq 0.5$ and $0 < MI \leq 0.15$ respectively. With saturation now removed, a quadratic increase of backscattered signal intensity with MI is observed.

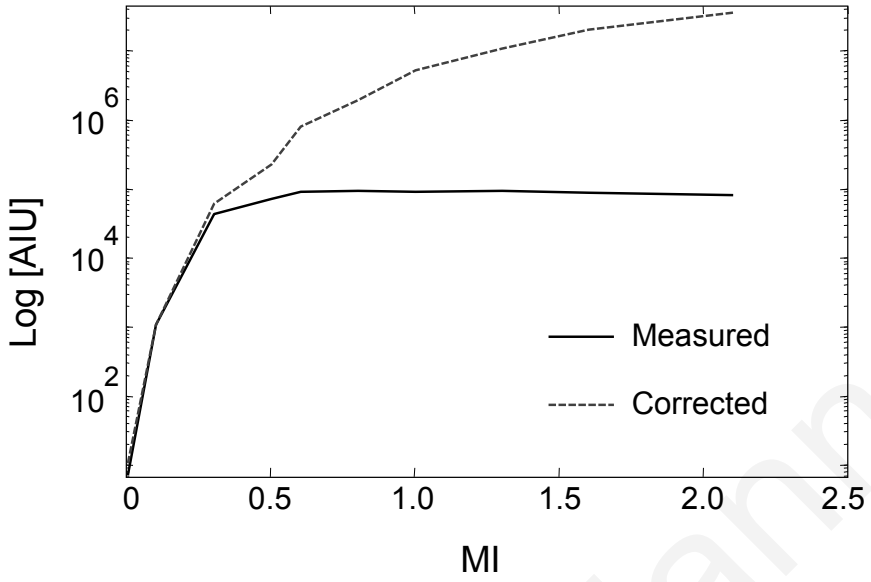

Figure 4-5: Contrast microbubble intensity as a function of MI. Measurements with 2D Gain fixed at 80 dB (solid line) compared to corrected values using the 2D Gain adjustment method (dashed line) for microbubble concentration of 0.1‰.

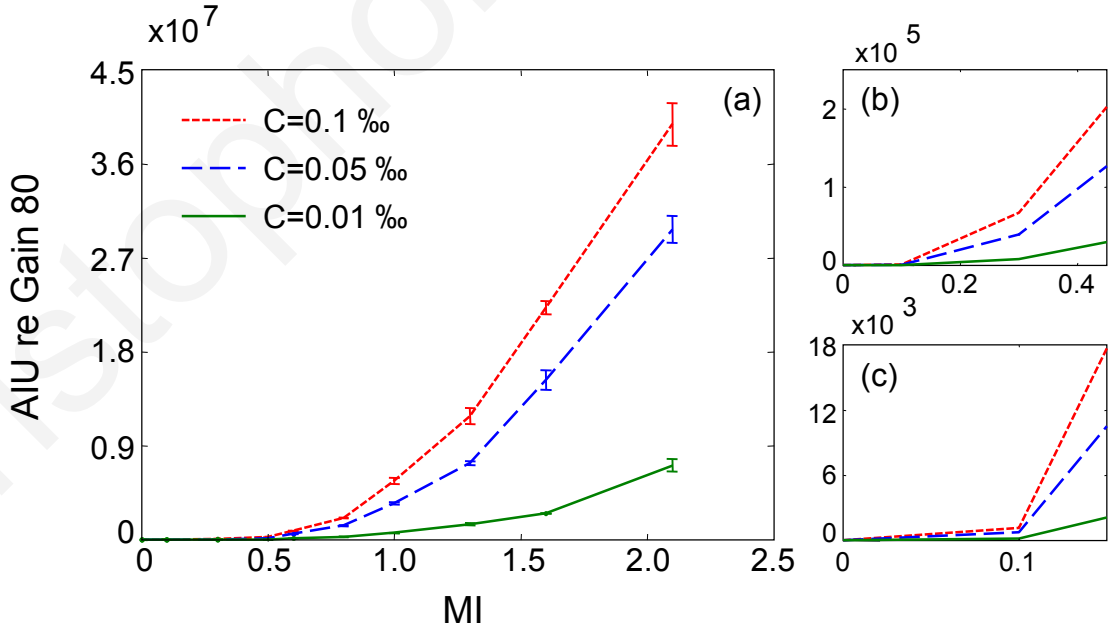

Figure 4-6: (a) Bubble backscattered signal intensity as a function of MI for 3 different concentrations. All values are adjusted to a reference 2D Gain of 80 dB. (b, c) Zoom into a smaller range of MIs, $0 \leq MI \leq 0.5$ and $0 \leq MI \leq 0.15$ respectively.

The backscattered intensity as a function of concentration for three different MIs (0.1, 1.0 and 2.1) is shown in Fig. 4-7. At MI=0.1, an almost linear relationship is observed, confirming previously published results [21]. There is some deviation from linearity at higher concentrations (not shown here). As the pressure increases however [Fig. 4-7 (b, c)], the deviation from linearity occurs at a lower concentrations.

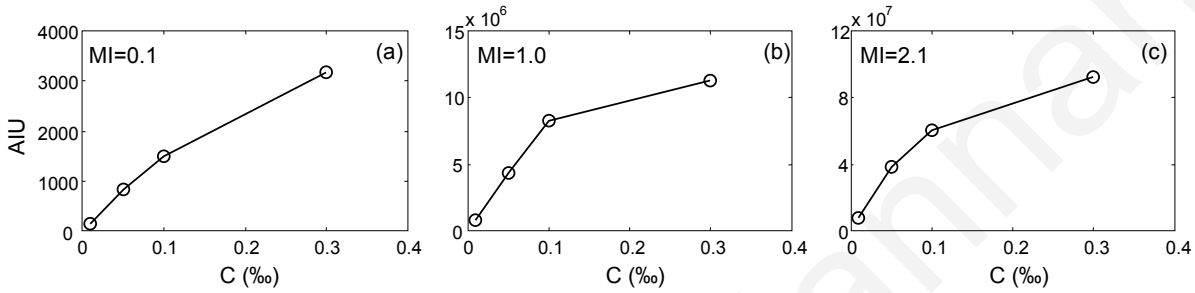

Figure 4-7: Intensity as a function of microbubble concentration for 3 different MIs. (a) MI=0.1, (b) MI=1.0 and (c) MI=2.1, adjusted to a reference 2D Gain of 80 dB.

To be able to isolate the effect of acoustic shadowing, the analysis of the signal from the vessel was repeated by placing two ROIs one at the top and one at the bottom of the tube as seen in Fig. 4-8 (a-d). The backscattered intensity as a function of MI for the two ROIs is shown in Figs. 4-7(e-h) for microbubble concentrations 0.01‰, 0.05‰, 0.1‰, and 0.3‰ respectively. The solid lines represent the top ROIs and the dashed lines the bottom ROIs. At low MIs we observe that the signal intensities from the two regions are very similar. As the pressure increases the backscatter intensity from the top region becomes significantly greater than the backscatter intensity from the bottom region. This difference is greater as the concentration increases and it is observed at a lower MI. At concentration 0.3‰, the deviation is observed as low as MI 0.15 while for concentration 0.01‰ there is no difference and two lines coincide though the entire MI range.

A comparison between tissue nonlinear echoes resulting from nonlinear propagation and microbubble backscattered nonlinear signal as a function of MI is shown in Fig. 4-9. The ROIs which were used to extract the signal for this plot (one in tissue and one in the phantom vessel) were placed at the same image depth. The dashed line shows the tissue and the solid line the microbubble signal intensity. Both the tissue and bubble signals increase with MI. The difference between the bubble and tissue signals (in dB), CTR, is shown in dashed line. Surprisingly, higher CTRs are observed with increasing MI.

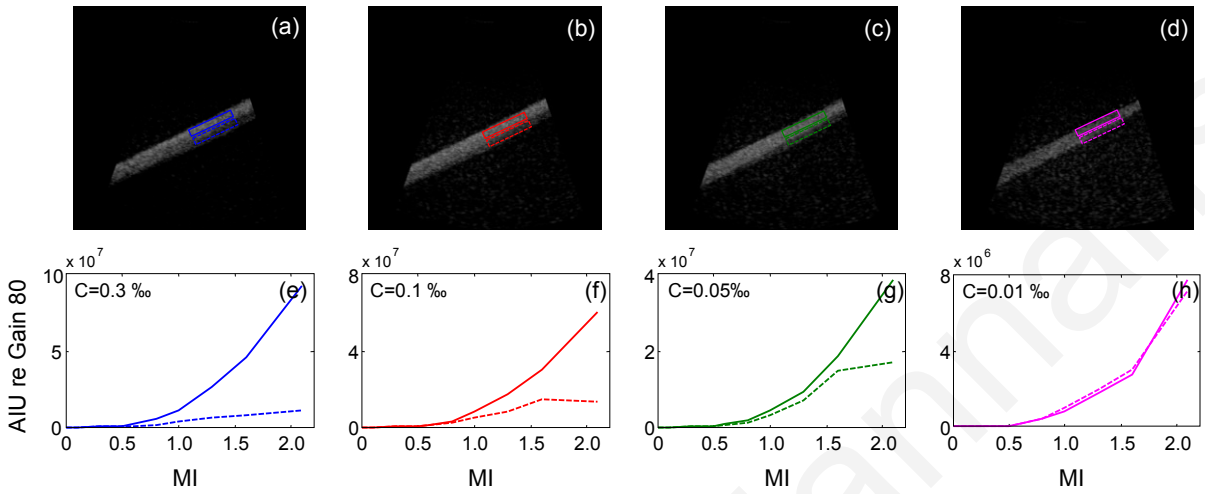

Figure 4-8: Images taken at MI=2.1 of the flow tube (a-d) and bubble backscattered signal intensity as a function of mechanical index (e-h) from 2 ROIs; one at the top and one at the bottom of the flow tube. All intensity plots are adjusted to a reference 2D Gain

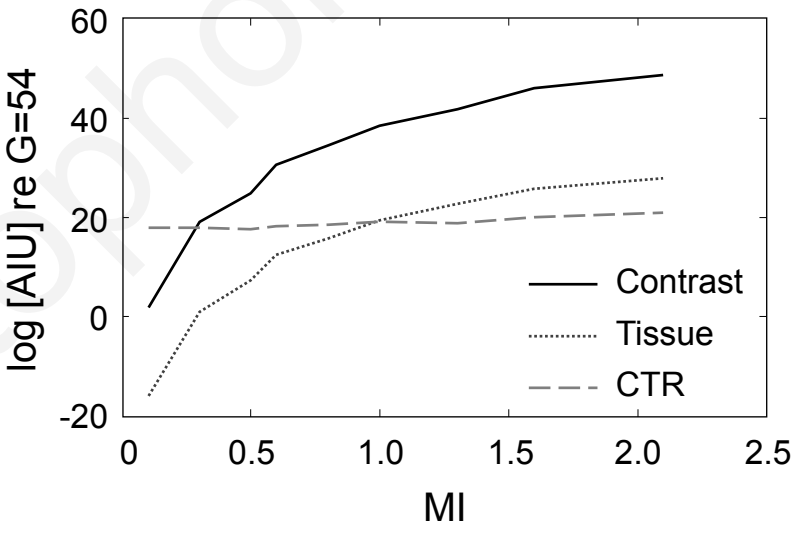

Figure 4-9: Tissue (dotted line) and contrast microbubbles (solid line) backscattered signal intensity at the second harmonic as a function of MI. The reference 2D Gain is 54 dB and the concentration 0.05‰. Contrast to tissue ratio (CTR), calculated as the difference in dB between microbubbles and tissue intensity is shown in dashed line.

4.4 Discussion

In this work, a diagnostic ultrasound scanner was used to accurately measure microbubble backscattering produced with large range of MIs (0.05-2.1). Despite the fact that this is a relatively simple task, it has not been addressed in the past and one of the main obstacles was signal saturation often present in diagnostic ultrasound scanners. The question of how the microbubbles behave as the MI is increased (even above the FDA imaging limit) was addressed. It was observed that up to acoustic pressures of 2.6 MPa, the backscattered intensity from microbubbles increased quadratically, in agreement with previously published results [45]. Specifically, in the work of Shi and Forsberg [45], the measured second harmonic of the backscattered signal as a function of acoustic pressure in double logarithmic scale could be fitted to curves with slopes of 1.8-1.9. Those results were in good agreement with theoretical predictions [46, 47] showing that the second harmonic bubble response amplitude is proportional to the square of the acoustic amplitude. Also in agreement with the above results, Sboros et al. [48] reported a linear increase in normalized scattering (with respect to the linear scattering from blood mimicking fluid particles) with increasing acoustic pressure.

A key factor in being able to accurately record backscattered signals at very high pressures was the 2D gain adjustment procedure. Knowledge of bubble response to a range of acoustic pressures is important when studying therapeutic applications of microbubbles and ultrasound such as sonoporation, sonothrombolysis, and gene transfection. The amplitude of bubble oscillations is important when considering the various sonoporation hypothesis relying on phenomena such as microjet formation and cell membrane disruption [49].

As seen in Fig. 4-7, with increasing MI there is a deviation from linearity in the intensity—concentration relationship. Since signal saturation was limited with the method of continuously adjusting the analog gain and accounting for it in the quantification software, the only other cause of this deviation from linearity is acoustic shadowing. It was confirmed from the results of Fig. 4-8 that acoustic shadowing was indeed present, as the signal from the top ROI increased quadratically while the signal from the bottom ROI plateaued at a certain value. As expected, acoustic shadowing increased with concentration. Additionally, according to the results of Fig. 4-7, shadowing also increases with increasing MI which is in agreement with previously published results [50].

Nonlinear propagation in tissue takes place as the transmitted pressure increases [51, 52]. The tissue harmonics are mixed with the microbubble harmonics at the higher MIs. The careful and accurate measurement of CTR has revealed that there is not an optimal MI at which microbubbles may be imaged, contrary to previous perception [14]. The low MI is chosen today in order to avoid bubble destruction, but microbubbles may be imaged equally well at larger MIs also. According to our results in Fig. 4-9, the general trend is that CTR increases with MI even at higher than diagnostic imaging MIs. For example, in drug delivery applications at MIs that cause bubble destruction, good triggered images (in order to allow for microbubble replenishment in the imaging plane) with nonlinear techniques (e.g. harmonic imaging) may be formed by simply thresholding the tissue signals due to nonlinear propagation. Based on our results, the only benefit of using a low MI is for enabling real-time imaging but it does not offer any increased CTR compared to using high MI.

An interesting outcome of our results is that both tissue and microbubble nonlinear signals continue to increase in the range of MIs considered. The tissue nonlinear signal from Fig. 4-9 is compared with a theoretical prediction based on the KZK equation [53] in Fig. 4-10. Propagation in a tissue like medium of a sound beam from a circular focused source was simulated. The excellent agreement of the measurement with theoretical predictions suggests once more that our method of adjusting the 2D gain to avoid signal saturation enables the true representation of the tissue response.

Nonlinear propagation can affect microbubble excitation pulses since at high pressures the propagated pulse gets distorted and also contains harmonic components in addition to the fundamental frequency. A change of the excitation pulse to include harmonic components has an impact on the microbubble response and has been briefly addressed before [54, 55], but it must be revisited again now when large amplitude pulses are used in therapeutic applications of ultrasound and microbubbles.

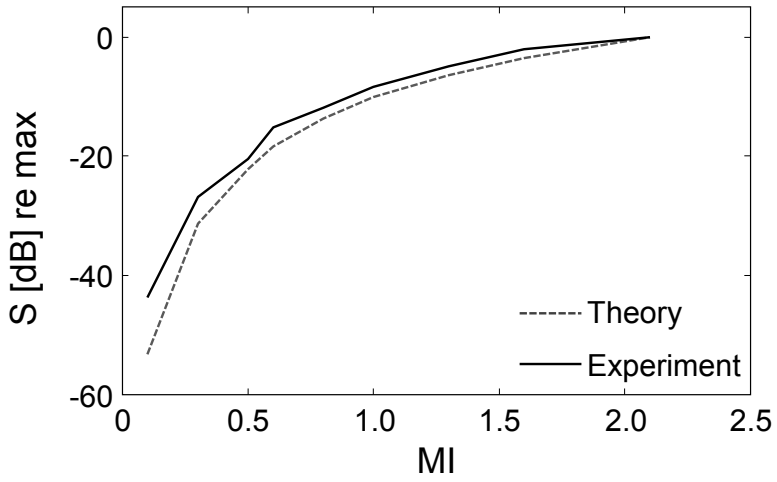

Figure 4-10: Theoretical prediction (dashed line) and measurements (solid line) of second harmonic echoes from tissue as a function of increasing amplitude.

4.5 Conclusion

A method for accurately and continuously adjusting the receive gain of ultrasound scanners and accounting for it in the quantification software in order to effectively limit signal saturation was developed. A quadratic relationship of backscattered pressure with acoustic excitation pressures for up to MI=2.1 was measured in a flow phantom. Contrast microbubbles produced higher responses with higher pressures without reaching any plateau. The intensity of the microbubbles echoes increased with concentration both at low MI, as previously measured, but also at high MIs. The contrast to tissue ratio was measured and found to increase with MI for all the range of MIs considered, thus allowing for imaging approaches in therapeutic procedures that use MIs above the bubble destruction threshold.

References

[1] M. Averkiou, et al., "Quantification of tumor microvascularity with respiratory gated contrast enhanced ultrasound for monitoring therapy," Ultrasound in Medicine & Biology, vol. 36, pp. 68-77, 2010/01// 2010.

[2] D. Cosgrove and N. Lassau, "Imaging of perfusion using ultrasound," European journal of nuclear medicine and molecular imaging, vol. 37 Suppl 1, pp. S65-85, 2010/08// 2010.

[3] V. Sboros and M. X. Tang, "The assessment of microvascular flow and tissue perfusion using ultrasound imaging," Proceedings of the Institution of Mechanical Engineers. Part H, Journal of engineering in medicine, vol. 224, pp. 273-290, 2010 2010.

[4] S. R. Wilson and P. N. Burns, "Microbubble-enhanced US in body imaging: what role?," Radiology, vol. 257, pp. 24-39, 2010/10// 2010.

[5] K. Wei, et al., "Quantification of myocardial blood flow with ultrasound-induced destruction of microbubbles administered as a constant venous infusion," Circulation, vol. 97, pp. 473-483, 1998/02/10/ 1998.

[6] E. Leen, et al., "Potential role of doppler perfusion index in selection of patients with colorectal cancer for adjuvant chemotherapy," Lancet, vol. 355, pp. 34-37, 2000/01/01/ 2000.

[7] S. R. Wilson and P. N. Burns, "Liver mass evaluation with ultrasound: the impact of microbubble contrast agents and pulse inversion imaging," Seminars in liver disease, vol. 21, pp. 147-159, 2001/05// 2001.

[8] J. R. Lindner, "Microbubbles in medical imaging: current applications and future directions," Nature reviews. Drug discovery, vol. 3, pp. 527-532, 2004/06// 2004.

[9] S. Mehier-Humbert, et al., "Ultrasound-mediated gene delivery: influence of contrast agent on transfection," Bioconjugate chemistry, vol. 18, pp. 652-662, 2007/06//May- undefined 2007.

[10] A. A. Rahim, et al., "Spatial and acoustic pressure dependence of microbubble-mediated gene delivery targeted using focused ultrasound," The journal of gene medicine, vol. 8, pp. 1347-1357, 2006/11// 2006.

[11] C. A. Molina, et al., "Microbubble administration accelerates clot lysis during continuous 2-MHz ultrasound monitoring in stroke patients treated with intravenous tissue plasminogen activator," Stroke; a Journal of Cerebral Circulation, vol. 37, pp. 425-429, 2006/02// 2006.

[12] M. R. Böhmer, et al., "Ultrasound triggered image-guided drug delivery," European Journal of Radiology, vol. 70, pp. 242-253, 2009/05// 2009.

[13] D. B. Ellegala, et al., "Imaging tumor angiogenesis with contrast ultrasound and microbubbles targeted to alpha(v)beta3," Circulation, vol. 108, pp. 336-341, 2003/07/22/ 2003.

[14] J.-M. Escoffre, et al., "Doxorubicin liposome-loaded microbubbles for contrast imaging and ultrasound-triggered drug delivery," IEEE Transactions on Ultrasonics, Ferroelectrics, and Frequency Control, vol. 60, pp. 78-87, 2013/01// 2013.

[15] C. Mannaris and M. A. Averkiou, "Investigation of microbubble response to long pulses used in ultrasound-enhanced drug delivery," Ultrasound in Medicine & Biology, vol. 38, pp. 681-691, 2012/04// 2012.

[16] G. E. R. Weller, et al., "Ultrasonic imaging of tumor angiogenesis using contrast microbubbles targeted via the tumor-binding peptide arginine-arginine-leucine," Cancer research, vol. 65, pp. 533-539, 2005/01/15/ 2005.

[17] D. H. Simpson, et al., "Pulse inversion Doppler: a new method for detecting nonlinear echoes from microbubble contrast agents," IEEE Transactions on Ultrasonics, Ferroelectrics, and Frequency Control, vol. 46, pp. 372-382, 1999 1999.

[18] M. A. Averkiou, et al., "Pulsing schemes for the detection of nonlinear echoes from contrast microbubbles," in 9th European Symposium on Ultrasound Contrast Imaging, 2004.

[19] M. Averkiou, et al., "Ultrasound contrast imaging research," Ultrasound quarterly, vol. 19, pp. 27-37, 2003/03// 2003.

[20] G. A. Brock-Fisher, et al., "Means for increasing sensitivity in non-linear ultrasound imaging systems," US5577505 A, Nov 26, 1996, 1996.

[21] M. Lampaskis and M. Averkiou, "Investigation of the relationship of nonlinear backscattered ultrasound intensity with microbubble concentration at low MI," Ultrasound in Medicine & Biology, vol. 36, pp. 306-312, 2010/02// 2010.

[22] R. E. Appel, "Possibility of microcavitation from diagnostic ultrasound," IEEE Transactions on Ultrasonics, Ferroelectrics, and Frequency Control, vol. 33, pp. 139-142, 1986 1986.

[23] C. K. Holland and R. E. Apfel, "Thresholds for transient cavitation produced by pulsed ultrasound in a controlled nuclei environment," The Journal of the Acoustical Society of America, vol. 88, pp. 2059-2069, 1990/11// 1990.

[24] W. T. Shi, et al., "Destruction of contrast microbubbles and the association with inertial cavitation," Ultrasound in Medicine & Biology, vol. 26, pp. 1009-1019, 2000/07// 2000.

[25] P. Marmottant and S. Hilgenfeldt, "Controlled vesicle deformation and lysis by single oscillating bubbles," Nature, vol. 423, pp. 153-156, 2003/05/08/ 2003.

[26] M. R. Böhmer, et al., "Focused ultrasound and microbubbles for enhanced extravasation," Journal of controlled release: official journal of the Controlled Release Society, vol. 148, pp. 18-24, 2010/11/20/ 2010.

[27] K. Ferrara, et al., "Ultrasound microbubble contrast agents: fundamentals and application to gene and drug delivery," Annual review of biomedical engineering, vol. 9, pp. 415-447, 2007 2007.

[28] K. Kooiman, et al., "Increasing the endothelial layer permeability through ultrasound-activated microbubbles," IEEE transactions on bio-medical engineering, vol. 57, pp. 29-32, 2010/01// 2010.

[29] A. Yudina, et al., "Evaluation of the temporal window for drug delivery following ultrasound-mediated membrane permeability enhancement," Molecular imaging and biology: MIB: the official publication of the Academy of Molecular Imaging, vol. 13, pp. 239-249, 2011/04// 2011.

[30] R. Bekeredjian, et al., "Augmentation of cardiac protein delivery using ultrasound targeted microbubble destruction," Ultrasound in Medicine & Biology, vol. 31, pp. 687-691, 2005/05// 2005.

[31] S. Chen, et al., "Optimization of ultrasound parameters for cardiac gene delivery of adenoviral or plasmid deoxyribonucleic acid by ultrasound-targeted microbubble destruction," Journal of the American College of Cardiology, vol. 42, pp. 301-308, 2003/07/16/ 2003.

[32] H. Fujii, et al., "Ultrasound-targeted gene delivery induces angiogenesis after a myocardial infarction in mice," JACC. Cardiovascular imaging, vol. 2, pp. 869-879, 2009/07// 2009.

[33] F. Xie, et al., "Diagnostic ultrasound combined with glycoprotein IIb/IIIa-targeted microbubbles improves microvascular recovery after acute coronary thrombotic occlusions," Circulation, vol. 119, pp. 1378-1385, 2009/03/17/ 2009.

[34] K. F. Bing, et al., "Blood-brain barrier (BBB) disruption using a diagnostic ultrasound scanner and Definity in Mice," Ultrasound in Medicine & Biology, vol. 35, pp. 1298-1308, 2009/08// 2009.

[35] S. Kotopoulis, et al., "Treatment of human pancreatic cancer using combined ultrasound, microbubbles, and gemcitabine: a clinical case study," Medical Physics, vol. 40, 2013/07// 2013.

[36] V. Sboros, et al., "Understanding the limitations of ultrasonic backscatter measurements from microbubble populations," Physics in Medicine and Biology, vol. 47, pp. 4287-4299, 2002/12/07/ 2002.

[37] T. P. Gauthier, et al., "Perfusion quantification using dynamic contrast-enhanced ultrasound: the impact of dynamic range and gain on time-intensity curves," Ultrasonics, vol. 51, pp. 102-106, 2011/01// 2011.

[38] S.-H. Hung, et al., "A simple method for quantifying ultrasound-triggered microbubble destruction," Ultrasound in Medicine & Biology, vol. 37, pp. 949-957, 2011/06// 2011.

[39] T. Schlosser, et al., "Echoscintigraphy: a new imaging modality for the reduction of color blooming and acoustic shadowing in contrast sonography," Ultrasound in Medicine & Biology, vol. 29, pp. 985-991, 2003/07// 2003.

[40] N. de Jong, "Mechanical index," European Journal of Echocardiography: The Journal of the Working Group on Echocardiography of the European Society of Cardiology, vol. 3, pp. 73-74, 2002/03// 2002.

[41] M. Schneider, et al., "Gray-scale liver enhancement in VX2 tumor-bearing rabbits using BR14, a new ultrasonographic contrast agent," Investigative Radiology, vol. 32, pp. 410-417, 1997/07// 1997.

[42] M.-X. Tang and R. J. Eckersley, "Nonlinear propagation of ultrasound through microbubble contrast agents and implications for imaging," IEEE Transactions on Ultrasonics, Ferroelectrics, and Frequency Control, vol. 53, pp. 2406-2415, 2006/12// 2006.

[43] A. Thapar, et al., "Dose-dependent artifact in the far wall of the carotid artery at dynamic contrast-enhanced US," Radiology, vol. 262, pp. 672-679, 2012/02// 2012.

[44] M. X. Tang, et al., "Quantitative contrast-enhanced ultrasound imaging: a review of sources of variability," Interface focus, vol. 1, pp. 520-539, 2011/08/06/ 2011.

[45] W. T. Shi and F. Forsberg, "Ultrasonic characterization of the nonlinear properties of contrast microbubbles," Ultrasound in Medicine & Biology, vol. 26, pp. 93-104, 2000/01// 2000.

[46] C. C. Church, "The effects of an elastic solid surface layer on the radial pulsations of gas bubbles," The Journal of the Acoustical Society of America, vol. 97, pp. 1510-1521, 1995 1995.

[47] N. de Jong, et al., "Higher harmonics of vibrating gas-filled microspheres. Part one: simulations," Ultrasonics, vol. 32, pp. 447-453, 1994/11// 1994.

[48] V. Sboros, et al., "The dependence of ultrasound contrast agents backscatter on acoustic pressure: theory versus experiment," Ultrasonics, vol. 40, pp. 579-583, 2002/05// 2002.

[49] I. Lentacker, et al., "Understanding ultrasound induced sonoporation: definitions and underlying mechanisms," Advanced Drug Delivery Reviews, 2013/11/21/ 2013.

[50] M.-X. Tang and R. J. Eckersley, "Frequency and pressure dependent attenuation and scattering by microbubbles," Ultrasound in Medicine & Biology, vol. 33, pp. 164-168, 2007/01// 2007.

[51] M. A. Averkiou, "Tissue harmonic ultrasonic imaging," Comptes Rendus de l'Academie des Sciences - Series IV: Physics, Astrophysics, vol. 2, pp. 1139-1151, 2001 2001.

[52] B. Ward, et al., "Nonlinear propagation applied to the improvement of resolution in diagnostic medical ultrasound," The Journal of the Acoustical Society of America, vol. 101, pp. 143-154, 1997/01// 1997.

[53] M. A. Averkiou and M. F. Hamilton, "Nonlinear distortion of short pulses radiated by plane and focused circular pistons," J Acoust Soc Am, vol. 102, pp. 2539-48, Nov 1997.

[54] E. J. Ayme and E. L. Carstensen, "Cavitation induced by asymmetric distorted pulses of ultrasound: theoretical predictions," IEEE Transactions on Ultrasonics, Ferroelectrics, and Frequency Control, vol. 36, pp. 32-40, 1989 1989.

[55] E. J. Aymé and E. L. Carstensen, "Occurrence of transient cavitation in pulsed sawtooth ultrasonic fields," The Journal of the Acoustical Society of America, vol. 84, pp. 1598-1605, 1988/11// 1988.

5

In vitro localized release of thermosensitive liposomes with ultrasound induced hyperthermia

Localized drug delivery with ultrasound induced hyperthermia can enhance the therapeutic index of chemotherapeutic drugs by improving the efficacy and reducing systemic toxicity. A novel *in vitro* method for the activation of drug loaded thermosensitive liposomes is presented. In particular, a dual compartment, acoustically transparent container is used where thermosensitive liposomes suspended in cell culture medium are immersed in a thermally absorptive medium, glycerol. Ultrasound induced hyperthermia is first applied in the glycerol which in turn heats the culture medium by thermal conduction. The method approximately mimics the *in vivo* scenario of thermosensitive liposomes collected in the interstitial spaces of tumors where ultrasound induces hyperthermia in the tumor tissue which in turn heats the thermosensitive liposomes by conduction and induces the release of the encapsulated drug. The acoustic conditions for the desired hyperthermia are derived theoretically and validated experimentally. An 80% release of doxorubicin from thermosensitive liposomes is achieved.

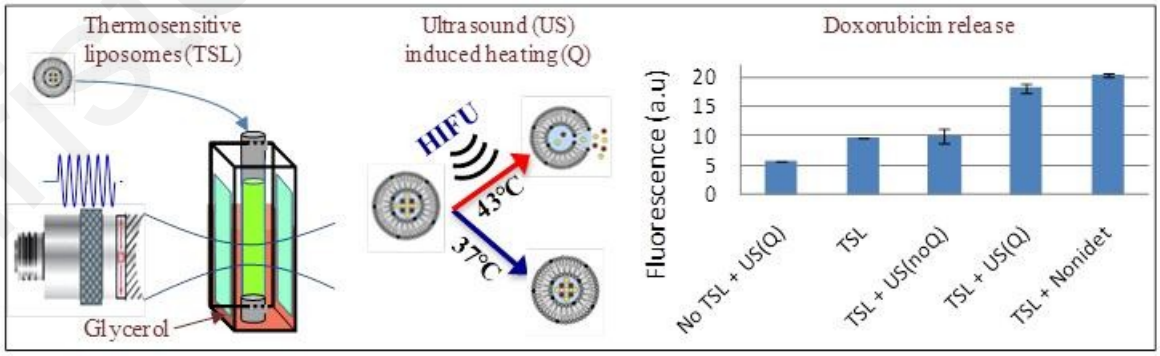

Published as: C. Mannaris, *et al.*, "In vitro localized release of thermosensitive liposomes with ultrasound-induced hyperthermia," *Ultrasound in Medicine & Biology,* vol. 39, pp. 2011-20, Nov 2013.

5.1 Introduction

Increasing the therapeutic index (the ratio of the average toxic dose to the average therapeutic dose) of anti-cancer pharmaceuticals is one of the main challenges in cancer therapy today. Conventional cancer treatment procedures using chemotherapy drugs, such as the widely used anthracycline doxorubicin, are limited mainly due to the severe and undesired side effects. Liposomes were initially designed as possible drug carriers for reduced systemic exposure. Nowadays, liposomal formulations of doxorubicin (Doxil®, Caelyx ®) are used in the clinic and have shown the ability to reduce cytotoxicity in healthy tissue compared to their unencapsulated counterpart [1, 2]. In addition, increased accumulation of the drug loaded liposomes was observed in tumors, mainly due to the enhanced permeability and retention (EPR) effect [1, 3-6]. A major drawback however was the limited bioavailability of the drug within the tumor. Despite the higher concentrations of liposomal drug present, the passive drug release from the liposomes is slow resulting in reduced drug effectiveness [7, 8].

Over the past 30 years, technological advances have resulted in the development of a variety of liposomes that can be triggered to release their payload following an external stimulus [9]. The use of mild hyperthermia as a stimulus for the activation of thermosensitive liposomes (TSLs) was first proposed in 1978 by Yatvin et al. [10] and has gained significant momentum over the last decade [11]. Furthermore, hyperthermia has also been known to increase the liposomal accumulation in tumors. In their review, Kong and Dewhirst [12] identify over 100 reports where tumors treated with hyperthermia exhibited increased drug accumulation as well as improved efficacy for a variety of drugs. Finally, pre-clinical studies have shown that hyperthermia may augment the potency of several chemotherapeutic agents [13, 14] in addition to itself being directly cytotoxic [15].

Thermosensitive liposomes remain stable for a long time in circulation under physiological temperatures and are able to quickly release their encapsulated content (e.g. doxorubicin) when heated near their phase transition temperature (T_m), where the liposome membrane changes from a gel to a liquid crystalline phase [8, 10, 12, 16-20]. Several sources of hyperthermia have been considered over the years, including superficial heating with water baths [8, 16, 19, 21-24], microwave radiation [25-27], infra-red radiation [28], and heating with invasive catheters [29-31]. Lately, the use of ultrasound as an external energy source to trigger drug release from thermosensitive liposomes is becoming increasingly more popular [32-34]. Briefly, focused ultrasound is used to non-invasively induce local hyperthermia with millimeter accuracy in a selected region of interest. Recent advances in electronic and mechanical ultrasound beam steering have enabled the uniform

heating of larger targets such as a tumor deep inside the human body while maintaining physiological temperatures in the surrounding tissue and along the path of ultrasound propagation [35-41]. The combined benefits of ultrasound, hyperthermia and drug loaded thermosensitive liposomes pose a very attractive localized drug delivery approach and show great potential in increasing the therapeutic index in cancer treatment.

Whereas more and more reports of *in vivo* studies with ultrasound as a source of hyperthermia are being published [32, 42-47], reports for *in vitro* work are scarce. *In vitro* work is a logical precursor to *in vivo* work since is allows simplifications of the system under study, offers a more predictable and controlled environment and is usually both time and cost efficient when compared to *in vivo* work. To our knowledge, no known *in vitro* drug delivery studies have been reported for the release of drug loaded thermosensitive liposomes where ultrasound is used as the source of hyperthermia. One of the main obstacles of ultrasound induced hyperthermia for drug delivery is finding an appropriate medium in which the experiments are to be carried out. An ideal medium should be biocompatible, it should not interact with liposomes in any way that may potentially compromise their stability and thermal properties, and it should have a high ultrasound thermoviscous absorption coefficient so that it may be heated with ultrasound energy. Cell culture media nearly satisfy all of the above criteria but have a very low thermoviscous absorption coefficient and are thus unable to be heated with ultrasound. Several other media (e.g. blood, serum, oils, glycerol, gels, etc) have been tested by the authors but finding a biocompatible, inert and high absorption coefficient medium has not been possible thus far.

In this work, an *in vitro* method for the controlled release of thermosensitive liposomes with ultrasound-induced hyperthermia is presented. The need for an "ideal" medium is overcome by the design of a dual compartment holder where the sample (suspension of TSLs in cell culture medium) is placed in an acoustically transparent holder which is immersed in glycerol. Hyperthermia is induced in the glycerol by a focused transducer and then heat is transferred to the sample via thermal conduction thus activating the drug loaded TSL. The proposed method resembles the *in vivo* scenario where ultrasound induces hyperthermia in the tumor tissue and the TSL (accumulated in the tumor interstitial spaces) are heated by thermal conduction. Theoretical predictions with the modified Pennes Bioheat equation [48] were first used to calculate the acoustic conditions needed for the desired temperature elevation. The theoretical predictions were then validated with measurements of the induced temperature elevation with fine wire

thermocouple in glycerol. *In vitro* activation of TSLs and doxorubicin release with the derived ultrasound conditions were evaluated.

5.2 Materials and Methods

5.2.1 Experimental Setup

A schematic of the experimental setup designed to implement the thermal conduction method is shown in Fig. 5-1. A 10x10x30 mm plastic cuvette (Fisher Scientific SAS, Illkirch, France) was filled with 99% glycerol (Sigma-Aldrich, Munich, Germany) that has high thermoviscous absorption coefficient α_0 = 3.6 Np/m at 1 MHz, where the frequency dependence of absorption is described with:

$$a = a_o * f^2, \tag{5.1}$$

Acoustically transparent Mylar windows were opened on all four cuvette walls to allow free propagation of ultrasound and avoid heating of the plastic walls. The TSL were suspended in cell culture medium, OptiMEM® (Gibco-Invitrogen, Carlsbad, CA) and placed in a cylindrical holder (outer diameter 3 mm) entirely made out of the same Mylar sheet. The sample holder was then immersed in the glycerol and a custom made single element focused transducer with center frequency 1.1 MHz, 51 mm diameter and 52 mm focus (radius of curvature) was used to induce hyperthermia in the glycerol. The transducer was placed in such a way so that the maximum pressure [1.7 mm before the focus (see Fig. 5-2a)] would be exactly halfway between the sample holder (with the OptiMEM and TSLs) and the cuvette wall (filled with glycerol). This provided the maximum heating effect. A focused transducer was used in order to ensure that a high enough pressure would result for the required temperature elevation. The TSL solution reached the desired temperature via thermal conduction that occurred fairly quickly (2-3 minutes) due to the small volume of the sample holder (> 0.5 ml). All experiments were carried out in a 37 °C water bath.

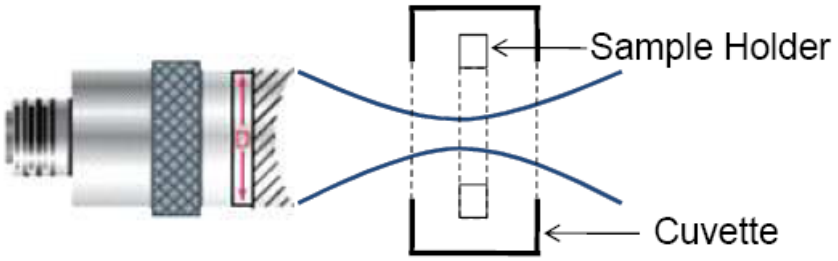

Figure 0-1: Ultrasound exposure setup with focused transducer and double compartment, the outer filled with glycerol and the inner filled with cell medium (OptiMEM®). Dotted lines represent Mylar acoustic windows on the cuvette (outer compartment with dimensions 10x10x30 mm) and sample holder (inner compartment with 3 mm diameter) walls. The sample holder is placed at the focus of the transducer.

Prior to the experiments, detailed characterization of the ultrasound field produced by the transducer was carried out. Propagation curves (variation of the acoustic pressure along the source axis) and beam patterns (distribution of the acoustic pressure on the transverse axis) at various fixed positions from the face of the source were measured using a calibrated 0.4 mm element membrane hydrophone (Precision Acoustics Ltd, Dorchester, UK). These were compared to the theoretical predictions (linear theory with the Rayleigh integral). A motorized 3-axis micro-positioning system (Newport, Irvine, California) was used to control the movement of the receiver along the linear (*x,y,z*) axis and a manual 360° rotation stage controlled the motion along the rotation axis, θ. The pressure at the focus as a function of input voltage was also measured using the calibrated membrane hydrophone.

5.2.2 Numerical simulation of temperature elevation

Numerical predictions of the ultrasound-induced temperature elevation were performed using a modified Pennes bio-heat transfer equation [48]. The bioheat equation calculates for the temperature distribution in tissue produced by ultrasound exposure taking into consideration perfusion and metabolic heat sources. During *in vitro* work, metabolic activity and perfusion are not present and therefore the corresponding terms may be neglected. The pressure field of the transducer was calculated with the Rayleigh Integral

$$p(x,y,z;t) = \frac{jk\rho_0 c_0 u_0 e^{j\omega t}}{2\pi}\int_S \frac{e^{-jkR}}{R}dS, \tag{5.2}$$

where, $R = \sqrt{(x-x')^2 + (y-y')^2 + z^2}$, for a planar source. For a circular focused source spherical coordinates are used and the surface R is transformed in to a curved interface R_f according to the radius of curvature.

The 3D volume pressure data was then imported in the bioheat equation and the predicted temperature distribution with respect to time and space was calculated. For the simulations, we assumed propagation in glycerol with density of 1258 kgm^{-3}, specific heat capacity of 2381 $Jkg^{-1}K^{-1}$, thermal diffusivity of 0.95 $e^{-7}m^2s^{-1}$, thermoviscous absorption coefficient of 3.6 $Npm^{-1}MHz^{-2}$ and speed of sound of 1935 ms^{-1}. Cooling due to streaming was not considered.

The objective of this work was to develop an *in vitro* method for the activation of thermosensitive liposomes using ultrasound induced hyperthermia and not experimentally verify the bioheat equation for the current setup. Temperature predictions were used in order to provide an estimate of the ultrasound conditions needed to produce the desired temperature elevation. Increased heating due to nonlinear propagation [49, 50] was also neglected as the acoustic amplitude used for a temperature elevation of 5-8°C is relatively small. According to the works of Bessanova et al. [51, 52] who investigated the influence of the nonlinear and diffraction effects on the amplification factors of focused ultrasound systems and the resulting effect on wave intensity and heat deposition, neglecting nonlinearity for the ultrasound settings used in our experiments was a valid assumption.

5.2.3 Temperature measurements

Temperature measurements were taken with a 50 μm K-type fine wire thermocouple. The transducer-thermocouple setup was immersed in a glycerol bath in the absence of the dual compartment setup and the thermocouple junction was first aligned with the focus of the transducer by maximizing the reflected echo in a pulse-echo system using a Ritec diplexer (RDX-6, Warwick, RI, USA). The final alignment was done by scanning the x, y and z planes for the point of maximum temperature elevation for a given ultrasound setting (0.5 MPa, 500 cycles, 45 % duty cycle for 4-5 seconds). Temperature readings were taken every 0.1 mm in the radial directions and 0.2 mm in the axial direction. For each step, the temperature was allowed to return to its ambient value before the next reading was taken. Once the alignment was complete, the temperature elevation as a function of pressure was captured with the fine wire thermocouple and recorded using a digital thermometer datalogger (TECPEL-DTM 318, Taipei, Taiwan). The ultrasound parameters used were 1.1 MHz frequency and 45% duty cycle and the heating time was 30 seconds with temperature recordings taken at a rate of 1 Hz.

The small diameter of the thermocouple (compared to the wavelength) allows for more accurate temperature readings but it is however still susceptible to the thermoviscous artifact [53, 54]. While this artifact is lessened when bare fine wire thermocouples are used [55], several authors have shown that it is still significant [56-58].

Temperature measurements as a function of time inside the sample holder were recorded in order to determine which ultrasound parameters are needed to induce a temperature elevation of 5-8 degrees as well as the rate of heating of the samples due to thermal conduction. In order to avoid any temperature measurement errors due to thermoviscous artifact, the thermocouple was fixed in the sample holder as far away from the ultrasound field as possible (about 6 mm away from the focus while the beam width is 2 mm [see Fig. 5-2b]). The produced acoustic streaming was effectively stirring the mixture during the 15-minute ultrasound application in order to produce a spatially uniform temperature.

5.2.4 Preparation of doxorubicin loaded thermosensitive liposomes:

Thermosensitive liposomes are prepared via the lipid film re-hydration method. Briefly, dipalmitoylphosphatidylcholine (DPPC), hydrogenated soybean phosphatidylcholine (HSPC), cholesterol (Chol) and distearylphosphatidylethanolamine-[methoxy(polyethylene glycol)-2000] (DSPE-PEG2000) are solubilized in chloroform in the molar ratio 100:33:27:7 (DPPC:HSPC:Chol:DSPE-PEG). The solvent is then evaporated under a nitrogen flow. Hydration of the lipid film is performed at 55 °C with 5mL of ammonium hydrogen phosphate 300 mM at pH 5 (pH was adjusted with HCl), so that the final lipid concentration is 20 mM. Freeze-thaw cycles are performed 6 times, by successively plunging the sample into liquid nitrogen and into a water bath regulated at 55 °C. Liposomes were then extruded at 55 °C five times through a 0.45 µm-sized and ten times through a 0.22 µm-sized polyvinylidene fluoride (PVDF) membrane filter at 55 °C. Their hydrodynamic diameter was measured by Dynamic Light Scattering (Zetasizer Nano ZS, Malvern) at 190 nm with a size distribution dispersity index of 0.17. The external buffer is then exchanged by dialysis in Hepes Buffer Saline (HEPES 25 mM, NaCl 140 mM, pH 7.4) with a 50 kDa dialysis membrane cutoff and a dialysis factor of 400*400*400. Doxorubicin was added to the liposomes solutions at a drug-to-lipid ratio of 0.1:1 (wt:wt) and incubated overnight at 37 °C [59-61]. Non-encapsulated doxorubicin was eliminated by size-exclusion chromatography on a Sephadex G50 column. The doxorubicin concentration of the purified doxorubicin-loaded liposomes was assayed by

UV-visible spectroscopy (Cary 100 Scan, Varian) against a calibration curve and was measured to be 194 μg/mL. The absorbance of doxorubicin was read at 485 nm.

5.2.5 Activation protocol

The TSL were diluted in fresh OptiMEM® medium to give a final doxorubicin concentration of 3 μg/mL. For each experiment, 0.5 ml of the TSL solution was used and each experiment was repeated three times. In order to ensure maximum drug release from the TSL (and following release mechanism experiments not shown here), experiment duration was 15 minutes. The experiments were divided in the following groups:

a) OptiMEM® alone (*No TSL*). This group is included to show the fluorescence of the cell medium itself. The text in the parenthesis denotes the label used in Figs. 5-6 and 5-7 and this applies to all groups described here.
b) OptiMEM® exposed to ultrasound [*No TSL+US(Q)*]. This group was included to check if ultrasound exposure alters the parameters of the cell medium when compared with the group above. The notation *US(Q)* denotes that the ultrasound applied is depositing heat and causes the desired hyperthermia.
c) TSL alone (*TSL*). This is the negative control group.
d) TSL exposed to ultrasound but without heating [*TSL+US(noQ)*]. By replacing the glycerol in the cuvette with water allows the same ultrasound exposure to be applied to the samples but without any induced heating since water has very low absorption. This is done to check if ultrasound alone (as mechanical energy) induces any release from the TSL. The notation *US(noQ)* denotes that the ultrasound applied is not depositing any heat.
e) TSL exposed to ultrasound and causing hyperthermia [*TSL+US(Q)*]. This is the group where the TSL are activated by ultrasound induced hyperthermia with the following acoustic conditions: 1.1 MHz, 500 cycles, 45% duty cycle, and 1.6 MPa.
f) TSL exposed to ultrasound and causing hyperthermia at higher pressure than group (v) [*TSL+US*(Q)*]. This group is very similar to (v) except that a higher acoustic pressure, 2.6 MPa, was used to see the effect of increased hyperthermia on TSL activation.
g) TSL in Nonidet P-40 (Sigma-Aldrich, St. Louis, MO, USA) solution (*TSL+Nonidet*). This group is the positive control since Nonidet P-40 detergent dissolves the liposomes causing 100 % release.

5.2.6 Release of Doxorubicin from TSLs

Doxorubicin is a naturally fluorescent molecule whose fluorescence is quenched when in the liposomal form. Therefore the fluorescence intensity of a doxorubicin containing medium is proportional to the extraliposomal doxorubicin or in this case the doxorubicin released from the TSL [62]. After the activation protocol was followed, 150 μl of solution was transferred to polystyrene 96-wells plate (Iwaki, Tokyo, Japan) and the fluorescence intensity was measured in a VICTOR™ X4 Multilabel Plate Reader (Perkin Elmer, Waltham MA, USA) at room temperature. The excitation, λ_{ex} and emission, λ_{em} wavelengths were 485 nm and 580 nm respectively. Each measurement was repeated three times and the results are presented as mean ± standard error. The % release of doxorubicin from the liposomes was evaluated according to the following equation [62]:

$$\%\ Release = \frac{I_{exp} - I_{neg}}{I_{pos} - I_{neg}}, \tag{5.3}$$

where I_{exp} is the intensity of the fluorescence after the application of hyperthermia, I_{neg} is the intensity of the fluorescence of the negative control, and I_{pos} is the intensity of the fluorescence after the addition of Nonidet P-40 (positive control).

5.3 Results

5.3.1 Focused ultrasound field

Measurements of the acoustic pressure of the ultrasound transducer are shown in Fig. 5-2 (solid line). The acoustic measurements are compared with theoretical predictions based on the Rayleigh integral (dashed lines in Fig. 5-2). The propagation curve (pressure as a function of axial distance) is shown in Fig. 5-2 (a) and the beam pattern (pressure as a function of radial distance) at the focus of the transducer (z=52 mm) in Fig. 5-2 (b). Good agreement is found between theory and experiment suggesting that our transducer is behaving like a typical piston source. This enables us to use the theoretical prediction for the calculation of the full 3D field instead of taking acoustic measurements. In addition, the focal dimensions (-6 dB down points) was calculated at 14 mm in the axial, and 2 mm in the transverse direction.

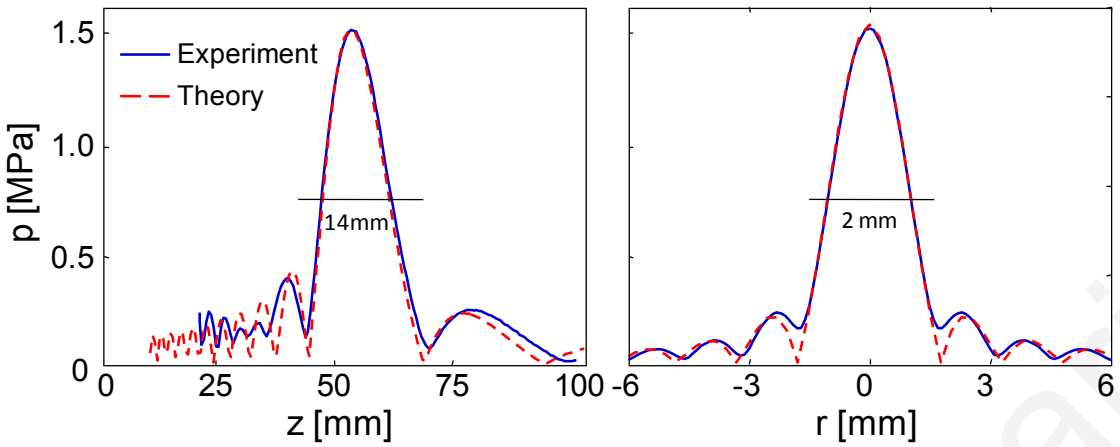

Figure 5-2: The acoustic pressure field [(a) axial and (b) transverse] of the transducer used for ultrasound induced hyperthermia. Solid lines are measurements and dashed lines are theoretical predictions from the Rayleigh Integral.

5.3.2 Numerical simulations and measurements of ultrasound induced temperature elevation

The pressure distribution field of our transducer calculated with the Rayleigh integral is shown in Fig. 5-3 (a). The acoustic pressure at the focus was 1.6 MPa, the frequency was 1.1 MHz and the duty cycle was 45% while a heating time of 20 sec was considered. Figures 5-3 (b) and (c) show the predicted temperature distributions for water and glycerol respectively (plotted in logarithmic scale). The predictions presented here are for free field (not for the dual compartment setup). It is evident from our results that water (or water-based media such as OptiMEM®) that has a low absorption coefficient does not heat up with ultrasound whereas higher absorption media such as glycerol may reach the desired temperature elevation with the given ultrasound parameters. As expected, the extent of the heated area closely resembles the extent of the pressure field. In Fig. 5-4, the predicted temperature elevation as a function of pressure (at the focus) is shown for various media. The results for water are shown in dash-dot line with solid squares, for olive oil in dashed line with open circles, and for 99% glycerol in dotted line with solid triangles. Heating of water using ultrasound is practically impossible whereas high absorption media (olive oil, glycerol) can be heated. According to these predictions, 1.6 MPa pressure at the focus is required to induce a 5 °C temperature rise in glycerol whereas 2.0 MPa would induce an 8 °C hyperthermia.

The theoretical predictions were compared to experimental measurements of ultrasound induced hyperthermia (after 20 sec exposure, 1 MHz frequency, 500 cycles, and 45% duty cycle) obtained with a 50 μm fine-wire thermocouple also shown in Fig. 5-4

(solid line with cross-hair markers). In order to compare the results with the theoretical predictions the experiments were carried out in a glycerol bath and the thermocouple was placed exactly at the focus of the transducer. At the lower acoustic pressures, the measured temperature is higher than the predicted value and this may be attributed to the thermoviscous heating artifact causing the thermocouple to record a higher value. At higher pressures (and overall intensities) there is increased acoustic streaming which causes cooling and reduction of the measured temperature. As a result, the predicted values become higher than the measured values (streaming is not taken into consideration in our heat transfer model). From Fig. 5-4, we confirm that a pressure of 1.6 MPa at the focus is adequate to raise the temperature in glycerol from 37 °C to 43 °C required for the thermal activation of the TSLs.

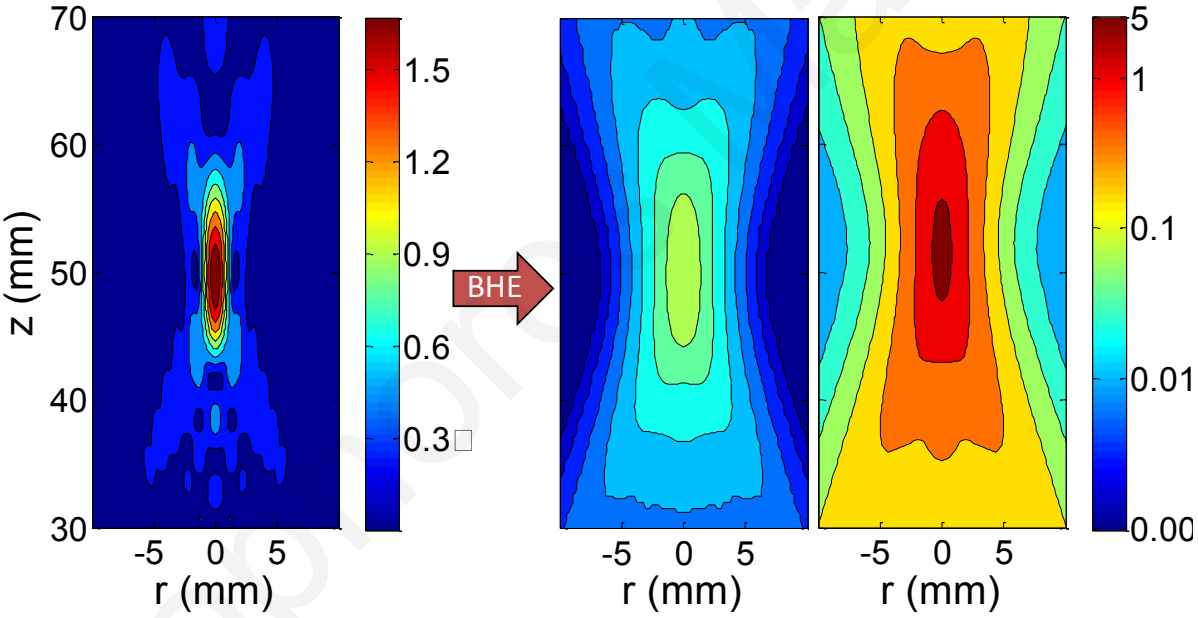

Figure 5-3: (a) Contour plot of the axial pressure distribution [plane (r=0, z)]. Predicted temperature elevation after 20 sec of ultrasound exposure in water (b), and glycerol(c).

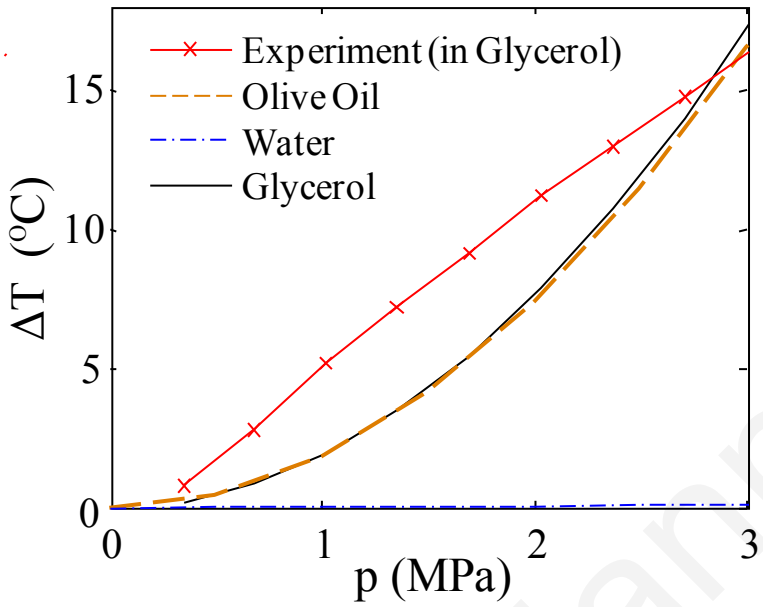

Figure 5-4: Predictions of temperature elevation as a function of pressure at focus for different media and comparison with measured values in glycerol. Ultrasound conditions: 1.1 MHz, 500 cycles, duty cycle= 45%, ultrasound exposure duration=20 sec.

The temperature elevation as a function of time inside the sample holder using the above ultrasound settings (1.6 MPa, 45 % DC) is shown in Fig. 5-5. While the target temperature is successfully reached, the rate of heating is slow requiring 2-3 minutes to reach 43 °C (ΔT= 6 °C) and about 6 minutes pass before equilibrium at 45 °C (ΔT= 8 °C) is reached.

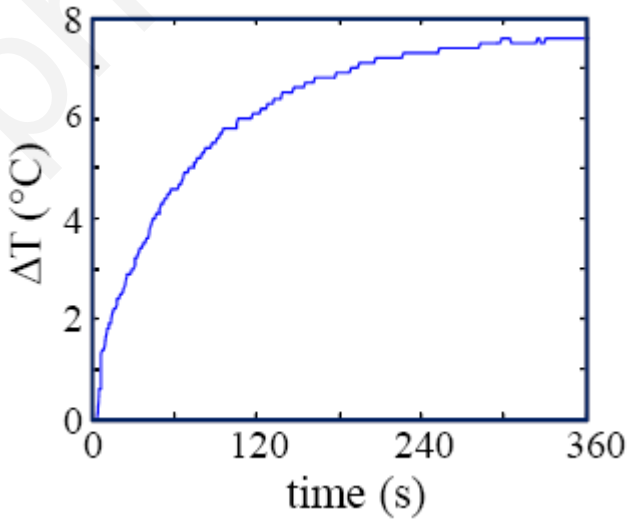

Figure 5-5: Temperature elevation of OptiMEM® in the sample holder due to thermal conduction from the glycerol. Ultrasound conditions: p=1.6 MPa, f=1.1 MHz, 500 cycles, 45% DC.

5.3.3 Doxorubicin release from TSL

TSL activation (mean fluorescence intensity) induced in the different experiment groups are shown in Fig. 5-6. Ultrasound alone does not affect the medium fluorescence since the natural fluorescent intensity of the medium remains the same before and after ultrasound sonication [*No TSL≈No TSL+US(Q)*]. Here we note that the background fluorescence of other media such as olive oil when insonified changes and thus it is not possible to quantify the drug release based on fluorescence alone.

Furthermore, ultrasound alone without hyperthermia does not influence the TSL or cause any release [*TSL≈TSL+US(noQ)*]. The higher intensity observed compared to the *No TSL* group is due to the quenched fluorescence of the liposomal doxorubicin.

When hyperthermia is induced with ultrasound [*TSL+US(Q)*], a significant amount of TSL activation is observed [about 80% of that of the positive control group (*TSL+Nonidet*)]. Further increasing the pressure to 2.6 MPa (group *TSL+US*(Q)*] which would correspond to temperatures above 50 °C does not show any increase in fluorescence.

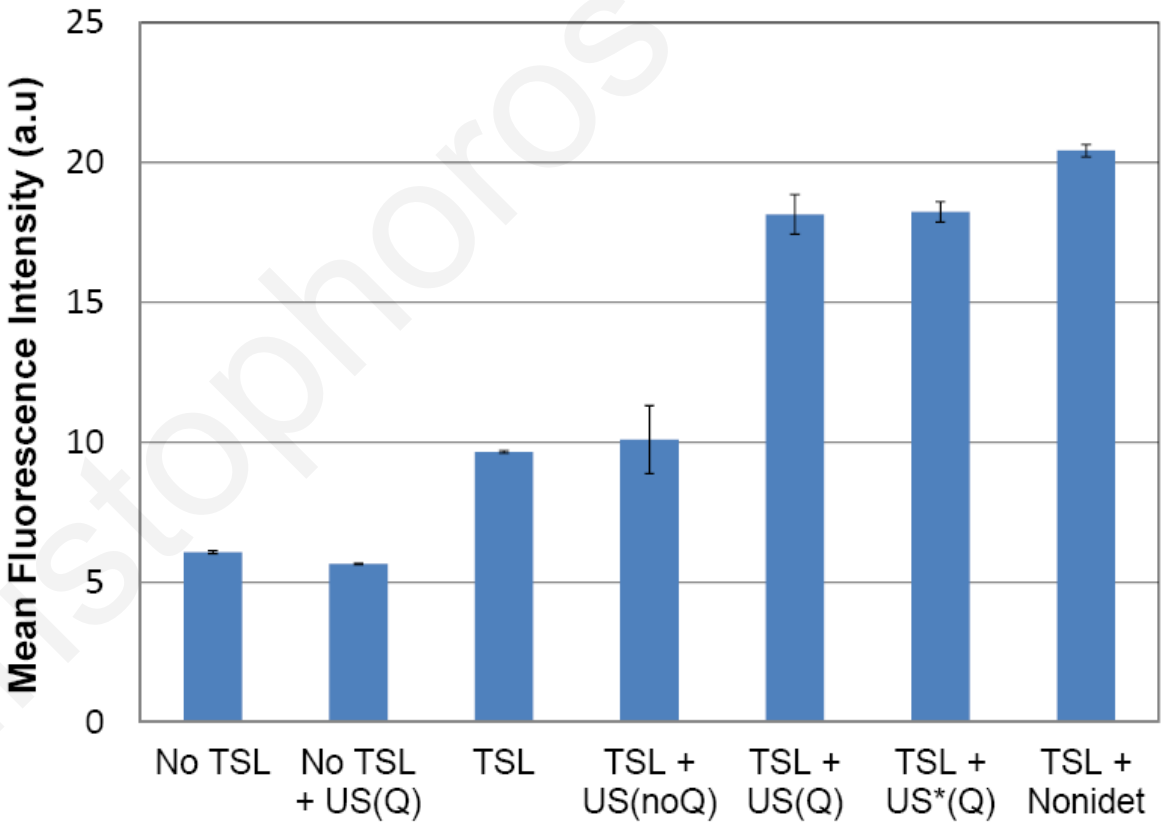

Figure 5-6: Mean fluorescence intensity (in arbitrary units) measurements of the different groups.

5.4 Discussion

An *in vitro* method for the controlled release of thermosensitive liposomes using ultrasound-induced temperature elevation was presented. The heating-by-conduction approach mimics the *in vivo* scenario of TSL in the interstitial tumor space where ultrasound induces hyperthermia in the tumor tissue and then by conduction the TSL are heated and activated to release their payload. Furthermore, it offers an *in vitro* method of TSL activation that eliminates the need for an ideal medium (biocompatible, inert with liposomes, high absorption coefficient) which is required for a single compartment *in vitro* setup and which has not been found yet. The proposed setup may be used to study the cell drug uptake by suspending cells together with the TSL in the culture medium. The secondary heating approach is also applicable to setups of seeded cells (e.g. heating in OptiCell™ chambers immersed in glycerol). Experimental setups with TSLs suspended tissue mimicking gel phantoms have also been used to study drug release (de Smet et al. 2011). However, the preparation of the gels as well as the analysis and quantification of the results is time demanding. In addition, accuracy may be compromised as cells and TSLs must be incorporated in the liquid gel before it solidifies. This of course may lead to cell death and premature activation of the TSL which will affect the results.

The choice of the focused transducers was to ensure the acoustic pressures required for 5-8° C temperature elevation without having a very strong power amplifier. However, in retrospect we have found out that we could have reached these temperatures even with unfocused transducers. The one clear advantage of the focused transducers is that the heated area is small and can easily be controlled and directed to a specific area. In addition, with our set-up and specific parameters, there is streaming that actually mixes the fluid and causes a more spatially uniform temperature.

A significant 80% doxorubicin release from the TSL is achieved with the proposed method. In Fig. 5-7 the % DOX release is shown for four of the groups: *TSL+US(noQ)*, *TSL+US(Q)*, *TSL+US*(Q)*, *TSL+Nonidet*. It is evident that the mechanical action of ultrasound alone is not inducing any TSL release. However, further improvements to the set-up and conditions may further increase drug release.

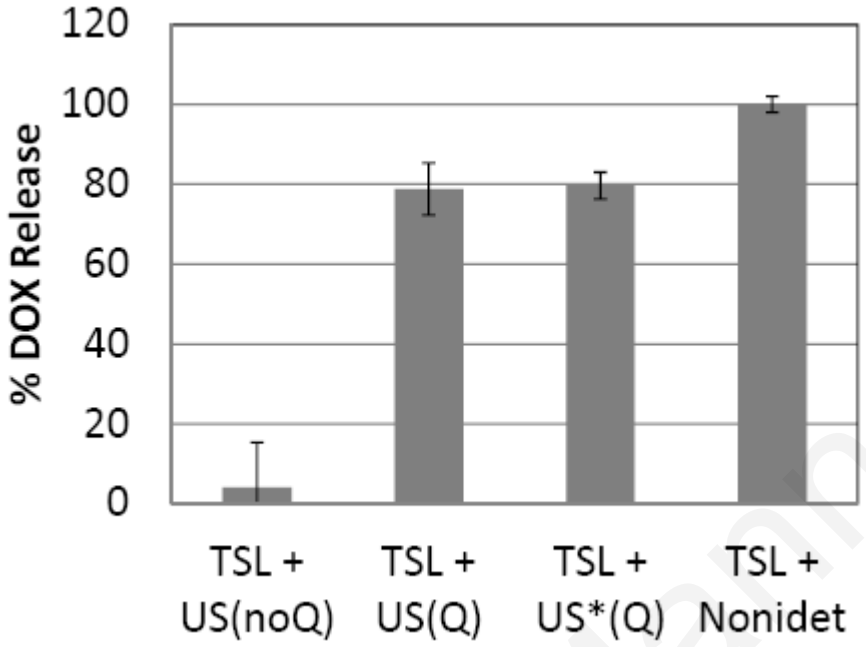

Figure 5-7: Percent Induced doxorubicin release from thermosensitive liposomes. Values calculated with equation (3).

Figure 5-5 shows the temperature evolution of the OptiMEM® in the sample holder with the proposed method. It takes about 300 seconds for the desired temperature to be reached whereas it is much faster when a heated water bath is used (data not shown here). One reason for the longer heating time is that focused transducers heat only a small area (see Fig. 5-3) and it takes much longer for the whole volume to heat up. It is possible to produce larger and more uniform heating areas with the use of flat or lightly focused transducers (currently under investigation) or even the nearfield of a focused transducer [63].

Methods of efficient mixing of the heated glycerol may also improve the uniformity of the heating. In the present work mixing is achieved due to acoustic streaming [64, 65]. Acoustic streaming has been shown to efficiently mix solutions in containers [66]. The ultrasound parameters considered here induce acoustic streaming [67] in both the glycerol and the cell medium. However, since both the cuvette and the inside cylindrical holder are small, the induced streaming causes a spatially uniform temperature elevation.

Often in ultrasound-induced thermal ablation applications (high intensity focused ultrasound—HIFU) nonlinear sound propagation plays an important role [50]. According to Bessanova et al. [51, 52] for the parameters used in this work, nonlinear wave propagation and the resulting effect on wave intensity and heat deposition is very small and was thus not included in our model.

5.5 Conclusion

A method for *in vitro* activation of thermosensitive liposomes with ultrasound induced hyperthermia has been developed. The use of ultrasound-induced hyperthermia offers the advantage of activation of localized delivery of drugs from thermosensitive liposomes. The method overcomes the problem of cell culture media such as OptiMEM® not being able to heat by ultrasound. This is achieved by using another thermally absorptive medium such as glycerol to heat by ultrasound which in turn heats the cell culture medium by conduction. The acoustic conditions for ultrasound induced hyperthermia and activation of TSL were first derived from theoretical models and then confirmed with pressure and temperature measurements. With the proposed method, 80% of the TSL were activated with 15 min exposure of 1.1 MHz, 1.6 MPa, 500 cycles, 45% duty cycle ultrasound.

Acknowledgments

The authors would like to acknowledge Christina Keravnou for her help with the theoretical predictions and Drs. Louiza Loizou and Andriani Odysseos, University of Cyprus and EPOS-Iasis Ltd for their help in the analysis of the results. We would also like to thank Dr. Ayache Bouakaz and Dr. J.M Escoffre, University François Rabelais-Tours for their collaboration. This work was funded by the EU FP7 Project Sonodrugs (NMP4-LA-2008-213706).

References

[1] D. W. Northfelt, et al., "Pegylated-liposomal doxorubicin versus doxorubicin, bleomycin, and vincristine in the treatment of AIDS-related Kaposi's sarcoma: Results of a randomized phase III clinical trial," J Clin Oncol., vol. 16, pp. 2445-2451, 1998.

[2] M. E. R. O'Brien, et al., "Reduced cardiotoxicity and comparable efficacy in a phase III trial of pegylated liposomal doxorubicin HCl (CAELYX™/Doxil®) versus conventional doxorubicin for first-line treatment of metastatic breast cancer," Annals of Oncology, vol. 15, pp. 440-449, 2004.

[3] D. C. Drummond, et al., "Optimizing liposomes for delivery of chemotherapeutic agents to solid tumors," Pharmacological Reviews, vol. 51, pp. 691-743, 1999.

[4] A. Gabizon, et al., "Prolonged circulation time and enhanced accumulation in malignant exudates of doxorubicin encapsulated in polyethylene-glycol coated liposomes," Cancer Research, vol. 54, pp. 987-992, 1994.

[5] A. A. Gabizon, "Selective tumor localization and improved therapeutic index of anthracyclines encapsulated in long-circulating liposomes," Cancer Research, vol. 52, pp. 891-896, 1992.

[6] D. W. Northfelt, et al., "Doxorubicin encapsulated in liposomes containing surface-bound polyethylene glycol: Pharmacokinetics, tumor localization, and safety in patients with AIDS-related Kaposi's sarcoma," J Clin Pharmacol., vol. 36, pp. 55-63, 1996.

[7] S. Bandak, et al., "Pharmacological studies of cisplatin encapsulated in long-circulating liposomes in mouse tumor models," Anti-Cancer Drugs, vol. 10, pp. 911-920, 1999.

[8] G. Kong, et al., "Efficacy of liposomes and hyperthermia in a human tumor xenograft model: Importance of triggered drug release," Cancer Research, vol. 60, pp. 6950-6957, 2000.

[9] V. P. Torchilin, "Recent advances with liposomes as pharmaceutical carriers," Nat Rev Drug Discov, vol. 4, pp. 145-160, 2005.

[10] M. B. Yatvin, et al., "Design of liposomes for enhanced local release of drugs by hyperthermia," Science, vol. 202, pp. 1290-1293, 1978.

[11] A. M. Ponce, et al., "Hyperthermia mediated liposomal drug delivery," Int J Hyperthermia, vol. 22, pp. 205-13, May 2006.

[12] G. Kong and M. W. Dewhirst, "Hyperthermia and liposomes," Int J Hyperthermia, vol. 15, pp. 345-370, 1999.

[13] G. M. Hahn, et al., "Thermochemotherapy: synergism between hyperthermia (42-43°) and adriamycin (or bleomycin) in mammalian cell inactivation," Proceedings of the National Academy of Sciences of the United States of America, vol. 72, pp. 937-940, 1975.

[14] T. S. Herman, "Temperature dependence of Adriamycin, cis-diamminedichloroplatinum, bleomycin, and 1,3-bis(2-chloroethyl)-1-nitrosourea cytotoxicity *in vitro*," Cancer Research, vol. 43, pp. 517-520, 1983.

[15] M. W. Dewhirst, et al., "Hyperthermic treatment of malignant diseases: Current status and a view toward the future," Seminars in Oncology, vol. 24, pp. 616-625, 1997.

[16] M. H. Gaber, et al., "Thermosensitive liposomes: Extravasation and release of contents in tumor microvascular networks," Int J Radiat Oncol Biol Phys, vol. 36, pp. 1177-1187, 1996.

[17] L. H. Lindner, et al., "Novel Temperature-Sensitive Liposomes with Prolonged Circulation Time," Clinical Cancer Research, vol. 10, pp. 2168-2178, 2004.

[18] J. K. Mills and D. Needham, "The materials engineering of temperature-sensitive liposomes," Methods in enzymology, vol. 387, pp. 82-113, 2004.

[19] D. Needham and M. W. Dewhirst, "The development and testing of a new temperature-sensitive drug delivery system for the treatment of solid tumors," Adv Drug Deliv Rev., vol. 53, pp. 285-305, 2001.

[20] D. Papahadjopoulos, et al., "Phase transitions in phospholipid vesicles. Fluorescence polarization and permeability measurements concerning the effect of temperature and cholesterol," Biochim Biophys Acta., vol. 311, pp. 330-348, 1973.

[21] Q. Chen, et al., "Tumor microvascular permeability is a key determinant for antivascular effects of doxorubicin encapsulated in a temperature sensitive liposome," Int J Hyperthermia, vol. 24, pp. 475-482, 2008.

[22] G. Kong, et al., "Hyperthermia enables tumor-specific nanoparticle delivery: Effect of particle size," Cancer Research, vol. 60, pp. 4440-4445, 2000.

[23] G. Kong, et al., "Characterization of the effect of hyperthermia on nanoparticle extravasation from tumor vasculature," Cancer Research, vol. 61, pp. 3027-3032, 2001.

[24] D. Needham, et al., "A new temperature-sensitive liposome for use with mild hyperthermia: Characterization and testing in a human tumor xenograft model," Cancer Research, vol. 60, pp. 1197-1201, 2000.

[25] B. Khoobehi, et al., "Hyperthermia and temperature-sensitive liposomes: Selective delivery of drugs into the eye," Jpn J Ophthalmol., vol. 33, pp. 405-412, 1989.

[26] M. L. Hauck, et al., "Phase I trial of doxorubicin-containing low temperature sensitive liposomes in spontaneous canine tumors," Clinical Cancer Research, vol. 12, pp. 4004-4010, 2006.

[27] S. K. Huang, et al., "Liposomes and hyperthermia in mice: Increased tumor uptake and therapeutic efficacy of doxorubicin in sterically stabilized liposomes," Cancer Research, vol. 54, pp. 2186-2191, 1994.

[28] R. Salomir, et al., "Local delivery of magnetic resonance (MR) contrast agent in kidney using thermosensitive liposomes and MR imaging-guided local

hyperthermia: A feasibility study *in vivo*," J Magn Reson Imaging, vol. 22, pp. 534-540, 2005.

[29] M. Ahmed and S. N. Goldberg, "Combination radiofrequency thermal ablation and adjuvant IV liposomal doxorubicin increases tissue coagulation and intratumoural drug accumulation," Int J Hyperthermia, vol. 20, pp. 781-802, 2004.

[30] A. M. Ponce, et al., "Magnetic resonance imaging of temperature- sensitive liposome release: Drug dose painting and antitumor effects," J Natl Cancer Inst., vol. 99, pp. 53-63, 2007.

[31] B. L. Viglianti, et al., "Chemodosimetry of *in vivo* tumor liposomal drug concentration using MRI," Magn Reson Med., vol. 56, pp. 1011-1018, 2006.

[32] S. Dromi, et al., "Pulsed-high intensity focused ultrasound and low temperature - Sensitive liposomes for enhanced targeted drug delivery and antitumor effect," Clinical Cancer Research, vol. 13, pp. 2722-2727, 2007.

[33] B. E. O'Neill and K. C. P. Li, "Augmentation of targeted delivery with pulsed high intensity focused ultrasound," Int J Hyperthermia, vol. 24, pp. 506-520, 2008.

[34] P. R. Patel, et al., "*In vitro* and *in vivo* evaluations of increased effective beam width for heat deposition using a split focus high intensity ultrasound (HIFU) transducer," Int J Hyperthermia, vol. 24, pp. 537-549, 2008.

[35] C. J. Diederich and K. Hynynen, "Ultrasound technology for hyperthermia," Ultrasound Med Biol, vol. 25, pp. 871-887, 1999.

[36] J. K. Enholm, et al., "Improved volumetric MR-HIFU ablation by robust binary feedback control," IEEE Trans Biomed Eng., vol. 57, pp. 103-113, 2010.

[37] P. M. Harari, et al., "Development of scanned focussed ultrasound hyperthermia: Clinical response evaluation," Int J Radiat Oncol Biol Phys, vol. 21, pp. 831-840, 1991.

[38] K. Hynynen, et al., "A scanned, focused, multiple transducer ultrasonic system for localized hyperthermia treatments," Int J Hyperthermia, vol. 3, pp. 21-35, 1987.

[39] M. O. Köhler, et al., "Volumetric HIFU ablation under 3D guidance of rapid MRI thermometry," Medical Physics, vol. 36, pp. 3521-3535, 2009.

[40] C. Mougenot, et al., "Quantification of near-field heating during volumetric MR-HIFU ablation," Medical Physics, vol. 38, pp. 272-282, 2011.

[41] P. R. Stauffer, "Evolving technology for thermal therapy of cancer," Int J Hyperthermia, vol. 21, pp. 731-744, 2005.

[42] M. de Smet, et al., "Magnetic resonance imaging of high intensity focused ultrasound mediated drug delivery from temperature-sensitive liposomes: an *in vivo* proof-of-concept study," J Control Release, vol. 150, pp. 102-10, Feb 28 2011.

[43] H. Grull and S. Langereis, "Hyperthermia-triggered drug delivery from temperature-sensitive liposomes using MRI-guided high intensity focused ultrasound," J Control Release, vol. 161, pp. 317-27, Jul 20 2012.

[44] K. Y. Ng and Y. Liu, "Therapeutic ultrasound: Its application in drug delivery," Med Res Rev, vol. 22, pp. 204-223, 2002.

[45] P. G. Sanches, et al., "See, reach, treat: Ultrasound-triggered image-guided drug delivery," Therapeutic Delivery, vol. 2, pp. 919-934, 2011.

[46] R. Staruch, et al., "Localised drug release using MRI-controlled focused ultrasound hyperthermia," Int J Hyperthermia, vol. 27, pp. 156-171, 2011.

[47] A. Yudina, et al., "Ultrasound-mediated intracellular drug delivery using microbubbles and temperature-sensitive liposomes," J Control Release, vol. 155, pp. 442-448, 2011.

[48] H. H. Pennes, "Analysis of tissue and arterial blood temperatures in the resting human forearm," J Appl Physiol, vol. 1, pp. 93-122, Aug 1948.

[49] D. R. Bacon and E. L. Carstensen, "Increased heating by diagnostic ultrasound due to nonlinear propagation," J Acoust Soc Am, vol. 88, pp. 26-34, Jul 1990.

[50] G. T. Haar and C. Coussios, "High intensity focused ultrasound: physical principles and devices," Int J Hyperthermia, vol. 23, pp. 89-104, Mar 2007.

[51] O. V. Bessonova, et al., "Focusing of high power ultrasound beams and limiting values of shock wave parameters," Acoustical Physics, vol. 55, pp. 463-473, 2009.

[52] O. V. Bessonova, et al., "A derating method for therapeutic applications of high intensity focused ultrasound," Acoustical Physics, vol. 56, pp. 354-363, 2010.

[53] W. J. Fry and R. B. Fry, "Determination of Absolute Sound Levels and Acoustic Absorption Coefficients by Thermocouple Probes---Experiment," J Acoust Soc Am, vol. 26, pp. 311-317, 1954.

[54] W. J. Fry and R. B. Fry, "Determination of Absolute Sound Levels and Acoustic Absorption Coefficients by Thermocouple Probes---Theory," J Acoust Soc Am, vol. 26, pp. 294-310, 1954.

[55] K. Hynynen, et al., "Errors in temperature measurement by thermocouple probes during ultrasound induced hyperthermia," Br J Radiol, vol. 56, pp. 969-70, Dec 1983.

[56] J. Huang, et al., "Experimental validation of a tractable numerical model for focused ultrasound heating in flow-through tissue phantoms," J Acoust Soc Am, vol. 116, pp. 2451-8, Oct 2004.

[57] K. Hynynen and D. K. Edwards, "Temperature measurements during ultrasound hyperthermia," Medical Physics, vol. 16, pp. 618-26, Jul-Aug 1989.

[58] H. Morris, et al., "Investigation of the viscous heating artefact arising from the use of thermocouples in a focused ultrasound field," Phys Med Biol, vol. 53, pp. 4759-76, Sep 7 2008.

[59] S. A. Abraham, et al., "The liposomal formulation of doxorubicin," vol. 391, ed, 2005, pp. 71-97.

[60] A. Fritze, et al., "Remote loading of doxorubicin into liposomes driven by a transmembrane phosphate gradient," Biochimica et Biophysica Acta - Biomembranes, vol. 1758, pp. 1633-1640, 2006.

[61] D. Zucker, et al., "Liposome drugs' loading efficiency: A working model based on loading conditions and drug's physicochemical properties," Journal of Controlled Release, vol. 139, pp. 73-80, 2009.

[62] M. de Smet, et al., "Temperature-sensitive liposomes for doxorubicin delivery under MRI guidance," J Control Release, vol. 143, pp. 120-127, 2010.

[63] A. Rahim, et al., "Physical parameters affecting ultrasound/microbubble-mediated gene delivery efficiency *in vitro*," Ultrasound Med Biol, vol. 32, pp. 1269-1279, 2006.

[64] H. C. Starritt, et al., "An experimental investigation of streaming in pulsed diagnostic ultrasound beams," Ultrasound Med Biol, vol. 15, pp. 363-73, 1989.

[65] S. Tjotta, "Some non-linear effects in sound fields☆," J Sound Vib, vol. 6, pp. 255-267, 1967.

[66] C. Suri, et al., "Chaotic mixing generated by acoustic streaming," Ultrasonics, vol. 40, pp. 393-396, 2002.

[67] C. Mannaris and M. A. Averkiou, "Investigation of Microbubble Response to Long Pulses Used in Ultrasound-Enhanced Drug Delivery," Ultrasound Med Biol, vol. 38, pp. 681-691, 2012.

6

Summary and Future directions

6.1 Summary

Image-guided ultrasound-enhanced drug delivery has gained increased attention over the past few years both in the clinic and in research. In particular, ultrasound energy is used as the facilitator in localized drug delivery applications while ultrasound imaging is the method of choice for tracking drug loaded carriers in circulation. This work was motivated by the need for a better understanding of the underlying mechanisms involved in both *pressure* and *temperature* activation approaches used in ultrasound-enhanced drug delivery. The physical acoustics and bubble dynamics related with the use of ultrasound in pressure activation with UCA were investigated in Chapters 2-4. The mechanisms of interaction between ultrasound, tissue and blood for the temperature activation of drug-loaded thermosensitive liposomes were explored in Chapter 5.

The response of microbubbles to ultrasound was investigated with specifically designed experiments in Chapter 2 using two *in vitro* set-ups: (a) a set-up with the microbubbles suspended in a large enclosure of deionized water; and (b) one with the microbubbles enclosed in a micron-sized cellulose tube. Experiments covered a wide range of ultrasonic pulse settings found in literature, claiming to be optimal for drug delivery.

Previous knowledge of the destruction characteristics of microbubbles was confirmed in both setups. At MIs<0.1, the microbubbles remained intact and kept oscillating for the duration of the pulse while at higher MIs disruption of the microbubbles and diffusion of the gas occurred. Bubble oscillations from very few even single microbubbles could be observed at various pressure and intensity settings due to the high receive sensitivity of a single element transducer that was used as a receiver (Fig. 3-1). Typical dilute bubble concentrations of 0.005‰ – 0.04‰, which correspond to roughly 1-8 bubbles/μL were utilized. The observation volume was 16 μL justifying that the detected signal originated from a few or even single microbubbles. The ability to observe the response to ultrasound from individual microbubbles is important as high microbubble concentrations involve complications such as multiple scatter and bubble–bubble interactions [1] which affect the behaviour of the microbubbles in the presence of the ultrasound field. In addition, in the microcirculation it is more likely to have concentrations closer to the ones mentioned above. The nonlinear (harmonic) content of the microbubble response was also accurately obtained following careful calibration of the frequency response of the receiver (see Ch.2 - Appendix).

Acoustic streaming (movement of the medium in the direction of propagation of ultrasound) in the microbubble suspensions resulted in bubble movement and thus not

allowing the observation of a bubble response to long pulses. An oscillating microbubble "pushed" out of the observation zone (due to acoustic streaming) produced a decrease in the detected signal that may be misinterpreted as a disrupted microbubble gradually diffusing. Bubble response investigation to long pulses is difficult (if not impossible) in analogous experimental setups with microbubbles in suspension, as they do not remain within the observation point for the duration of the pulse.

Acoustic streaming was successully eliminated by allowing the microbubbles to flow in a 200-μm acoustically transparent cellulose capillary. This set-up resulted in a more accurate observation and measurement of the bubble response to longer ultrasound pulses suggested for use in therapeutic applications. In addition, the capillary setup better mimics the *in vivo* geometry of microbubbles in the microcirculation. An important observation was that at MI>0.4, microbubbles were destroyed and any bubble activity disappeared within 100 cycles or 100 μs (at 1 MHz) irrespective of the pulse length (Fig. 3-8). Theory predicts that a gas-filled micron-sized bubble requires 10-100 ms to diffuse to the surrounding medium [2]. Destruction and breakage of the bubble into several smaller bubbles however (as is the case with long high MI pulses) greatly influences and accelerates the diffusion process. With the microbubbles destroyed and the gas diffused, any bubble related bioeffects associated with enhanced drug delivery (e.g. cavitation and microstreaming), probably cease to be in effect during the remaining several hundred cycles!

Based on the observed bubble behavior two options for drug delivery were suggested: (a) a long pulse (100-1000 cycles) at low amplitude, MI<0.1 for a prolonged stable nonlinear oscillation; and (b) a shorter, 100 cycle pulse at high amplitude, MI>0.4, for a destructive highly nonlinear oscillation. Longer than 100 cycles pulses at high amplitude do not produce any added benefit in terms of the bubble oscillation. The influence of other biological factors should be carefully considered by drug delivery reports suggesting that pulses with thousands of cycles are more effective in delivering the drugs. Ultrasound-induced hyperthermia for example has been previously shown to enhance drug delivery as discussed in chapter 5. A single 20000 cycle, 2 MPa burst would result in a temperature rise of 0.2 degrees in tissue. For a continuous 1 MHz, 0.5 MPa wave, a temperature rise of 2 degrees Celsius is expected within 3 seconds. These are significant changes and should be taken into consideration. Transient opening of pores on vessel walls (extravasation) and on cell membranes (sonoporation) occur either due to microstreaming from cavitating microbubbles or due to massaging of the membrane from oscillating microbubbles [3]. Acoustic streaming which occurs during long pulses could

potentially "push" the drug through these micropores resulting in increased uptake of the drug.

Chapter 3 reported on the therapeutic efficacy of novel DOX liposome-loaded microbubbles [4] following ultrasound enhanced drug delivery on human glioblastoma cells. A synergistic effect between ultrasound and DOX liposome-loaded microbubbles was demonstrated. A much higher glioblastoma cell death was induced with the above combination compared to treatment with free DOX or DOX liposome-loaded microbubbles alone (Fig. 3-6). We have also demonstrated that the enhanced therapeutic efficiency is associated with (i) an ultrasound-triggered release of DOX from the DOX liposome-loaded microbubbles (Fig. 3-8) and (ii) an enhanced uptake of free DOX by the cells (Fig. 3-7) confirming the hypothesis that sonoporation improves the cellular uptake of free DOX [5, 6]. The ability to track the drug loaded agents *in vivo* using real time imaging is essential in localized drug delivery applications, thus the imaging and destruction properties of the DOX liposome-loaded microbubbles were also evaluated. Ideally, the drug carrier should be able to be tracked *in vivo* using low mechanical index (MI) imaging and once at the desired location, high MI ultrasound may be used to trigger the drug release on site. Experiments with a commercial ultrasound scanner showed that real time non-destructive imaging is possible with these DOX liposome-loaded microbubbles which qualify as a hybrid imaging/therapeutic agent to be used in targeted drug delivery under ultrasound imaging guidance.

In Chapter 4 we considered the use of a diagnostic ultrasound scanner as both a therapy and imaging device. Specifically, we have considered the accurate measurement of microbubble oscillations and evaluated possible imaging approaches under these conditions.

Signal saturation was limited by continuously adjusting the scanner's 2D analog gain and accounting for it in the quantification software. This simple and yet crucial improvement on bubble response measurement under high MIs may have considerable impact on drug delivery approaches such as sonoporation which seems to depend on bubble response to ultrasound. Acoustic pressures equivalent with MIs up to 2.1 (which is higher than the allowed diagnostic limit) were considered while various concentrations, were used. A quadratic relationship of backscattered pressure with acoustic excitation pressures was observed while the CTR was found to increase with MI, contrary to previous perception [15]. This allows for imaging approaches in therapeutic procedures where the MI used is greater than the bubble destruction threshold.

In vitro localized drug release from DOX-loaded thermosensitive liposomes was presented in Chapter 5. Numerical simulations of the ultrasound induced temperature elevation were carried out using a code solving the modified Pennes Bioheat equation [7]. The theoretical predictions acted as a guide for selecting the acoustic parameters needed to produce the desired temperature elevation as well as to design specific pulsing schemes in order to maintain constant heating over prolonged periods. The predictions were validated with measurements of the induced hyperthermia with fine a wire thermocouple and a good agreement was found.

One of the main obstacles encountered in the work of Chapter 5 was finding an appropriate medium to perform the experiments. An ideal medium should be biocompatible, it should not interact with liposomes in any way that may potentially compromise their stability and it should have a high ultrasound thermoviscous absorption coefficient so that it may be heated with ultrasound energy. Such a medium does not exist and explains why most temperature activation studies are done *in vivo* while reports for *in vitro* work are scarce. The need for an "ideal" medium was overcome by the design of a dual compartment holder where the sample (TSLs suspended in cell culture medium) was placed in an acoustically transparent holder immersed in glycerol which is a thermoviscous medium. Hyperthermia was induced in the glycerol by ultrasound and then heat was transferred to the sample via thermal conduction thus activating the drug loaded TSL. The proposed method, which to the best of our knowledge may be the first of its kind, resembles the *in vivo* scenario where ultrasound induces hyperthermia in the tumor tissue and the TSL (accumulated in the tumor interstitial spaces) are heated by thermal conduction (Fig. 6-1).

A significant 80% doxorubicin release from the TSL was achieved. Further improvements to the set-up and conditions used are needed to decrease activation times and further increase drug release. Flat or lightly focused transducers, able to produce hyperthermia in a much wider area, will significantly decrease the time required for the whole compartment to reach the desired temperature elevation. The current set-up and future modified ones may be used to quickly and accurately investigate the release dynamics of new thermosensitive agents as well as their therapeutic effectiveness on cell cultures. Tissue mimicking gel phantoms populated with small capillaries or even small tumor models perfused with TSL in solution may use the same ideas developed here offering a more realistic *in vitro* model with all its apparent benefits.

Last but not least, the importance of the detailed geometric shape (diffraction pattern) of the focused sound field and its possible influence on the drug delivery

applications was considered throughout this work. We have showed that the expected temperature elevation strongly depends on the special pressure distribution (Fig. 5-3) and should be taken into consideration during temperature activation approaches. Similarly, pressure activation studies should carefully consider the effect of the diffraction pattern on different microbubbles in the acoustic field before coming to conclusions. As the field varies in amplitude, different bubbles in the field experience a different acoustic pressure (Fig. 6-2). Bubble related bioeffects such as inertial cavitation, micro-streaming and sonoporation as well as localized increases in stress and temperature are highly dependent on the applied pressure field intensity and the type of bubble oscillation.

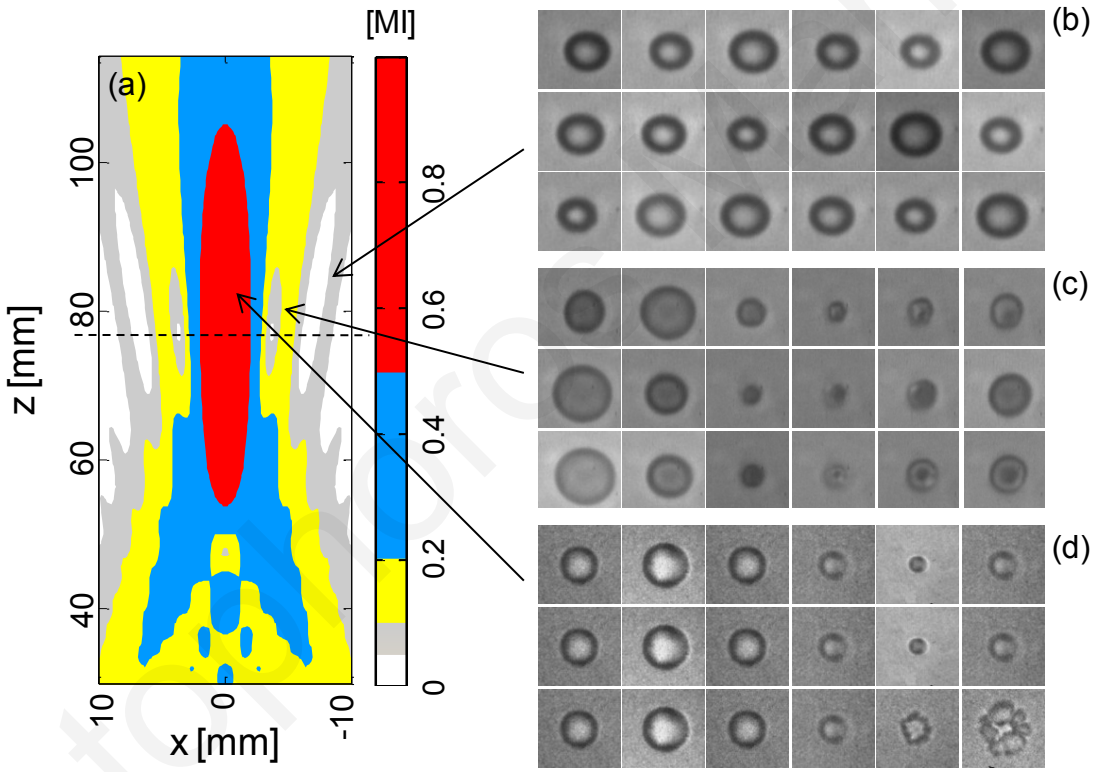

Figure 6-1: Effect of diffraction pattern on UCA response. (a) the axial plane of a 1 MHz transmitter (calculated with the KZK equation). Four MI ranges shown: 0-0.1 (white), 0.1-0.2 (yellow), 0.2-0.5 (blue), and 0.5-1.0 (red). In (b-d) – high frame rate images of bubble oscillations acquired by the Brandaris-128 high frame rate camera [8]; (b) 0.05<MI<0.1; stable linear oscillation observed, (c) 0.1<MI<0.2; nonlinear oscillations, (d) violent oscillations and destruction

6.2 List of Original Contributions

- This thesis offered imaging contributions in the area of image-guided drug delivery and specifically, considered the properties of drug carrying microbubbles and developed imaging methods for such carriers. A method that eliminates signal saturation was developed and this allowed to accurately measuring the contrast to tissue ratio with increasing MI, which was not done in the past.

- Another important finding is that the tissue nonlinearity dependence with acoustic pressure is actually very similar to that of microbubbles (contrary to the current understanding) and thus the contrast to tissue ratio is constant across all acoustic pressures. This finding allows the imaging of drug carrying microbubbles equally effectively at both low non-destructive MI's and high destructive MI's.

- The current work elucidated the role of acoustic streaming in set-ups with freely suspended microbubbles and pointed out the limitations of this set-up in an effort to avoid reaching possible false explanations of the bubble responses to long pulses when studying ultrasound enhanced drug delivery.

- Expanded the overall understanding of bubble response to long ultrasonic pulses in a capillary tube set-up that closely mimics the *in vivo* case. A very important finding is that all microbubbles are completely diffused (disappear) in about 100 ms irrespective of the acoustic pulse duration. Thus, the successful use of longer pulses in previously published *in vivo* works suggests that the drug delivery enhancement is also due to the interaction of ultrasound with the cells themselves after an interaction of microbubbles with ultrasound and the cells was preceded.

- Optimal ultrasound parameters for both low and high amplitude excitations were derived and suggested for future use in preclinical and clinical work.

- Methods and techniques were developed for effective drug delivery of Dox-liposome loaded microbubbles. A 4-fold decrease of cell viability compared to free or encapsulated Dox was measured in *in vitro* experiments with cancer cells. The ultrasound enhancement techniques developed here both enhance Doxorubicin release from liposomes and Doxorubicin internalization into the cancer cells which are

directly related to the enhanced therapeutic efficacy observed with the current technique.

- A novel method and set-up for *in vitro* activation of thermosensitive liposomes with focused ultrasound was developed, tested, and validated. This unique set-up, which resembles the *in vivo* case of liposomes in the tumor interstitial spaces, consists of a dual compartment where the cells and liposomes are in one compartment and heated with conduction from a thermally absorbing fluid in a second compartment that is heated by focused ultrasound. Using this *in vitro* setup, a significant 80% release of doxorubicin from TSLs was achieved.

6.3 Conclusion

More than 100 years ago, Paul Ehrlich [9] envisioned that synthetic compounds could be made to selectively target and destroy disease causing microorganisms but not damage anything else in the patient's body. He termed these drugs ‘magic bullets’ inspiring generations of scientists to devise new methods and therapeutics in the fight against cancer. Image-guided ultrasound-enhanced drug delivery shows great potential in fulfilling Dr. Ehrlich’s vision. A complete understanding of the underlying mechanisms will offer more control of the associated bioeffects and will allow increased efficiency in drug delivery. From the studies performed in this thesis, some answers were offered and some new important questions were raised. Nevertheless, steps have been taken forward and methods have been developed that will act as a stepping stone for further studies attempting to further advance the state of the art in ultrasound enhanced drug delivery.

REFERENCES

[1] V. Sboros, et al., "Understanding the limitations of ultrasonic backscatter measurements from microbubble populations," Physics in Medicine and Biology, vol. 47, pp. 4287-4299, 2002/12/07/ 2002.

[2] P. S. Epstein and M. S. Plesset, "On the stability of gas bubbles in liquid-gas solutions," The Journal of Chemical Physics, vol. 18, pp. 1505-1509, 1950.

[3] T. A. Tran, et al., "Effect of ultrasound-activated microbubbles on the cell electrophysiological properties," Ultrasound in Medicine and Biology, vol. 33, pp. 158-163, 2007.

[4] B. Geers, et al., "Self-assembled liposome-loaded microbubbles: The missing link for safe and efficient ultrasound triggered drug-delivery," Journal of Controlled Release, vol. 152, pp. 249-56, Jun 10 2011.

[5] J. M. Escoffre, et al., "Doxorubicin delivery into tumor cells with ultrasound and microbubbles," Mol Pharm, vol. 8, pp. 799-806, Jun 6 2011.

[6] B. Geers, et al., "Self-assembled liposome-loaded microbubbles: The missing link for safe and efficient ultrasound triggered drug-delivery," J Control Release, vol. 152, pp. 249-56, Jun 10 2011.

[7] H. H. Pennes, "Analysis of tissue and arterial blood temperatures in the resting human forearm," J Appl Physiol, vol. 1, pp. 93-122, Aug 1948.

[8] C. T. Chin, et al., "Brandaris 128: A digital 25 million frames per second camera with 128 highly sensitive frames," Review of Scientific Instruments, vol. 74, pp. 5026-5034, 2003.

[9] F. Winau, et al., "Paul Ehrlich - In search of the magic bullet," Microbes and Infection, vol. 6, pp. 786-789, 2004.

List of publications

Journal Articles

1. "Investigation of Microbubble Response to Long Pulses Used in Ultrasound-Enhanced Drug Delivery," **Mannaris, C.** and Averkiou, M. A., Ultrasound in medicine & biology, vol. 38, pp. 681-691, 2012

2. "Dose-dependent artifact in the far wall of the carotid artery at dynamic contrast-enhanced US," Thapar, A., Shalhoub, J., Averkiou, M., **Mannaris, C.**, Davies, A. H., Leen, E. L., Radiology, vol. 262, pp. 672-9, Feb 2012.

3. "Doxorubicin liposome-loaded microbubbles for contrast imaging and ultrasound-triggered drug delivery," Escoffre, J. M.*, **Mannaris, C.*** et al., IEEE Transactions on Ultrasonics, Ferroelectrics, and Frequency Control, vol. 60, pp. 78-87, Jan 2013. *equal contribution

4. "*In vitro* localized release of thermosensitive liposomes with ultrasound-induced hyperthermia," **Mannaris, C**, Efthymiou, E, Meyre, M. E, Averkiou, M.A, Ultrasound in Medicine & Biology, vol. 39, pp. 2011-20, Nov 2013.

5. "Accurate measurement of microbubble response to ultrasound with a diagnostic ultrasound scanner," C. Keravnou*, **Mannaris C.*** and M. Averkiou, IEEE Transactions on Ultrasonics, Ferroelectrics, and Frequency Control, 2014 (under review) *equal contribution

Book Chapters

1. Averkiou, M.A, **Mannaris, C**., Nicolaides, A., "Vascular Ultrasound Imaging with Contrast Agents: Carotid Plaque Neovascularization and the Hyperplastic Vasa Vasorum Network", in *Ultrasound and carotid bifurcation atherosclerosis,* Nicolaides, A.N., et al., eds.. 2012, Springer London: New York.

Conference Proceedings

1. "Nonlinear pulsing schemes for the detection of ultrasound contrast agents", Averkiou, MA, Mannaris, C, Bruce, M, Powers, J, Proc. Acoustics'08 Paris, 2008.

2. "Experimental investigation of microbubble response to ultrasonic pulses used in therapeutic applications", Mannaris C, Stylianou K, de Jong N, Averkiou M, 15th European Symposium on Ultrasound Contrast Imaging, Rotterdam (NL), Jan. 2010.
3. 'High-intensity focused ultrasound-mediated doxorubicin delivery with thermosensitive liposomes', Escoffre JM, Mannaris C, Rio L, Meyre ME, Germain M, Averkiou M, Bouakaz A, International Symposium on Therapeutic Ultrasound, New York, USA, April 2011.
4. 'Use of high intensity focused ultrasound for localized activation of thermosensitive liposomes for drug delivery.' Mannaris C, Efthymiou E, Khokhlova VA, Ilin SA, Escoffre JM, Bouakaz A, Mathieu G, Averkiou MA, 161st Meeting of the Acoustical Society of America, Seattle, USA, May 2011.
5. 'Investigation of microbubble response to long ultrasonic pulses used in therapeutic applications', Mannaris C, Averkiou M, 161st Meeting of the Acoustical Society of America, Seattle, USA, May 2011.
6. '*In vitro* evaluation of thermosensitive liposomes for high-intensity focused ultrasound-triggered doxorubicin delivery', Escoffre JM, Mannaris C, Efthymiou E, Novell A, Meyre M-E, Germain M, Averkiou M, Bouakaz A, IEEE International Ultrasonics Symposium, Orlando (USA), Oct 2011
7. 'Ultrasound-induced temperature elevation for *in vitro* controlled release of thermo-sensitive liposomes', Mannaris C, Efthymiou E, Meyre M-E, Rio L, Germain M, Pottier A, Levy L, Averkiou MA, 162nd Meeting of the Acoustical Society of America, San Diego (USA), Oct-Nov 2011
8. 'Ultrasound-induced temperature elevation for *in vitro* controlled release of thermosensitive liposomes', Mannaris C, Escoffre J-M, Bouakaz A, Meyre M-E, Germain M, Averkiou MA, 17th European symposium on ultrasound contrast imaging, Rotterdam (NL), Jan 2012
9. 'Role of thermal and mechanical effects on drug release from thermosensitive nanocarriers', Novell A, Escoffre JM, Al-sabbagh C, Mannaris C, Fattal E, Tsapis N, Averkiou M, Bouakaz A, IEEE International US Symposium, Dresden (DE), Oct 2012